ISTITUTO NAZIONALE DI FISICA NUCLEARE - ISTITUTO NAZIONALE DI FISICA NUCLEARE - ISTITUTO NAZIONALE DI FISICA NUCLEARE - ISTITUTO NAZIONALE DI FISICA NUCLEARE - ISTITUTO NAZIONALE DI FISICA NUCLEARE - ISTITUTO NAZIONALE DI FISICA NUCLEARE - ISTITUTO NAZIONALE DI

Laboratori Nazionali di Frascati

LNF-96/043 (IR)
3 Settembre 1996

The KLOE Collaboration

THE KLOE TRIGGER SYSTEM

ADDENDUM TO THE KLOE TECHNICAL PROPOSAL

PACS.: 11.30.Er; 13.20.Eb; 13.20.Jf; 29.40.Gx; 29.40.Vj

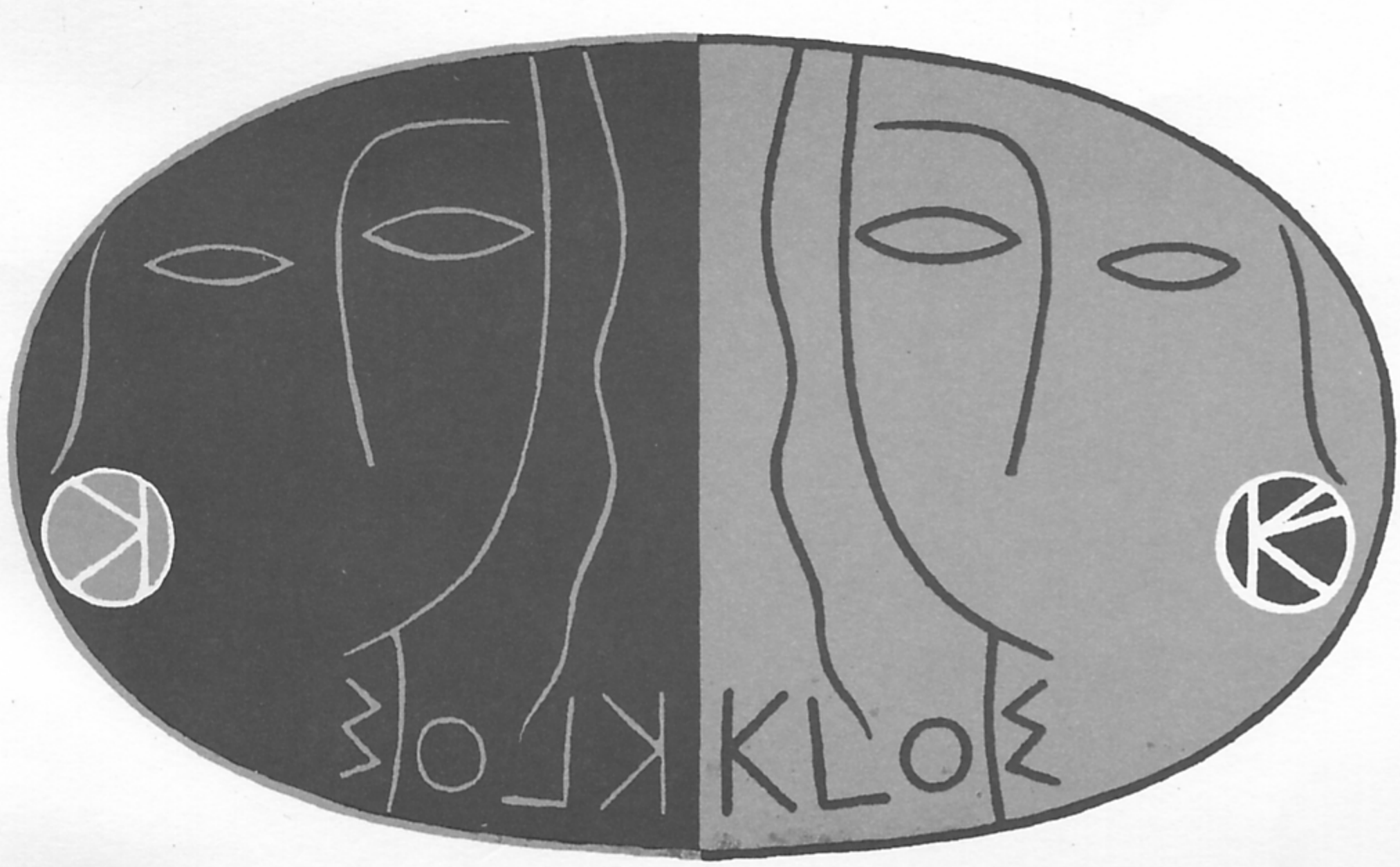

SIS–Pubblicazioni
dei Laboratori Nazionali di Frascati
P.O. Box 13 – 00044 Frascati (Italy)

LNF-96/043 (IR)
3 Settembre 1996

The KLOE Collaboration

THE KLOE TRIGGER SYSTEM

ADDENDUM TO THE KLOE TECHNICAL PROPOSAL

PACS.: 11.30.Er; 13.20.Eb; 13.20.Jf; 29.40.Gx; 29.40.Vj

THE KLOE COLLABORATION

A. Aloisio[f] A. Andryakov[c] A. Antonelli[c] M. Antonelli[c] F. Anulli[c]
C. Avanzini[i] C. Bacci[l] R. Baldini-Ferroli[c] G. Barbiellini[o] V. Baturin[f]
H. Beker[i] G. Bencivenni[c] S. Bertolucci[c] M. Billich[d] C. Bini[i] C. Bloise[c]
V. Bocci[k] F. Bossi[c] P. Branchini[m] L. Bucci[i] A. Calcaterra[c] R. Caloi[i]
P. Campana[c] G. Capon[c] M. Carboni[c] G. Cataldi[e] S. Cavaliere[f]
F. Ceradini[l] M. Cerù[i] F. Cervelli[h] F. Cevenini[f] G. Chiefari[f]
P. Creti[e] R. De Sangro[c] P. De Simone[c] G. De Zorzi[i] S. Dell'Agnello[c]
D. Della Volpe[f] A. Denig[d] A. Di Benedetto[k] G. Di Cosimo[i]
A. Di Domenico[i] S. Di Falco[h] R. Di Stefano[c] A. Doria[f] F. Donno[c]
E. Drago[f] V. Elia[e] O. Erriquez[a] A. Farilla[a] G. Felici[c] A. Ferrari[h]
M. L. Ferrer[c] G. Finocchiaro[c] D. Fiore[f] G. Foti[o] A. Franceschi[c]
P. Franzini[i,g] A. Gaddi[c] C. Gatto[f] P. Gauzzi[i] E. Gero[c] S. Giovannella[i]
V. Golovatyuk[e] E. Gorini[e] F. Grancagnolo[e] W. Grandegger[c]
E. Graziani[m] U. v. Hagel[d] S. W. Han[c,b] M. Imhof[d] M. Incagli[h]
L. Ingrosso[c] L. Keeble[c] W. Kim[n] W. Kluge[d] F. Lacava[i] G. Lanfranchi[i]
P. Laurelli[c] J. Lee-Franzini[c,n] T. Lomtadze[h] G. Margutti[i] A. Martini[c]
A. Martinis[o] M. M. Massai[h] R. Messi[k] L. Merola[f] S. Miscetti[c]
S. Moccia[c] F. Murtas[c] M. Napolitano[f] G. F. Palamà[e] M. Panareo[e]
L. Paoluzi[k] E. Pasqualucci[k] L. Passalacqua[c] M. Passaseo[i]
A. Passeri[m] V. Patera[j,c] F. Pelucchi[c] E. Petrolo[i] G. Petrucci[c]
M. Piccolo[c] A. Pintus[c] M. Pollack[n] L. Pontecorvo[i] M. Primavera[e]
F. Ruggieri[a] R. D. Schamberger[n] C. Schwick[c] A. Sciubba[j,c] F. Scuri[o]
F. Shoenleber[d] A. Smilzo[f] S. Spagnolo[e] E. Spiriti[m] C. Stanescu[m]
L. Tortora[m] P. M. Tuts[g] E. Valente[i] P. Valente[c] G. Venanzoni[h]
S. Veneziano[i] D. Vettoretti[c] S. Weseler[d] R. Wieser[d] S. Wölfle[c]
A. Zallo[c] P. P. Zhao[c,b] C. D. Zhang[c,b] J. Q. Zhang[c,b] A. Zott[d]

[a] Dipartimento di Fisica dell'Università e Sezione INFN, Bari
[b] Institute of High Energy Physics of Academica Sinica, Beijing, China
[c] Laboratori Nazionali di Frascati dell'INFN, Frascati
[d] Institut für Experimentelle Kernphysik, Universität Karlsruhe
[e] Dipartimento di Fisica dell'Università e Sezione INFN, Lecce
[f] Dipartimento di Scienze Fisiche dell'Università e Sezione INFN, Napoli
[g] Physics Department, Columbia University, New York
[h] Dipartimento di Fisica dell'Università e Sezione INFN, Pisa
[i] Dipartimento di Fisica dell'Università e Sezione INFN, Roma I
[j] Dipartimento di Energetica dell'Università, Roma I
[k] Dipartimento di Fisica dell'Università e Sezione INFN, Roma II
[l] Dipartimento di Fisica dell'Università di Roma III e Sezione INFN, Roma I
[m] Istituto Superiore di Sanità and Sezione INFN, ISS, Roma.
[n] Physics Department, State University of New York at Stony Brook
[o] Dipartimento di Fisica dell'Università e Sezione INFN, Trieste/Udine

TABLE OF CONTENTS

1. OVERVIEW

1.1 INTRODUCTION

The KLOE detector,[1–4] at present under construction for operation at the Frascati ϕ–factory DAΦNE,[5] is a general purpose detector whose major aim is the study of direct CP violation in the neutral kaon system. As in all e^+e^- collider experiments background levels at KLOE are *low*, allowing for efficient selection of high purity K_S–K_L event samples. However, the aim of KLOE is to reach an accuracy in the measurement of $\Re(\epsilon'/\epsilon)$ of $\sim\mathcal{O}(10^{-4})$. Such accuracies are not common in particle physics and impose stringent requirements on the detector performance and the trigger system. In particular the trigger should have the same efficiency for the several channels involved in the measurement of the parameters describing CP violation, with particular care for those channels which have 4 pions in all possible charge combinations. This requirement can best be achieved by insuring that the inefficiencies in triggering on different event configurations be kept at the level of few$\times 10^{-3}$. At the same time a highly redundant trigger can allow the measurement of these efficiencies, to the required accuracy of $0.3\text{x}10^{-3}$.

It should be noted that in principle an inefficient trigger can be acceptable for performing a measurement of $\Re(\epsilon'/\epsilon)$ by the double ratio method tagging K_S and K_L by detection respectively of a K_L or K_S decay because after event reconstruction one can establish that the event was indeed triggered by one or the other channel and thus remove event dependent biases. Nevertheless, we prefer to operate at the inefficiency levels mentioned above, not only for redundancy and safety reasons, but also because we are interested in the observation of interference patterns.[1]

1.1.1 Backgrounds

The main backgrounds in KLOE are due to electromagnetic processes, Bhabha and radiative Bhabha scattering from collisions of the two beams, as well as Coulomb scattering and Bremsstrahlung in the residual vacuum chamber gas and, finally Touschek scattering in the single bunches. These backgrounds become of importance because the resulting very small angle photons and electrons shower in the quadrupoles of the low β insertion which is fully contained inside the KLOE detector. Cosmic rays are another important class of background events. Rates from these processes are high compared to those from processes at interest, and they must be efficiently rejected by the trigger, while maintaining the aimed efficiencies for ϕ decays, especially in the K_SK_L channel.

1.1.2 Rates

At full luminosity, $\mathcal{L}$=10^{33} cm^{-2} s^{-1}, the ϕ production rate is $\sim$5 kHz and the Bhabha rate, for $9°<\theta<171°$is $\sim$40 kHz. The machine background gives a contribution that depends upon the details of the accelerator parameters but is of the same order of magnitude as the Bhabha's. Cosmic rays reaching the apparatus yield and additional $\sim$5 kHz.

The KLOE DAQ has been designed for an average throughput of 50 Mbytes s^{-1}, equivalent to a total trigger rate of 10 kHz. This is a necessary requirement which the

trigger must satisfy, while recognizing and scaling Bhabha's and Cosmic Rays, and rejecting background.

1.2 General Considerations

As will be proved in the following, the high efficiency for ϕ decays and high rejection of the various backgrounds is achievable. Some aspects of the trigger are determined by the properties of the front end electronics (FEE), the detector and the DAQ system. Studies of the constraints from physics and from the detector have been performed with specially developed software tools, *i.e.* Monte Carlo programs based on GEANFI[6] for the simulation of the response of the calorimeter, the tracking chamber and trigger hardware. These studies have led to the development of a two levels trigger scheme which satisfies all the requirements given above.

In this scheme the electromagnetic calorimeter, EmC, is the main trigger device, since it is particularly suited to provide a fast and efficient trigger. However some simple considerations immediately preclude a trigger based on total energy deposit in the EmC. For the case of the processes $e^+e^- \to K^0\bar{K}^0 \to \pi^0\pi^0\pi^0\pi^0$, the energy deposit in the calorimeter is ~1020 MeV, assuming that all particles reach the calorimeter. For Bhabha scattering, the energy deposit is also 1020 MeV. For the process $e^+e^- \to K^0\bar{K}^0 \to \pi^+\pi^-\pi^+\pi^-$ the visible energy in the calorimeter will be ~600 MeV due to the different response of the calorimeter to charged pions and electromagnetic showering particles (see chapter 2). The presence of obstructions, in particular the quadrupoles of the low β insertion, leads to losses in visible energy for all types of events. In addition, it produces background from the large number of small angle Bhabha's showering in the quadrupoles with a total energy distribution ranging from 0 MeV to 1020 MeV.

To avoid these difficulties the trigger described in the following is based on combining informations from local energy deposits in the calorimeter and clusters of hits in the drift chamber. The simplicity of this scheme and the modularity of its implementation facilitate monitoring and maintenance of the hardware. Possible malfunction can be detected online with the help of simple monitoring programs. Finally, since for almost all events the trigger is highly redundant, it allows the possibility in the offline analysis, to determine the efficiencies to high precision from the data themselves.

Our adopted scheme is not the most general possible trigger. One could, for example, construct a universal weighing function of the ~5000 calorimeter read-out signals, correlations included, and realize a filter which could ideally best discriminate between all event classes of interest. However, the very complexity of such a scheme might result in the impossibility of verifying the correctness of its performance.

The presentation of this paper is structured as follows. In chapter two we describe the characteristics of the various types of both background and physics events. Together with other requirements they form the bases of the trigger method described in chapter three. The results of the Monte Carlo simulation of the proposed trigger scheme are shown in

chapter four. A detailed description follows of the hardware, including the electronics necessary for handling calorimeter and drift chamber signals, and a description of the interface to the DAQ[4] system. We conclude with a time schedule and estimates for the cost of the trigger system.

2. PHYSICS AND BACKGROUND SIGNALS

The trigger essentially has to separate events of physical interest from the various background sources, at a rate with which these events occur in KLOE. To achieve an optimal performance their characteristics have to be studied with care.

2.1 ϕ DECAYS

The ϕ decay channels of interest for the study of CP violation have a quite wide spectrum of detector's responses. We have performed Monte Carlo studies on the following channels:

a) $K_S \to \pi^+\pi^-$, $K_L \to \pi^+\pi^-$
b) $K_S \to \pi^+\pi^-$, $K_L \to \pi^0\pi^0$, and $K_L \to \pi^+\pi^-$, $K_S \to \pi^0\pi^0$
c) $K_S \to \pi^0\pi^0$, $K_L \to \pi^0\pi^0$
d) $K_S \to \pi^+\pi^-$, $K_L \to \pi^\pm\ell^\mp\nu$

to which we will refer from now on as $\pi^{\pm,\pm}$, $\pi^{\pm,00}$, $\pi^{00,00}$, $\pi^{\pm,\pi\ell}$ respectively.

Events are generated according to the correct angular and energy distributions and propagated through the detector by GEANFI, in which the KLOE geometry is embedded.

The total reconstructed energy deposition inside the calorimeter for the four classes of events is shown in fig. 2.1. The mean value of this distribution is lower for events richer in charged particles, for many reasons. The rest mass of pions and/or muons is mostly lost from the energy deposit signal. Neutrinos from semileptonic K_L decays are another loss in visible energy. Furthermore charged particles are more easily lost because of the focussing effect of the detector solenoidal field, whereby spiralizing particles are absorbed in the quadrupoles. This last effect results in about 15% of the $\pi^{\pm,\pm}$ or $\pi^{\pm,\pi\ell}$ events depositing their energy entirely in the calorimeter's end caps, while for 99 % of the $\pi^{00,00}$ events there are at least 30 MeV deposited in the calorimeter barrel.

The average number of particles impinging on the calorimeter, as a function of the particle's minimal energy, is shown for the various classes of events in fig. 2.2. For all event classes there are on average $\sim$3 particles with at least 100 MeV in each event. For higher energies this multiplicity tends to rapidly decrease.

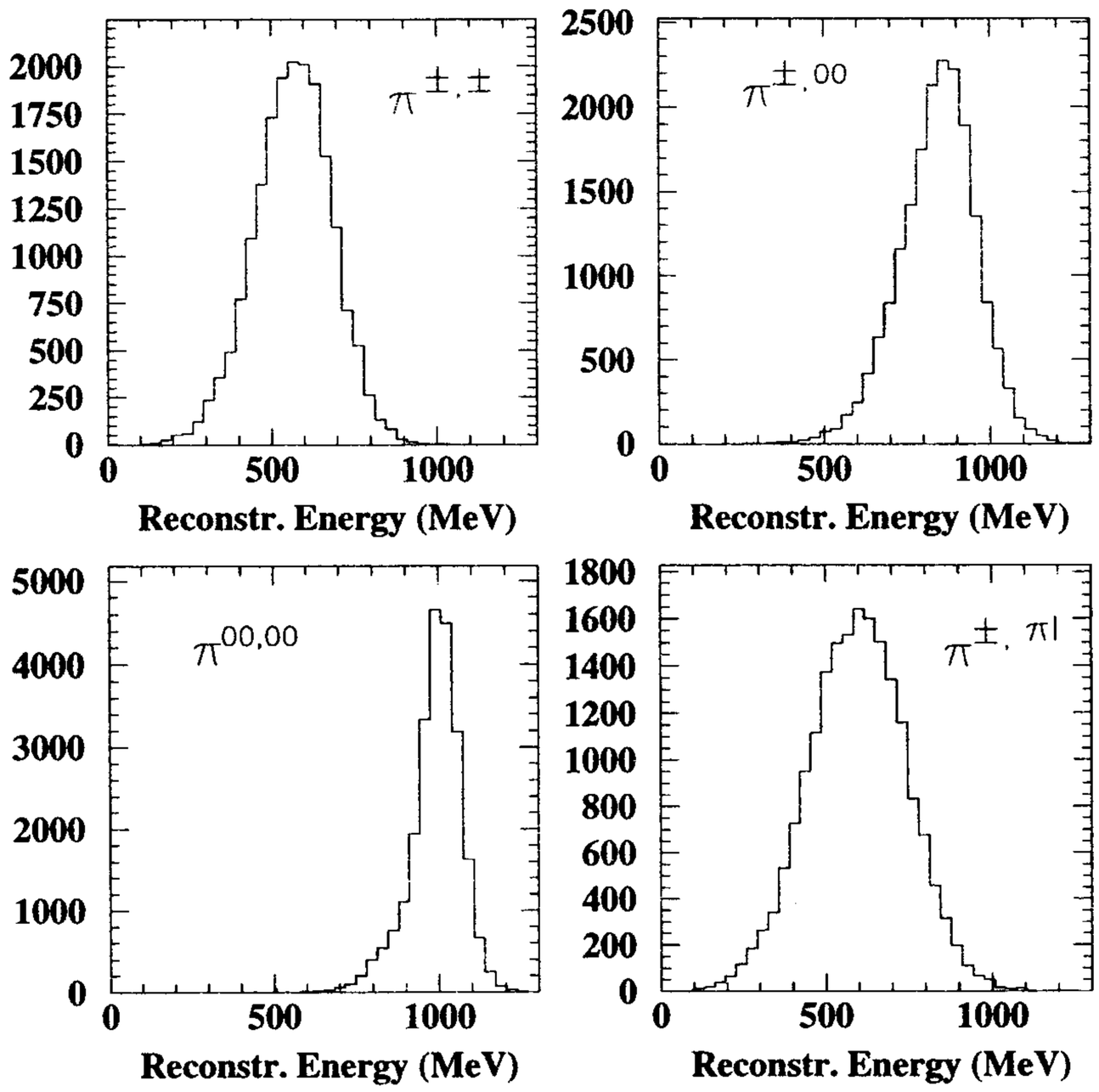

Figure 2.1. Distributions of the calorimeter response for four channels, see text.

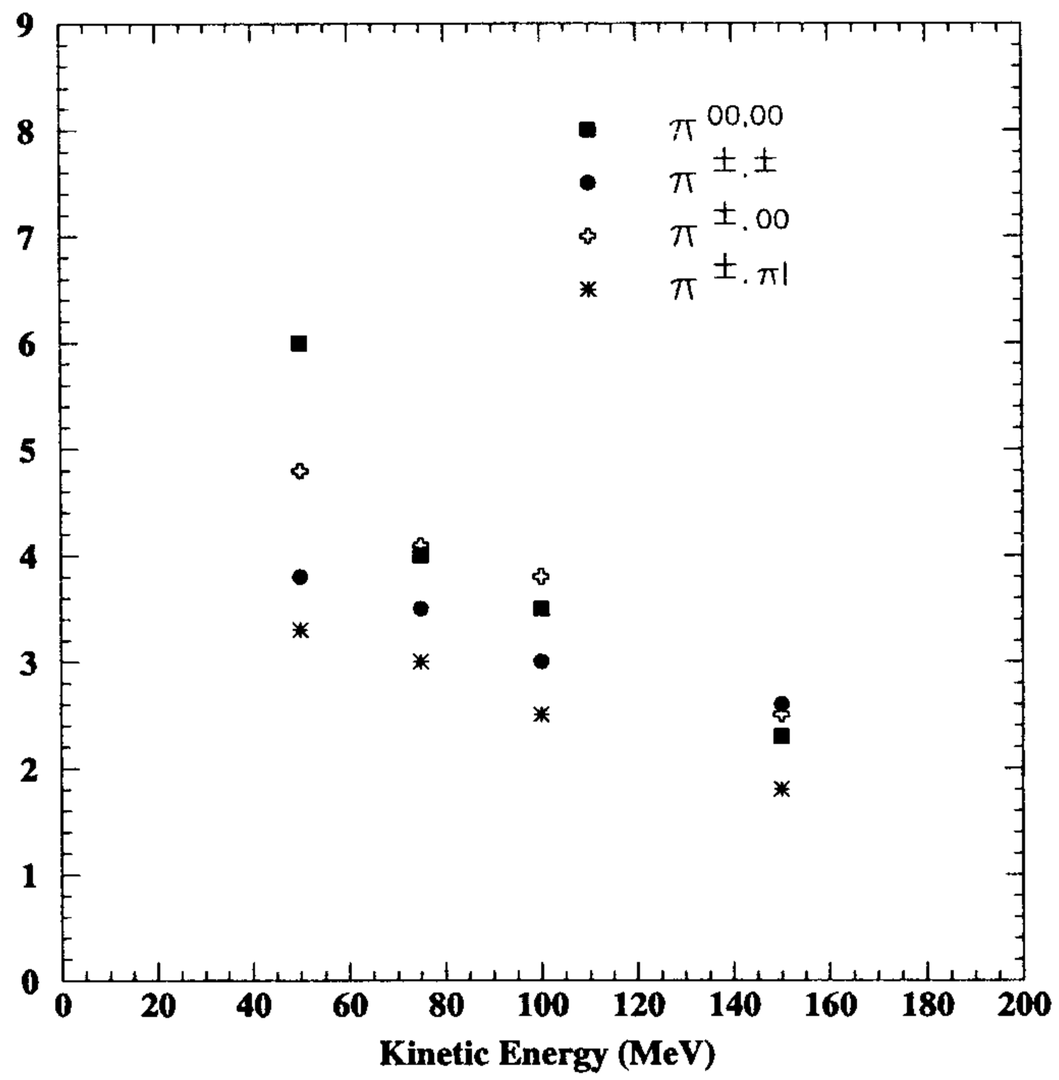

Figure 2.2. Expected particle multiplicities per event as a function of the minimal energy of the particles for the different event classes defined in the text.

Due to the relatively high value of the magnetic field, 0.6 T, charged particles produced in the K^0 decays spiralize in the drift chamber, DC, before reaching the calorimeter; therefore the multiplicity of DC hits is generally high for these classes of events, as shown in fig. 2.3.

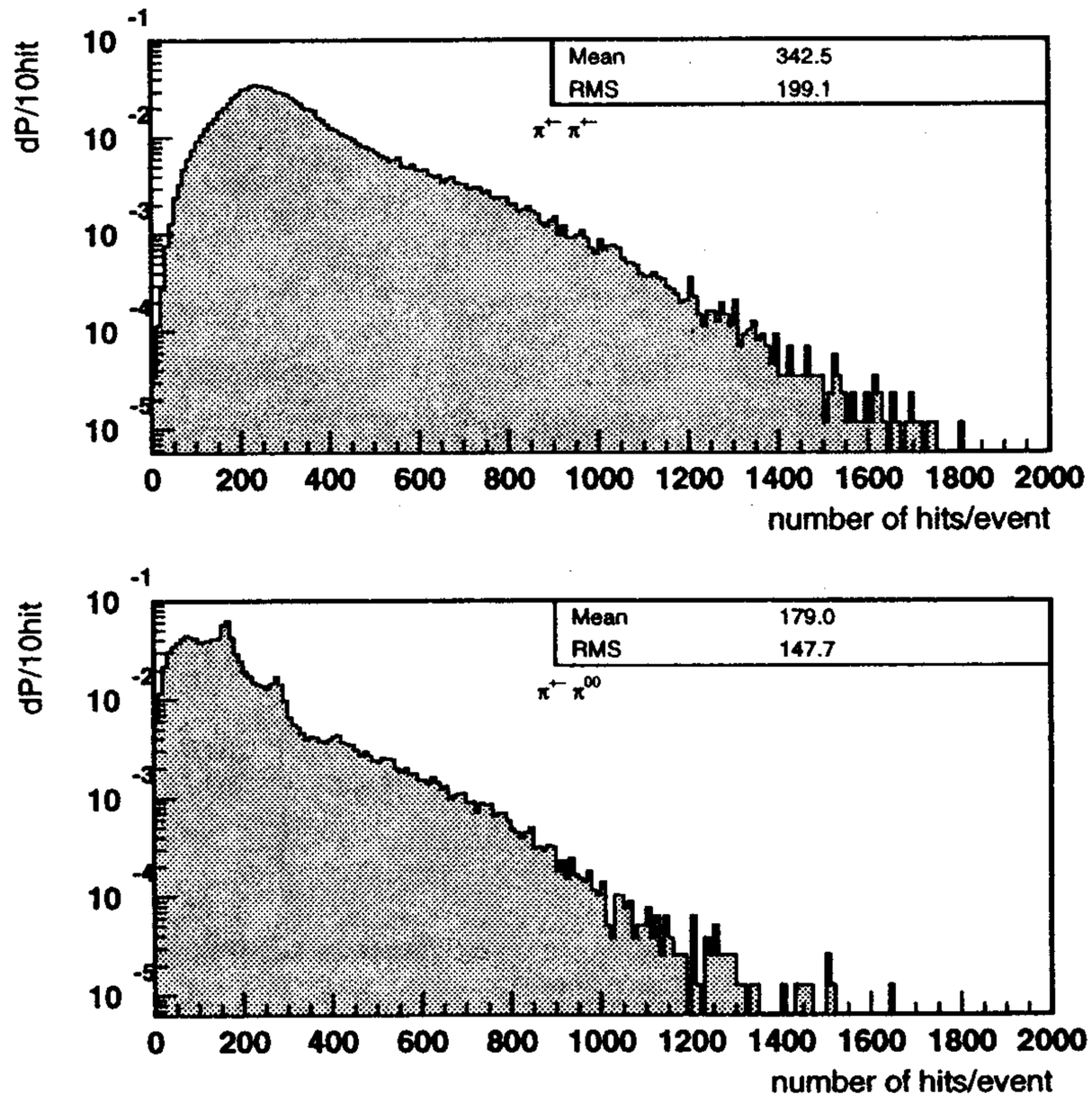

Figure 2.3. Number of DC hits for $\pi^{\pm,00}$,$\pi^{\pm,\pm}$ events

2.2 BHABHA EVENTS

At the maximum luminosity of 10^{33} cm^{-2} s^{-1}, the Bhabha event rate in the angular range $1°<\theta<179°$ exceeds 4 MHz. Due to the steep dependence on θ, the rate for Bhabha events depositing their entire energy in the calorimeter is ~30 kHz. These events can be easily tagged and downscaled as required. Note that these events are fundamental for the calibration of the time and energy scales of the calorimeter.

For events produced at $3°<\theta<9°$, ~300 kHz, the electron (positron) interacts with the material inside KLOE, mainly the quadrupoles, initiating an electromagnetic shower with some energy reaching the calorimeter. The distribution of the energy deposit for all Bhabha's is shown in fig. 2.4. In addition to the peak at 1.02 GeV due to wide angle events, there is an almost continuous tail due to the 'energy degraded' events. This distribution has to be compared with those shown in fig. 2.1, once the relative rates are properly taken into account. Making a cut at, say, 400 MeV, and properly downscaling the wide angle Bhabhas, results in an inefficiency of about 5% in the $\pi^{\pm,\pm}$ channel with a residual Bhabha background of about 7 kHz, still too high to be acceptable.

A striking feature of the Bhabha events is the energy release concentration in the endcaps; at maximum luminosity the rate of events reaching the barrel region is only ~1.5 kHz.

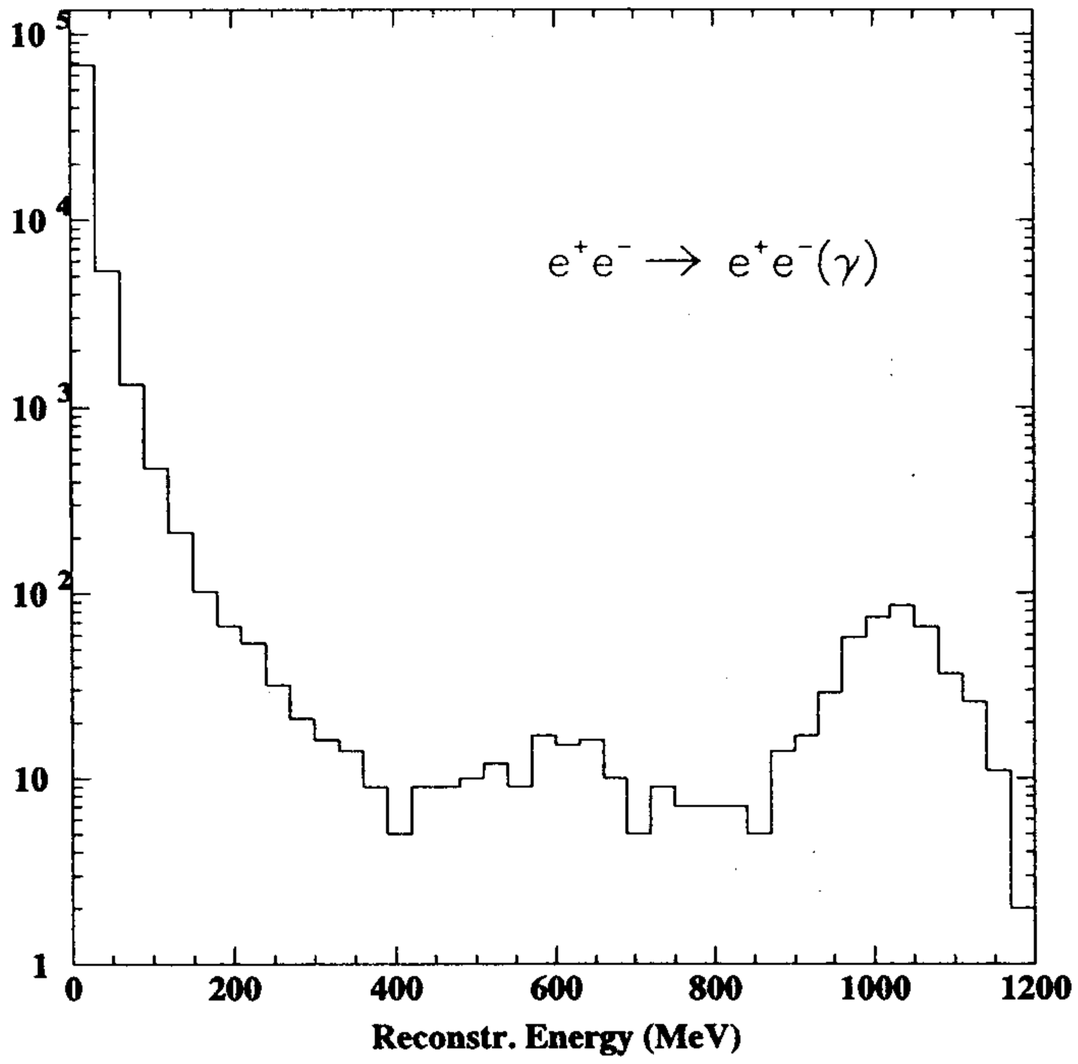

Figure 2.4. Energy deposited in the entire calorimeter for Bhabha events in the angular range $1°<\theta<179°$.

The hit multiplicity in the DC for Bhabhas is shown in fig. 2.5. It is interesting to compare this distribution with the one shown in fig. 2.3. As expected, ϕ decays have on average a much higher multiplicity with respect to Bhabhas (note the different scale on the horizontal axis).

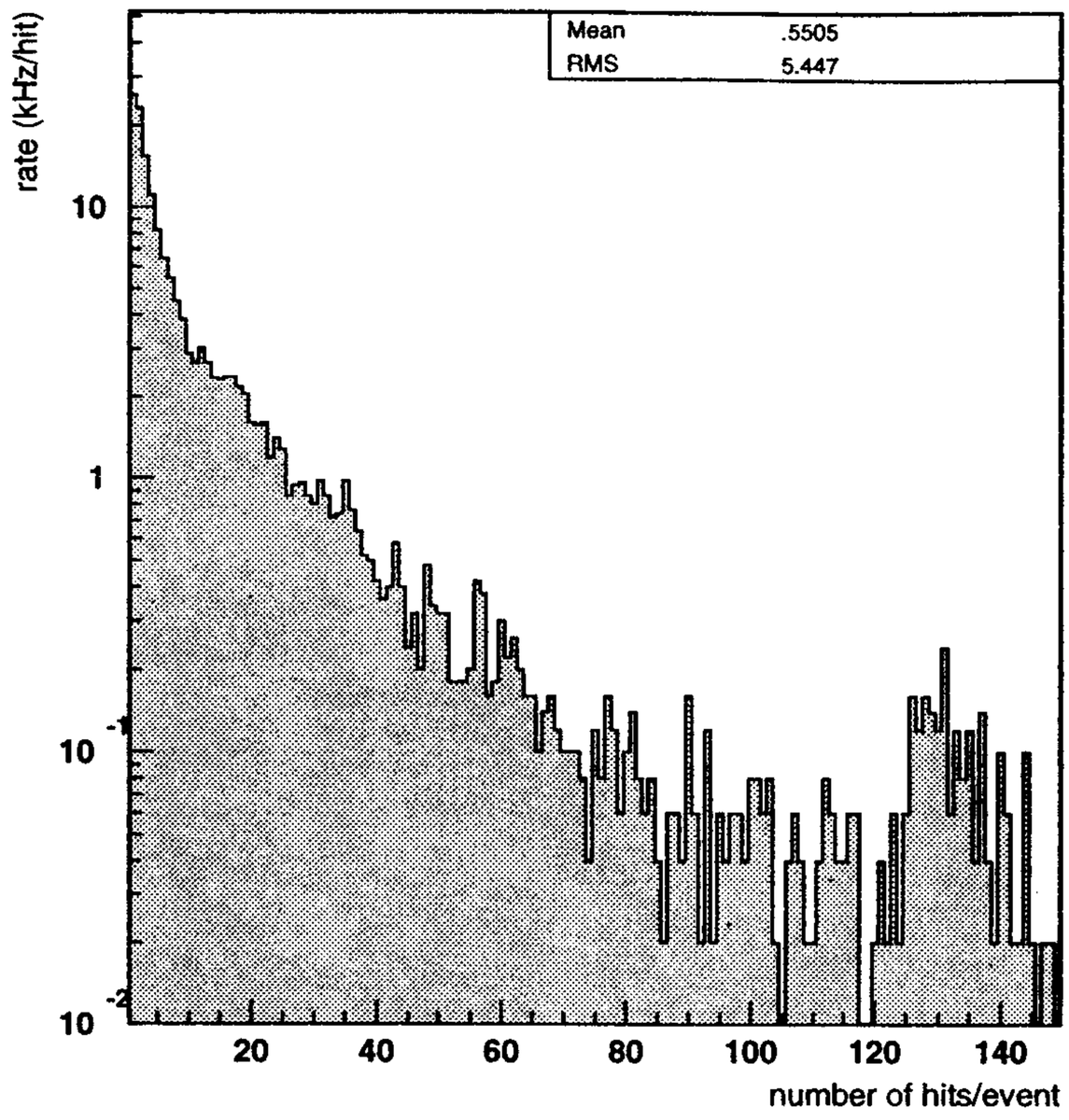

Figure 2.5. Number of DC hits for Bhabha events in the angular range $1°<\theta<179°$

2.3 Machine Background

Large particles fluxes inside KLOE can be generated by beam particles interacting with the residual gas in the pipe, or with other particles in the same bunch (Touschek effect). In order to study the effects of these events on the trigger rate, an intense program of simulation has been done, in close discussion with the DAΦNE machine division.

The program KTURTLE[7] has been used to track electrons and positrons through the machine elements and the KLOE solenoidal field and simulate their interactions with the residual gas. Particles are then tracked through the apparatus via GEANFI. An actual mapping of the pressure in the interaction region, shown in fig. 2.6, has been used.

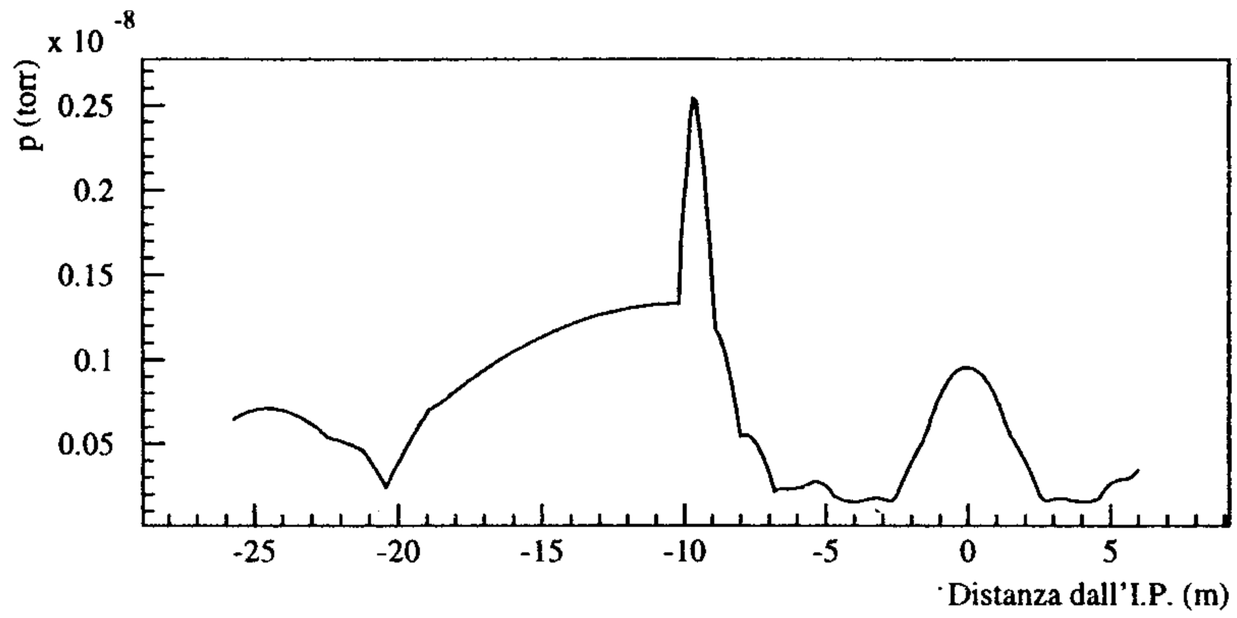

Figure 2.6. Distribution of the residual gas pressure along the beam pipe

Events	Energy (MeV)	Rate† (kHz)
Brems e^+	$500 < E < 510$	0.04
	$410 < E < 500$	703
	$2 < E < 410$	181
Brems photons	$0.05 < E < 10$	240
	$10 < E < 100$	118
	$100 < E < 508$	65
	θ (mrad)	
Coulomb e^+	$3 < \theta < 500$	606
Touschek e^+		110

† Before masking.

Table 2.1. Background rates.

There are three physics processes that contribute to machine background in KLOE: Coulomb scattering, beam gas bremsstrahlung, and Touscheck effect. Calculations show that the insertion of horizontal scrapers before the DAΦNE splitter magnet reduces drastically the last contribution.[8] . Table 2.1 shows the rates of particles *per beam* expected to cross the beam pipe in the KLOE region, i.e. within ±200 cm from the interaction point. Most of these particles are almost parallel to the beams, and tend to deposit their

energy onto the focussing quadrupoles.

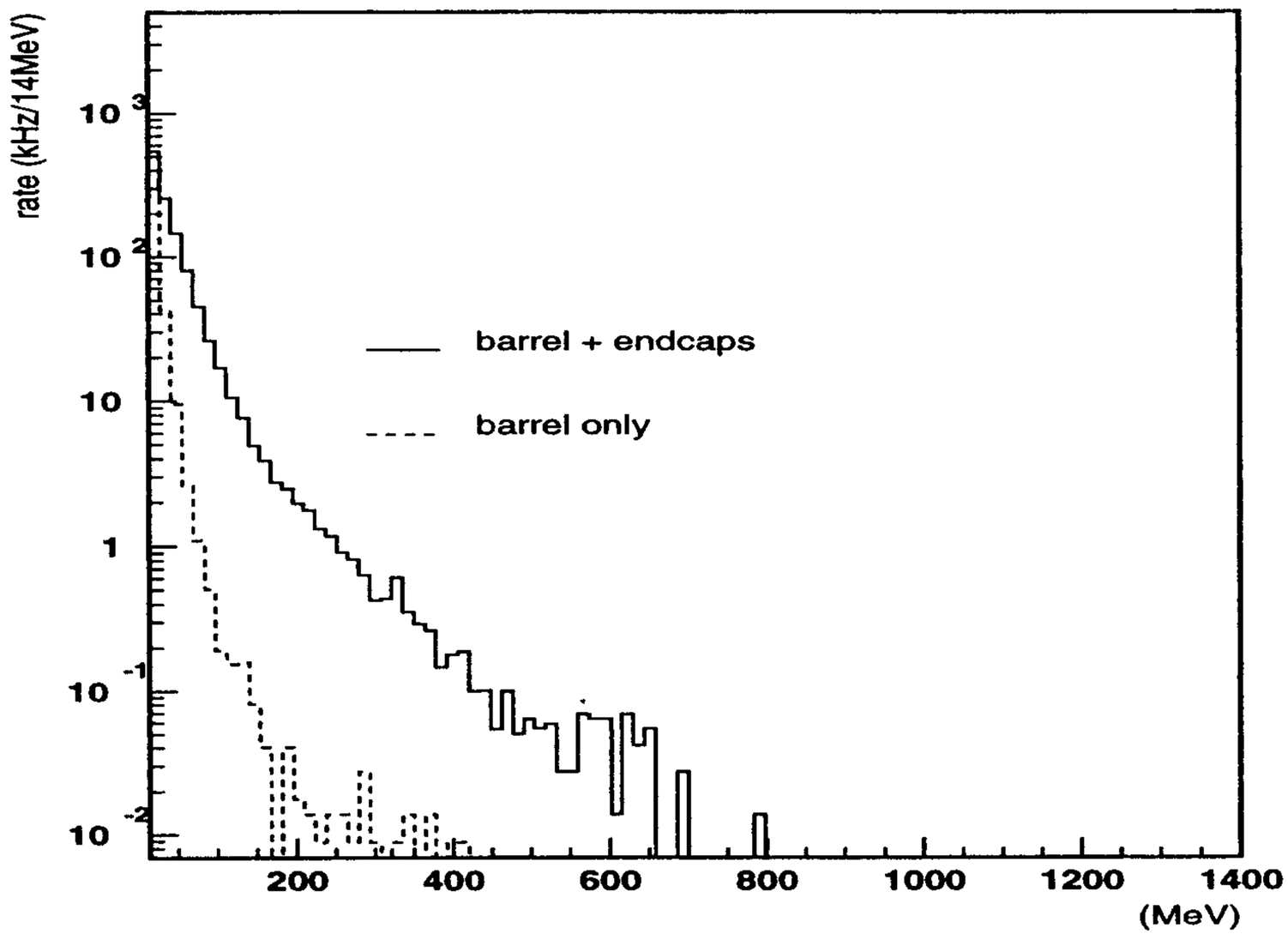

Figure 2.7. Energy deposited in the EMC by background radiation.

To reduce some of the remaining background we have considered inserting more absorbers at ± 170 cm from the interaction point, in the form of two lead rings, 12 cm long and 4.5 cm thick. The energy deposited in the calorimeter by the surviving events is shown in fig. 2.7. Similarly to the Bhabhas, energy is deposited mostly in the forward region.

Another similarity with Bhabhas is the fact that machine background produces a modest hit multiplicity in the DC, as shown in fig. 2.8. Again, a comparison with fig. 2.3 shows the different behaviour for ϕ and background events of this variable.

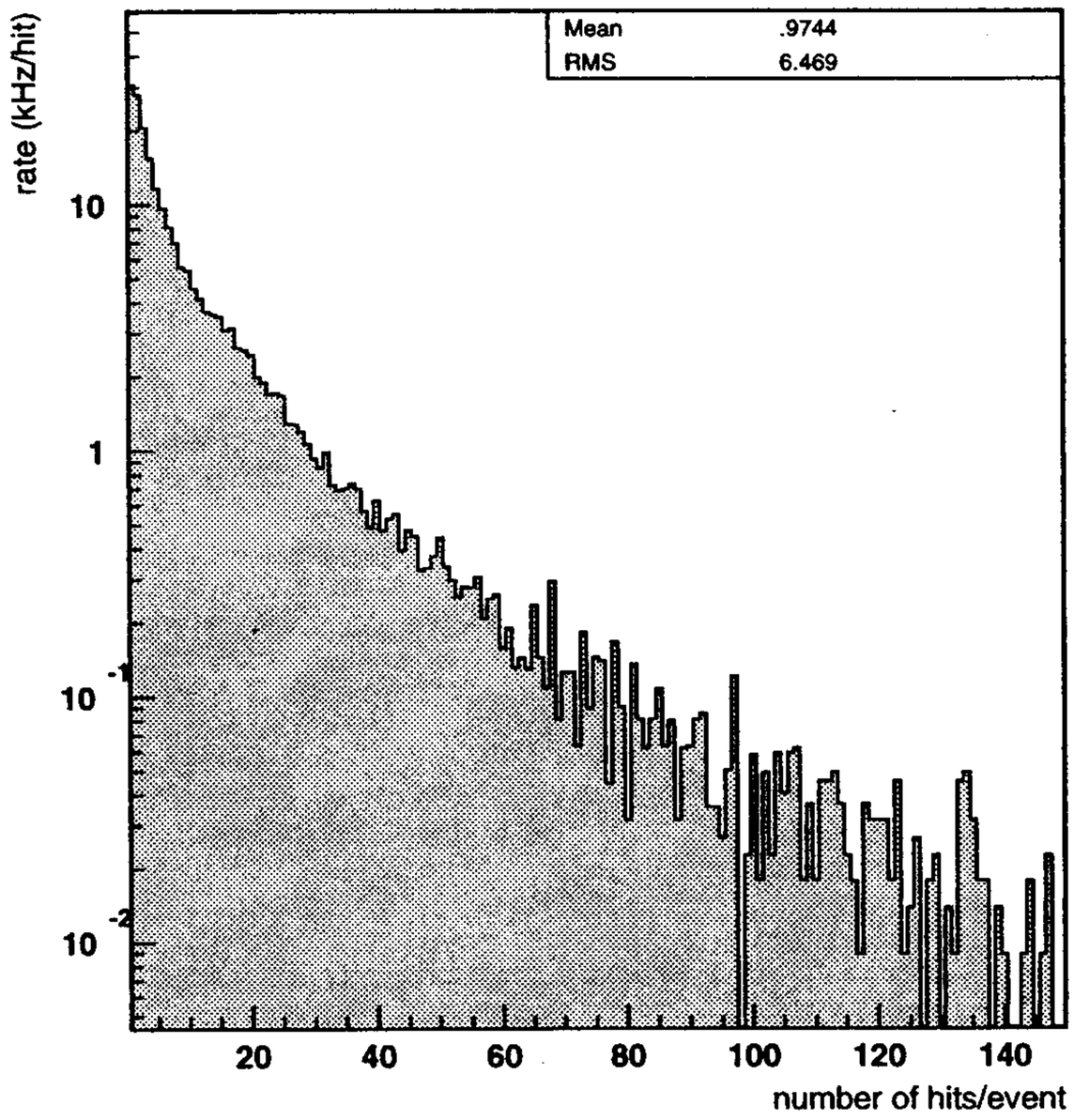

Figure 2.8. Number of DC hits for Machine Background events

2.4 Cosmic Rays

At Frascati's latitudes, a cosmic rays flux of about 4-5 kHz is expected to penetrate through the 40 cm iron shield provided by the yoke and to enter KLOE. Most of these particles are energetic muons which release on average about 30-40 MeV of equivalent energy in each calorimeter's cell.

A Monte Carlo cosmic ray generator has been written,[9] using energy and angle distributions based on the Dar formulae.[10] Particles are generated with an energy larger than 200 MeV, and then tracked via GEANFI through the apparatus including the iron shield.

The distribution of the energy deposited in the calorimeter is shown in fig. 2.9. We find that for 85% of the cases energy is deposited in the barrel. Any criteria based on total energy is clearly ineffective to reject these events without loosing efficiency on ϕ decays.

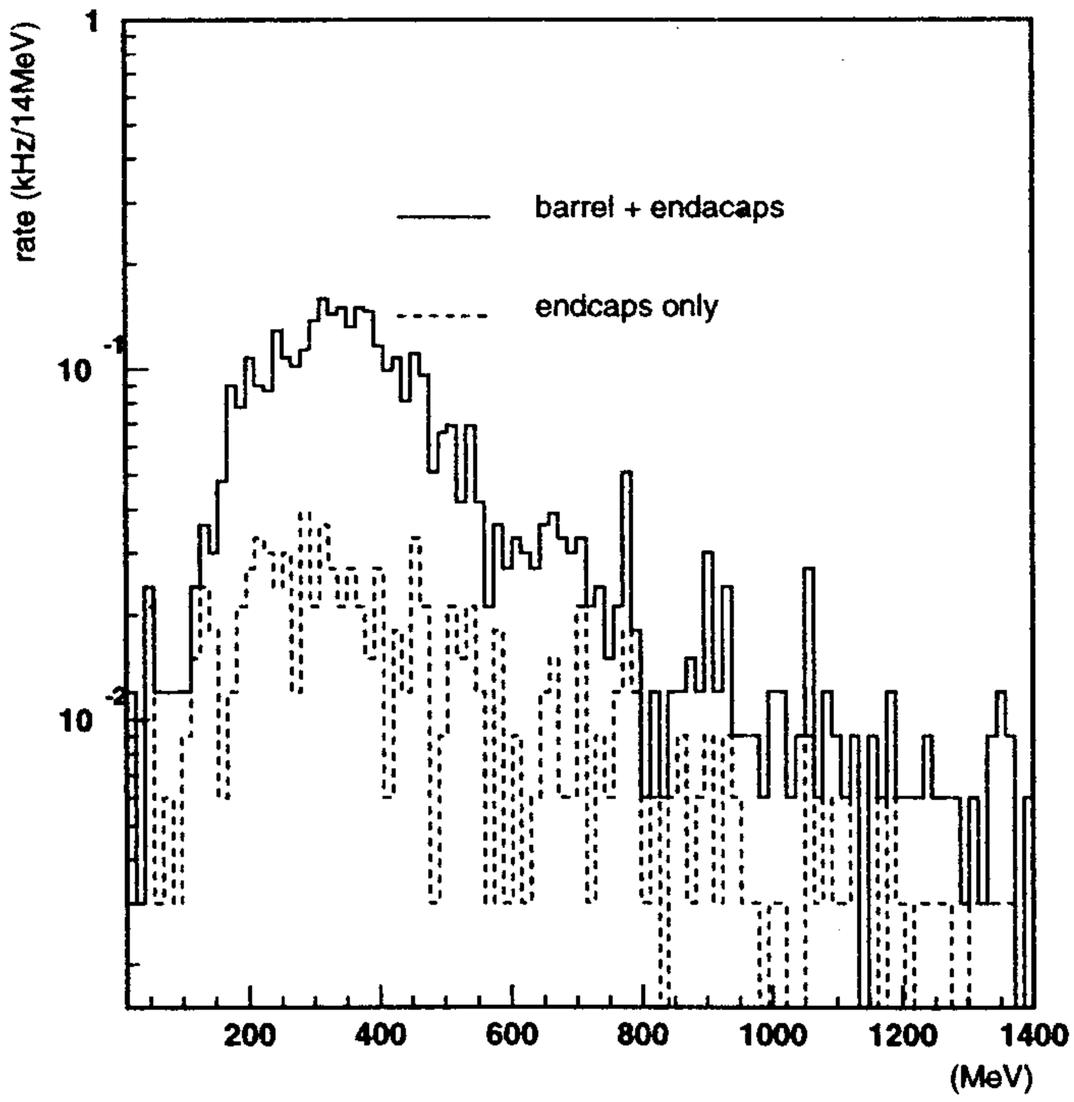

Figure 2.9. Energy deposited by cosmic rays.

In addition, the DC hit multiplicity for cosmic rays events is more similar to that of ϕ decays in contrast to the other background's types (see fig. 2.10). A dedicated trigger must therefore be developed to reject this particular class of events.

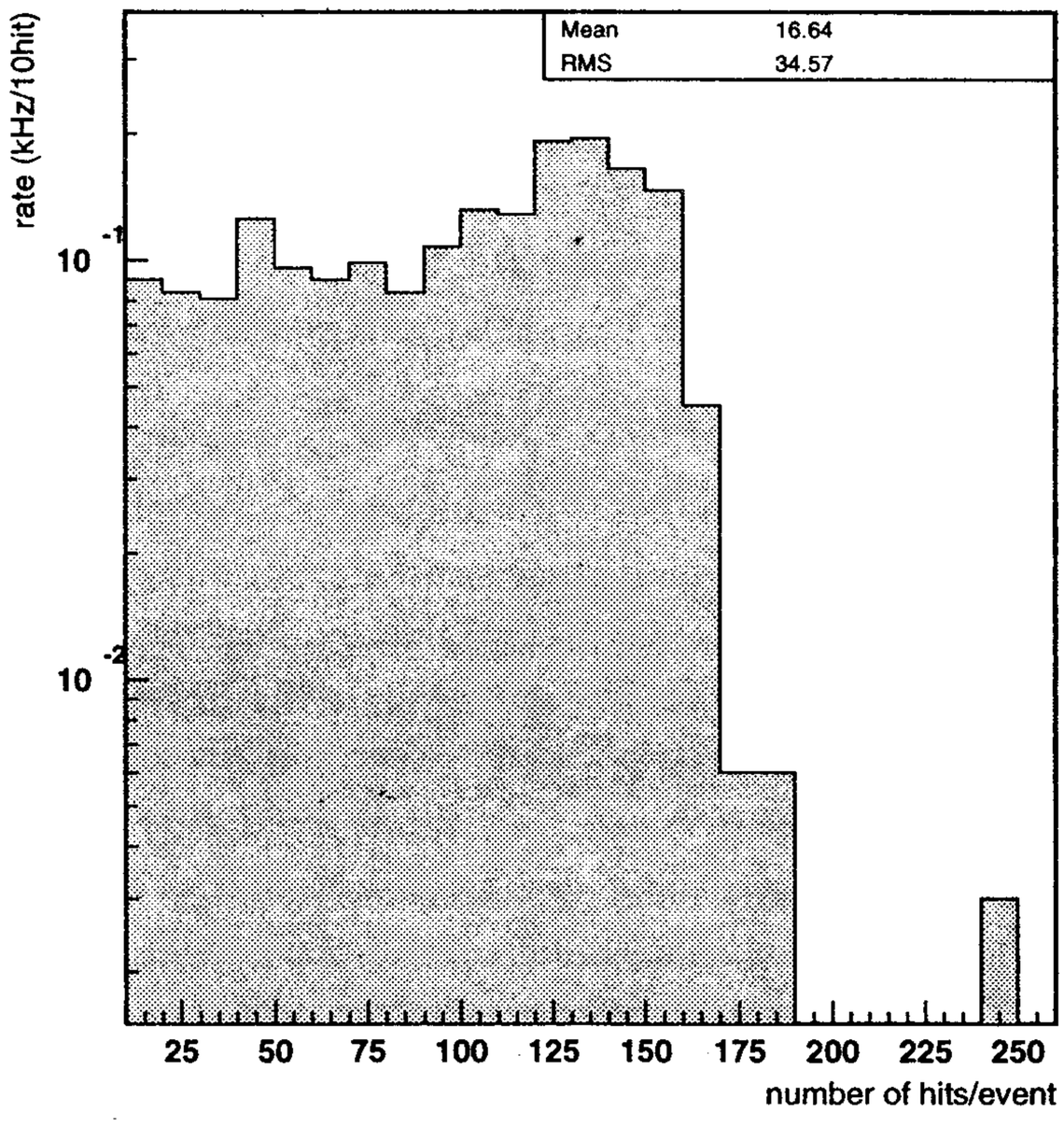

Figure 2.10. Number of DC hits for Cosmic rays events

3. THE PRINCIPLE OF THE KLOE TRIGGER

As already mentioned, the KLOE DAQ is quite safely designed for a maximum throughput of 10,000 good events per second.* The trigger system must therefore reduce the rate of good Bhabha events and the various backgrounds discussed in chapter two down to 5 $\sim$ kHz while retaining full efficiency for ϕ decays.† In the first section of this chapter we review some properties of DAΦNE and of the different event types, to properly motivate the choices for the KLOE trigger presented in the second section.

3.1 Requirements of the KLOE Trigger

In addition to the general requirements discussed in the introduction, the total deadtime must be kept small, a few %, which corresponds to an acceptable loss of luminosity. The two level trigger proposed achieves all this by using both calorimeter and drift chamber information, as explained in the following. While the efficiency for the various decay modes of interest can be known with negligible statistical error, systematic errors are harder to control. Systematic effects can only be studied on subsamples of the whole data set. We therefore require that efficiencies be close to unity, thus requiring only small corrections. This also ensures that the efficiency functions are "flat" and therefore can be safely extrapolated from the study of data sample with redundant trigger information and Monte Carlo computations.

3.1.1 Constraints due to event configuration

Since K_L mesons can decay everywhere in the detector volume, we cannot impose as a trigger requirement that particles originate at the IP, which would greatly help in removing cosmic rays and machine backgrounds. On the other hand, Bhabhas and machine backgrounds are concentrated in the forward direction. This suggests a trigger with different thresholds for the different regions of the detector. Energy thresholds in the forward directions will typically be set higher than at large angle. However since $\pi^{\pm,\pm}$ and $\pi^{\pm,\pi\ell}$ events reach more frequently the endcaps than $\pi^{\pm,00}$ and $\pi^{00,00}$ events (see section 2.1), the use of the calorimeter alone, with different thresholds would introduce appreciable differences in the efficiencies for the various channels. In order to improve the efficiency for the charged decays without increasing the background rates, we intend to use information from the drift chamber.

The energy deposit of cosmic ray muons in the calorimeter is similar to those of particles from ϕ decays and therefore can not be used to suppress cosmic ray events by itself. To reject these events the trigger has to exploit the fact that cosmic particles do not originate inside of the detector.

3.1.2 Constraints from DAΦNE

In DAΦNE the time between bunch crossings is $\sim$2.7 ns. Since it is not possible to

---

⋆ A good event has an average size of 5 kbytes, background events tend to be smaller.

† Another class of events with physical interest are $\gamma\gamma$ events. Since the rate of these events is very small, $\sim$0.4 Hz, they are ignored here.

generate a trigger in this time, the KLOE trigger must operate in a continuous mode. After some appropriate decision has been generated, the outgoing trigger signal must however be synchronized to the bunch crossing time, modulo n crossings, to allow precise event reconstruction. The situation is further complicated by the fact that the arrival time of particles to the calorimeter has an intrinsic spread mainly due to the random origin of the decay products of K_L's and spiraling of charged particles in the magnetic field. The arrival time of the particles hitting the calorimeter is shown in fig. 3.1 for various classes of ϕ decays.

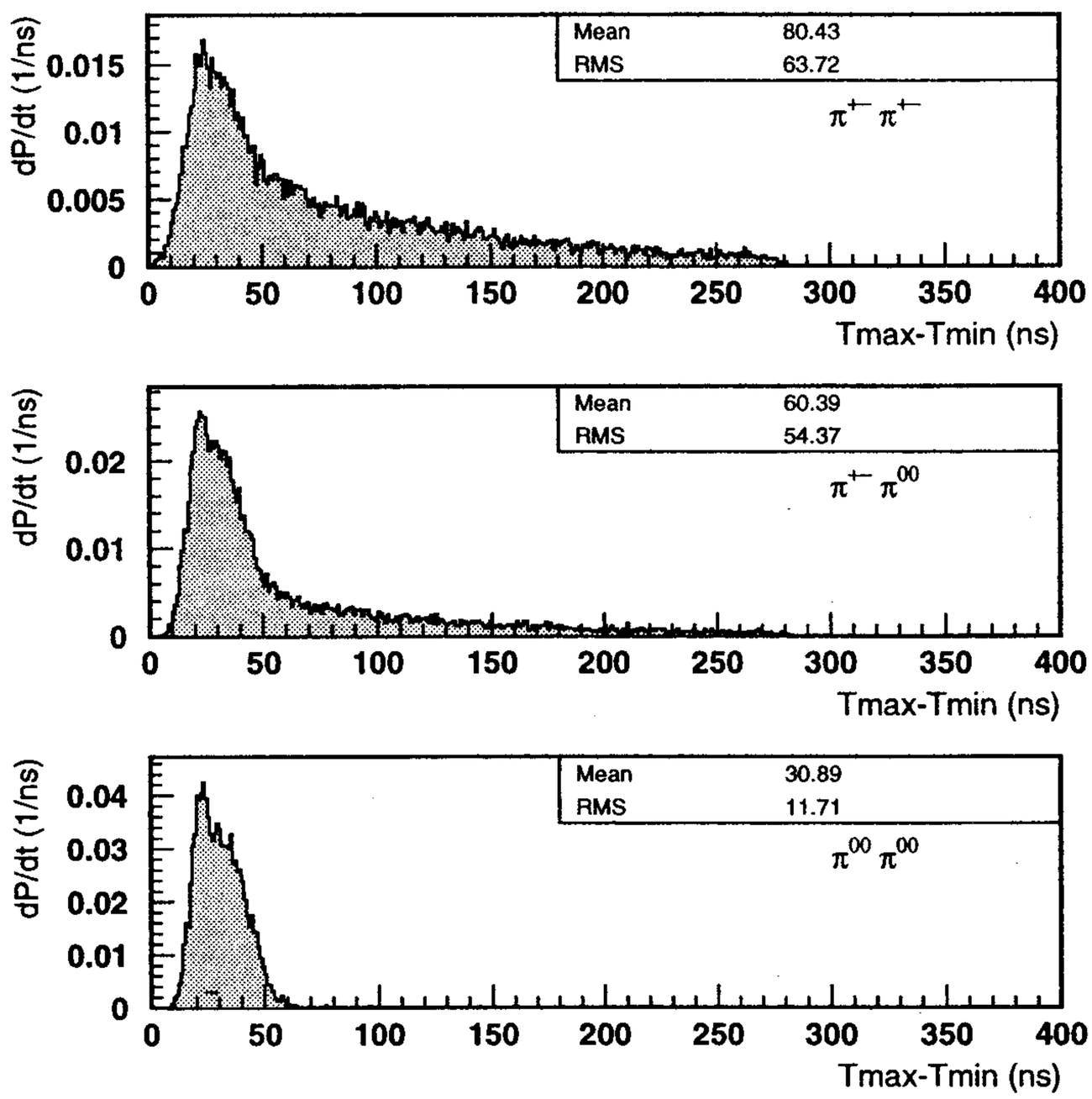

Figure 3.1. Distribution of arrival times at the calorimeter.

3.1.3 Constraints due to the FEE

The Front-end electronics, FEE, cannot accept triggers less than 2 μs apart in time, which for an average first level trigger rate of 10 kHz corresponds to a fractional loss of luminosity F_d=2%. In our proposed two level trigger scheme the second level trigger does not cause additional deadtime whereas every first level trigger causes a fixed deadtime of 2 μs. The total deadtime fraction F_d of the KLOE experiment in per cent is therefore given by $F_d = f_1 \times 2 \times 10^{-6} \times 100$, where f_1 is the trigger rate of the 1st level trigger. A deadtime of ~5%, which is still an acceptable loss of luminosity, corresponds to a first

level trigger rate of 25 kHz.

The flight path of the K_L mesons decaying to $\pi^0\pi^0$ is obtained in KLOE from time of flight measurements. These are performed with TDC's with a resolution of ~30 ps/count. The TDCs are started by the trigger signal and stopped by the delayed calorimeter signals. This common start mode of operation is better suited for asynchronous operation. The calorimeter signals cannot however be delayed by more than ~200 ns while retaining the accuracy required. The first level trigger decision must therefore be generated within this time interval after the arrival of the first signal from the calorimeter. This constraint requires that the first level trigger decision be made with fast analog sums of calorimeter signals and counts of chamber hits in a short time window of ~150 ns.

3.2 The KLOE Trigger

The KLOE trigger is based on local energy deposits in calorimeter sectors and multiplicity information from the drift chamber. The two level scheme has been adopted in order to both produce an early trigger with good timing information to start the FEE operation and to use as much information as possible from the drift chamber. Specifically, after the arrival of a first level trigger, additional information is collected from the drift chamber, which is used, together with the calorimetric information, to confirm the former and start the DAQ system.

The trigger logic is shown in fig. 3.2. The first level trigger can be vetoed if the event is identified as a Bhabha or a cosmic ray event. Details are given in the following sections.

3.2.1 Triggering With the Calorimeter

For trigger purposes the fine granularity of the calorimeter is not needed and therefore as first step we concentrate the 5000 readout elements into ~200 summed signals. The granularity of this concentration is a compromise between minimizing the number of trigger signals and the desire of triggering on single particles. The calorimeter barrel drives 96 trigger channels, each organised in two groups of 5×6 readout elements for each side of the barrel modules. Sums of the signals from five radial readout elements are produced by the FEE adders. A second level of adders in the trigger system adds six of the above sums. The grouping of the readout elements is indicated in fig. 3.3. In order to guarantee that each "particle" is fully contained in at least one sum, the calorimeter signals are added twice in a staggered way to form a set of totally overlapping calorimeter sectors.

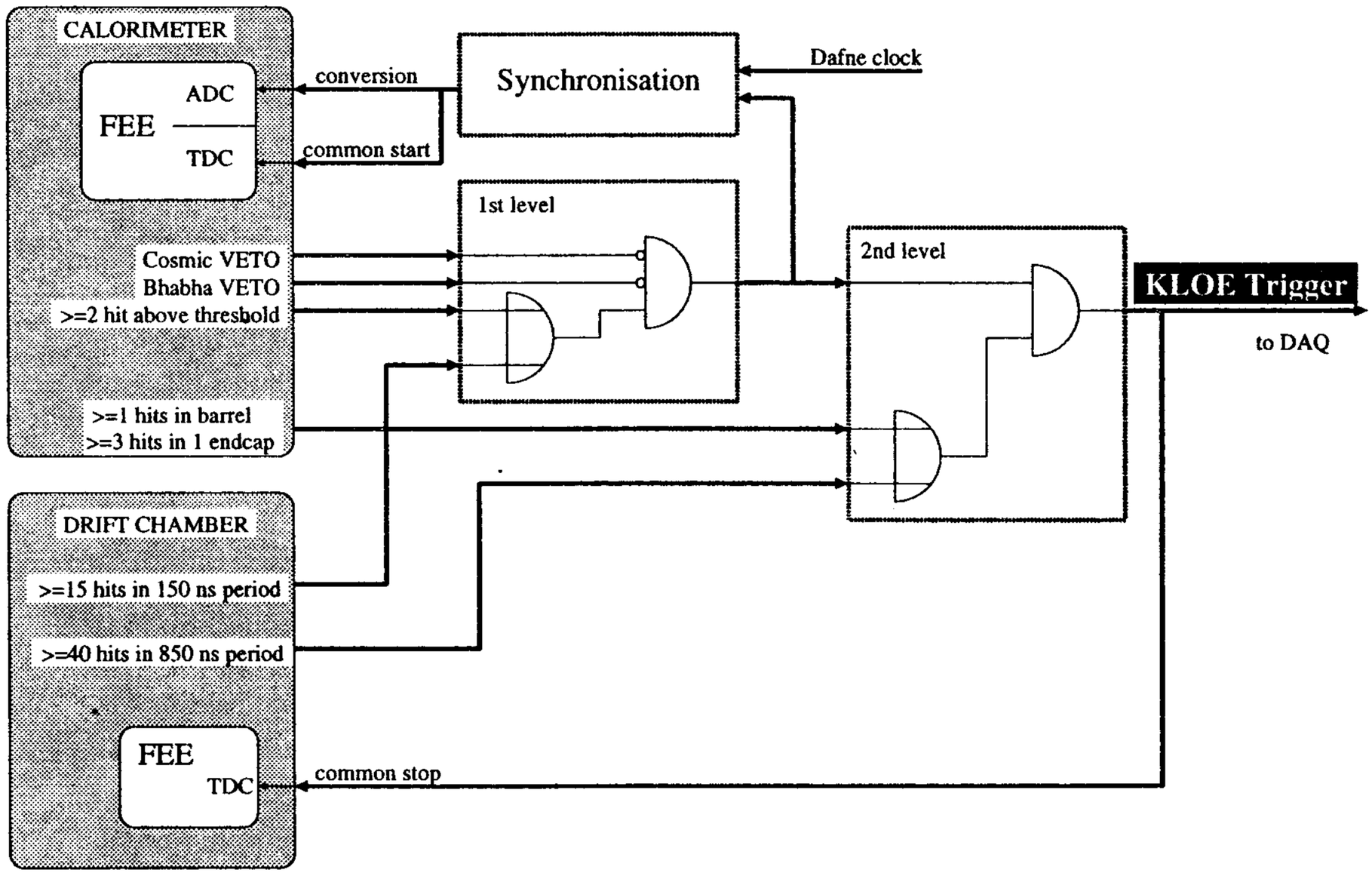

Figure 3.2. Block diagram of the two level trigger.

Since the particle multiplicity is higher in the forward region, mostly for background events, the end caps are segmented in groups of 4 columns in the zone close to the beam axis and of 6 columns elsewhere. Again, one column comprises 5 readout elements, resulting in 36 trigger channels for each endcap (see fig. 3.4).

The calorimeter triggers on local energy deposits larger than a programmable threshold. Two thresholds are given for each channel. One at low energy (~30 MeV) in order to trigger on low energy particles from ϕ decays entering the calorimeter (low energy trigger, LET), and one at high energy (~400 MeV) in order to identify and downscale Bhabha events at the trigger level (Bhabha trigger, BBT).

3.2.2 EMC trigger signal generation

In practice it is not a trivial task to apply a threshold which correponds to a constant energy deposit equivalent to the calorimeter signals because the signal amplitude depends on the z position* of the incident particle. This is due to the attenuation of the scintillator light in the optical fibers with an average attenuation length λ=3.5 m.

$\star$ By z-position we intend the position along the fibers. This becomes the vertical direction for the endcap modules.

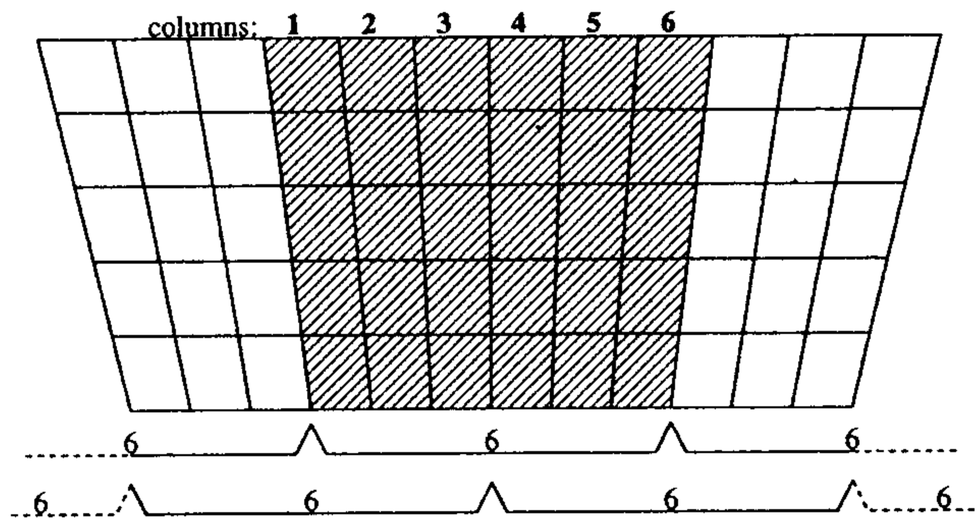

Figure 3.3. Division of the barrel into trigger elements. The brackets at the bottom of the figure indicate how readout columns are grouped together in overlapping trigger channels.

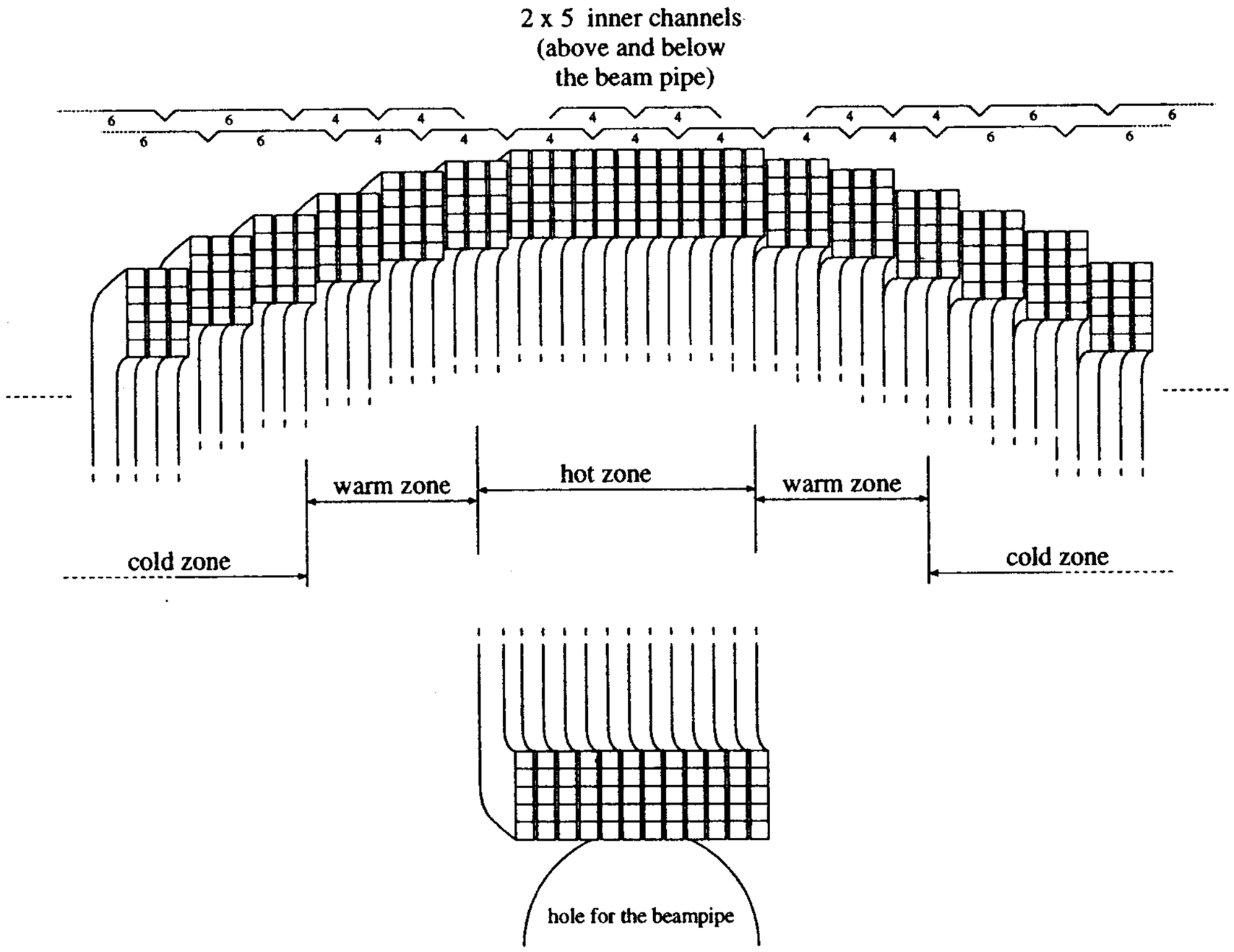

Figure 3.4. Division of the endcap into trigger channels. The brackets indicate the groups of column which form a trigger channel. The numbers indicate the number of columns in the trigger channel. The region close to the beampipe has finer granularity, while the outer channels have the same granularity as the barrel (6 columns per channel). The total number of endcap channels is 72 (both endcaps).

In order to reduce the dependence on z, in principle, signals from both sides of the calorimeter could be added. However, for the endcap elements a non uniform effective trigger threshold is aimed at as will be shown below. In addition, this method would cause some technical problems. The trigger thresholds would be applied to the amplitude of the signals. Due to the time light needs to travel along the fibres of the calorimeter module (up to 27 ns), the signals would arrive at the adders at different times. Since the duration of the signals is very short, ~5 ns, they would have to be integrated in order to get an amplitude at the output of the summer which would be proportional to the sum of the amplitudes of the input signals. To guarantee a precision of ~10%, the time constant of the integrator would have to be chosen so large that at full DAΦNE luminosity pile up would start to cause problems, in addition to delaying the trigger response. Finally, since an unique design for endcap and barrel was preferred, another method to generate the trigger thresholds has been chosen.

EMC trigger thresholds

In the proposed scheme the analog information of each adder is first digitized by comparing the signal to two different programmable thresholds. The comparator outputs are shaped to pulses of a well defined length and then combined logically as shown in fig. 3.5. This scheme allows to apply a large variety of effective thresholds with different characteristics with respect to their dependence on z.

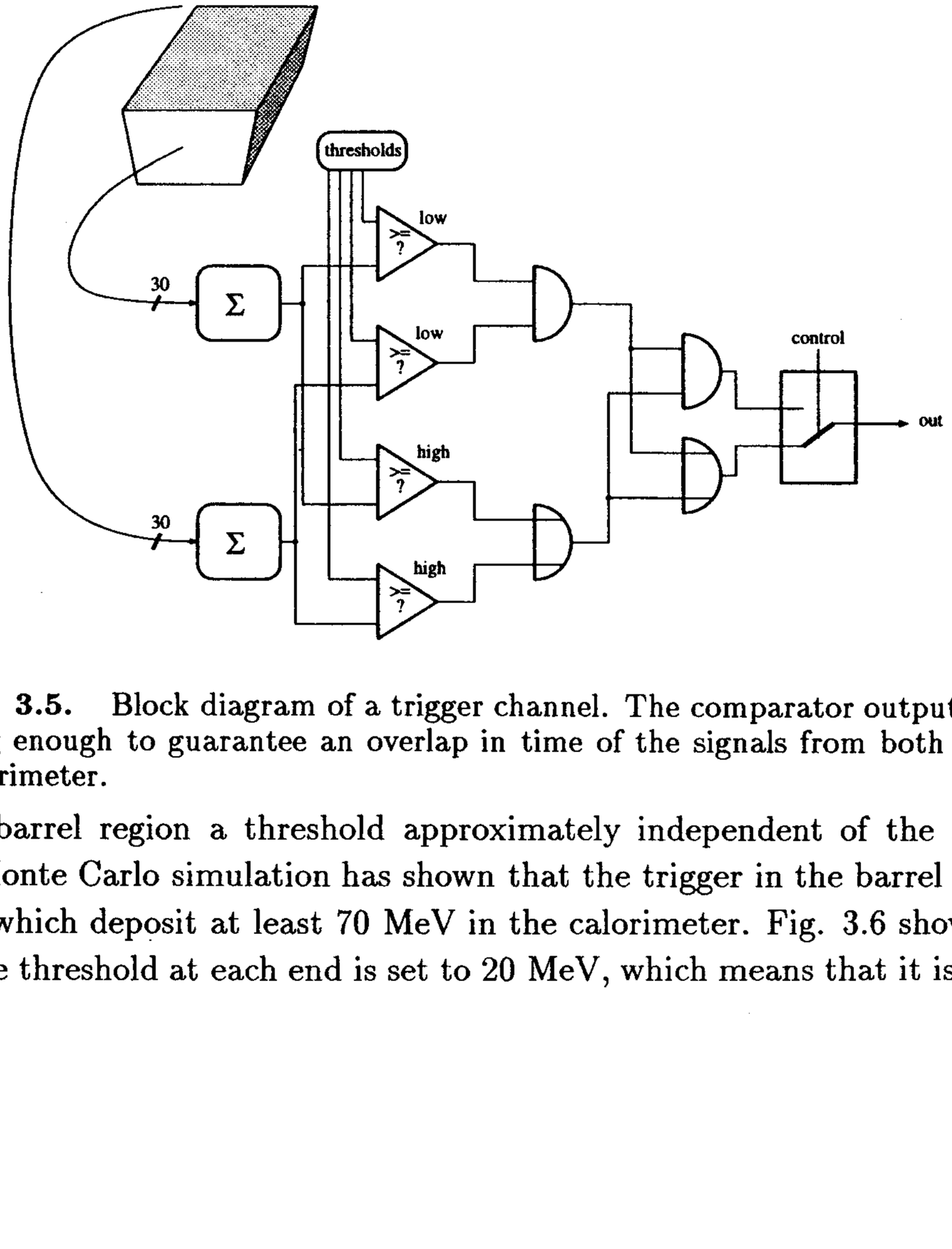

Figure 3.5. Block diagram of a trigger channel. The comparator output signals are long enough to guarantee an overlap in time of the signals from both sides of the calorimeter.

For the barrel region a threshold approximately independent of the z position is aimed for. Monte Carlo simulation has shown that the trigger in the barrel should select all particles which deposit at least 70 MeV in the calorimeter. Fig. 3.6 shows a possible solution. One threshold at each end is set to 20 MeV, which means that it is exceeded by

the signal of an electromagnetic showering particle of ~20 MeV entering the calorimeter near the corresponding photomultiplier. The logical "AND" of the two comparators is formed. The other two thresholds are set to ~37 MeV and combined as an "OR". If at least one of the two gates is active, the trigger is activated. (This means that the "OR" of the two digital signals is chosen in fig. 3.5.) The effective trigger threshold is shown in fig. 3.6 as a function of the z position of incident particle. The fractional *rms* variation of the threshold is less than half of the energy resolution of the calorimeter for particles in this low energy range ($\sim 5\%/\sqrt{E\ (\mathrm{GeV})}$=22% for particles of 50 MeV).

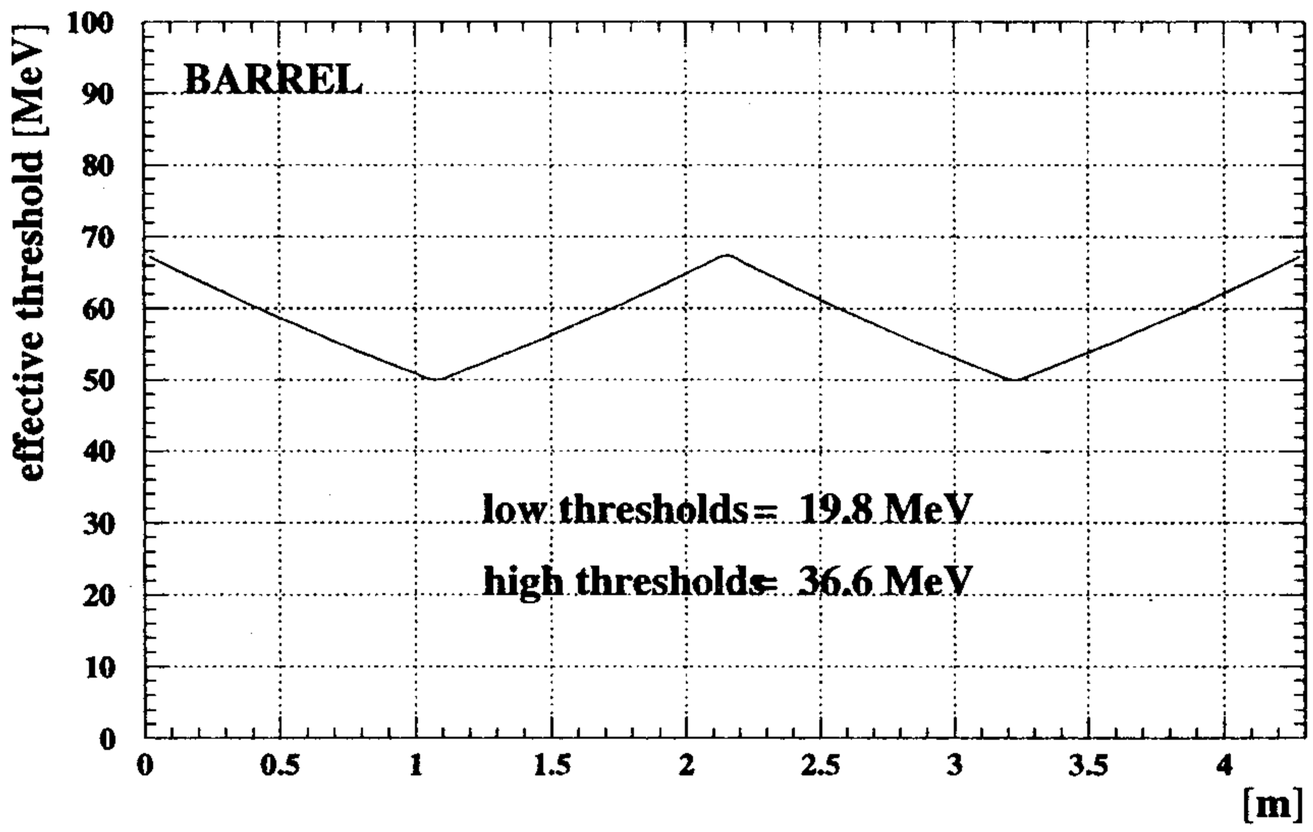

Figure 3.6. The effective trigger threshold as a function of z of the incident particle. Thresholds are adjusted to result in a minimal variation of the effective threshold along the z - direction. An average attenuation length of 3.5 m is assumed.

In the endcap region the background is concentrated around the beam pipe. With the proposed scheme thresholds can be adjusted such that in the zone around the beampipe the effective threshold for particles is higher than elsewhere. Fig. 3.7 shows a possible solution used in the Monte Carlo simulation. In the outer regions of the endcap the thresholds at both ends of the readout elements are adjusted symmetrically and in a way such that the variation of the effective trigger threshold is minimal. Particles with less than 50 MeV would not produce a trigger signal. The first two plots show the effective threshold for two readout elements with different lengths. The variation of the effective threshold is smaller for the short readout elements because of the limited effect of the light attenuation in shorter fibres. In the center of the endcap the thresholds are adjusted such that they are effectively higher close to the hole for the beam pipe. This is shown in the third and fourth plot. The "warm zone" comprises 80 readout elements per endcap on the right and the left of the beam pipe hole. For the elements above and below the hole ("hot zone") the thresholds are chosen asymmetrically in order to result in a higher effective threshold close to the beam pipe.

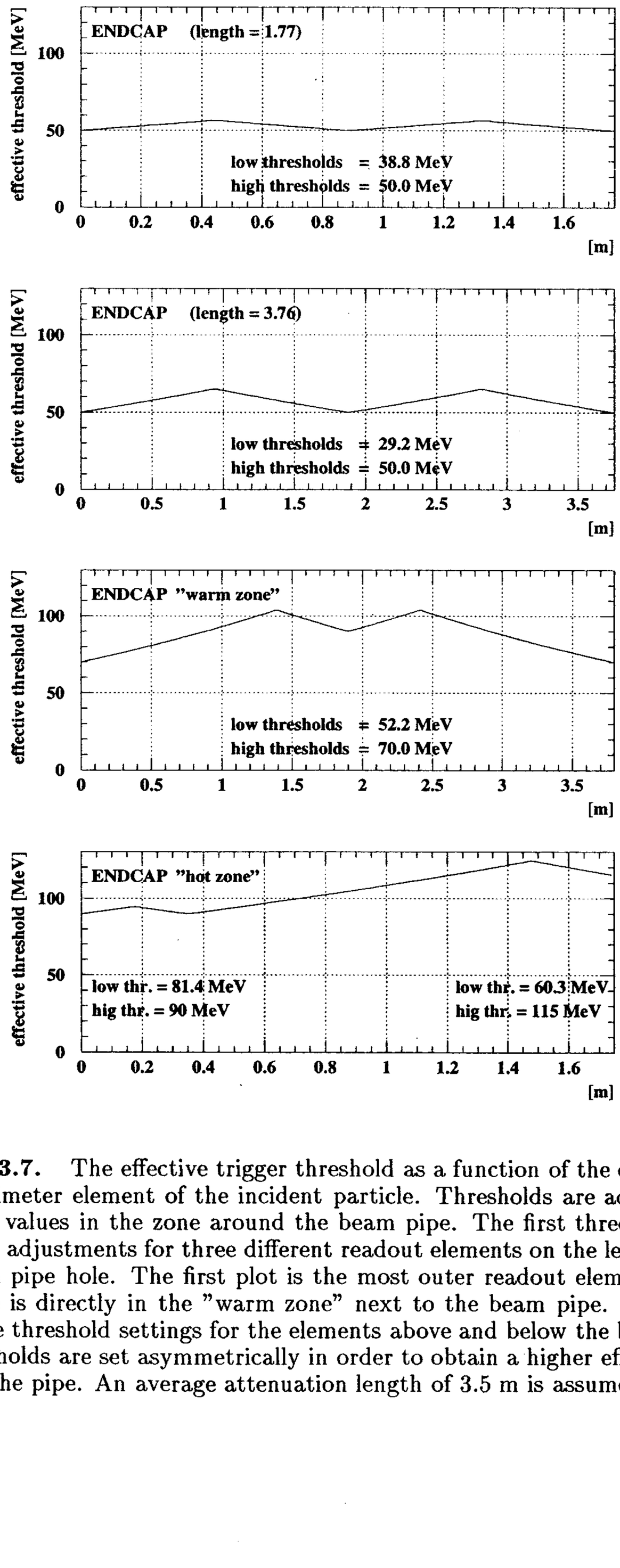

Figure 3.7. The effective trigger threshold as a function of the coordinate along the calorimeter element of the incident particle. Thresholds are adjusted to result in higher values in the zone around the beam pipe. The first three plots show the threshold adjustments for three different readout elements on the left or the right of the beam pipe hole. The first plot is the most outer readout element whereas the third one is directly in the "warm zone" next to the beam pipe. The fourth plot shows the threshold settings for the elements above and below the beam pipe. Here the thresholds are set asymmetrically in order to obtain a higher effective threshold close to the pipe. An average attenuation length of 3.5 m is assumed.

3.2.3 Triggering with the Drift Chamber

Drift chamber (DC) information can be used to produce an efficient trigger for the $\pi^{\pm,\pm}$ and $\pi^{\pm,00}$ channels, for which the calorimeter is less effective. In addition, it adds redundancy and self-checking capability to the whole trigger system also in the ϕ decay channels where the calorimeter is highly efficent. The main requirements for the DC trigger, which is used in combination with the calorimeter trigger, are listed below:

1. High efficiency for $\pi^{\pm,\pm}$ decays for which the calorimeter is relatively inefficient.

2. Provide a reduction of the Bhabha background to a 1–2 kHz level.

3. Be produced within an interval $t_{max} \leq 150$ ns after the ϕ decay time, such as to be usable as start for the calorimeter TDC's.

4. Reduce machine background below 1–2 kHz.

Chamber response

Details on the KLOE DC can be found in reference[3] . The chamber has ~12500 square cells, 2×2 cm^2 for 27 cm $<r<$61 cm and 3×3 cm^2 for 61 cm $<r<$191 cm, where r is the radius of the cylindrical chamber.

The average space-time relation for a 3×3 cell is shown in fig. 3.8. For K_L decays the drift distance distribution for all cells is essentially flat between 0 cm and 1.5 cm because of the high value of the B/p_t ratio in KLOE and the randomness of the decay point. The folding of these features with the cell space-time relations of fig. 3.8 gives the drift time distribution shown in fig. 3.9. Only signals arriving at a time $t < t_{max}$ from the ϕ decay instant can be used to generate a fast trigger. In practice t_{max} is chosen ~150 ns corresponding to ~20% of all chamber hits (see fig. 3.9).

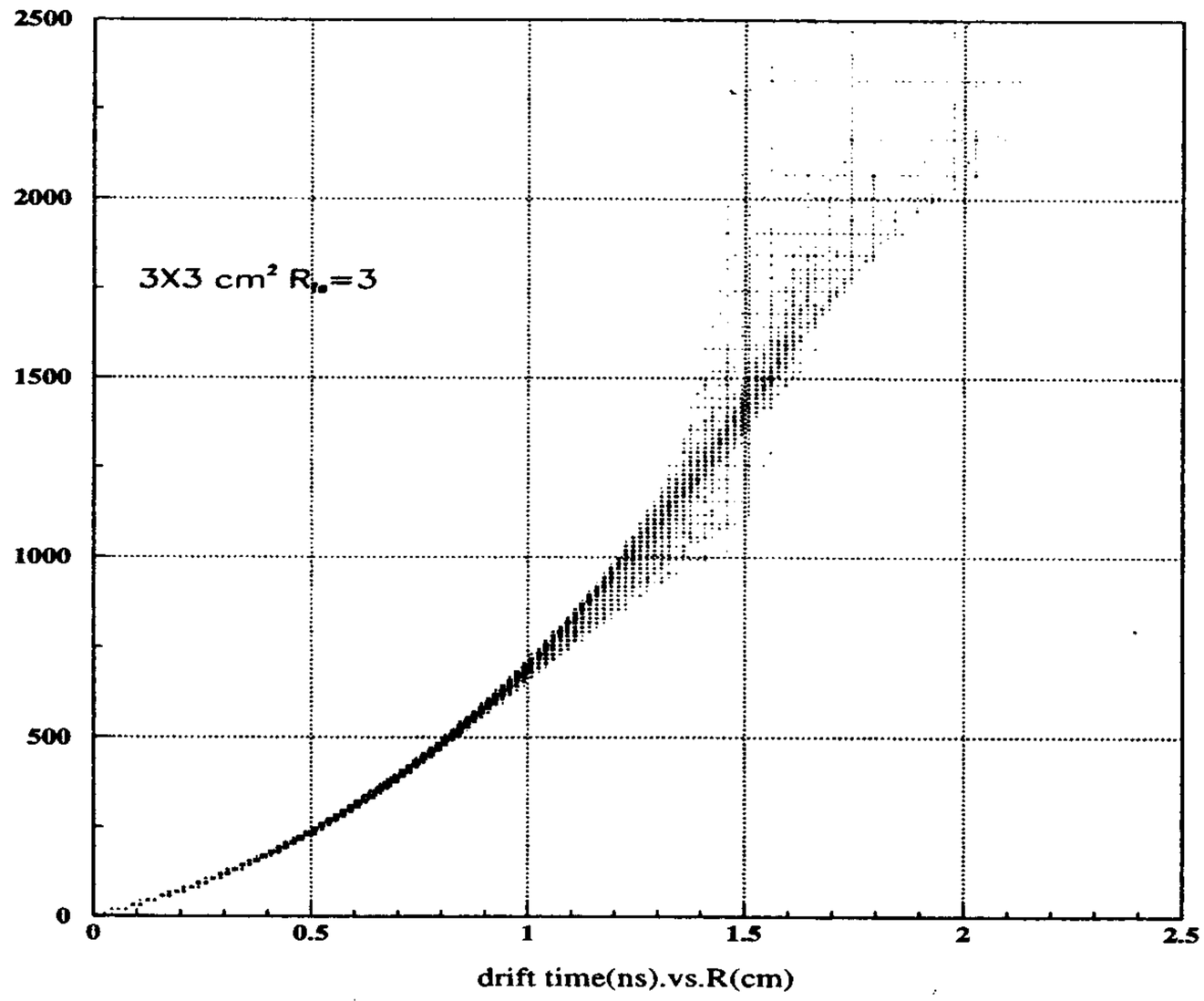

Figure 3.8. Space-time relation for a 3x3 cm^2 cell.

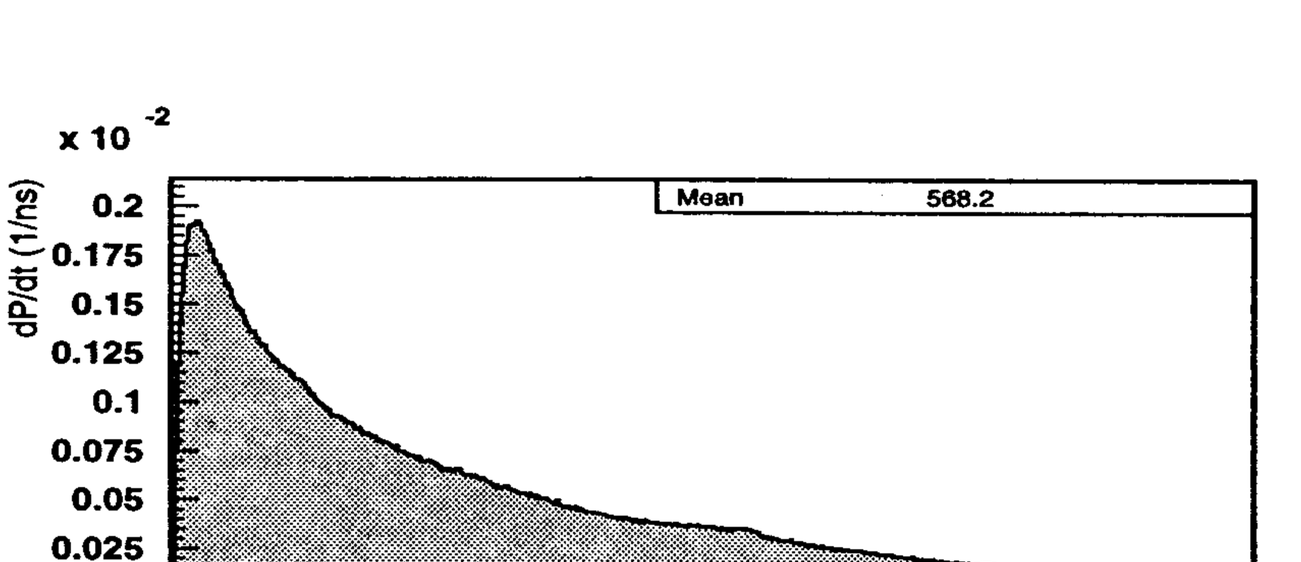

Figure 3.9. Differential and integral time distributions of the DC hits for a 3×3 cell. The time is measured from the bunch crossing and include TOF, drift and propagation along wire.

For $\pi^{\pm,\pm}$ events the mean hit number is ~350 (see fig. 2.3), so that on average ~70 wires are fired within $t_{max} = 150$ ns. Since for background events this number is much lower, good rejection factors can be easily achived.

The DC trigger signal

The high helium content in the drift chamber gas leads to a low primary ionization. As a consequence discrete clusters of charge are formed along the particle's paths which cause trains of pulses at the wires, with an average pulse separation of ~25 ns. After having exceeded an appropriate threshold, the wire signals trigger the formation of a logic signal of 150 ns duration. (This duration implements the length of t_{max}.)

Since many of the pulses in the train will cross the threshold the logic output would be an almost continuous signal lasting on the average ~1.5 μs $- t_{drift}$~1 μs. Coincidences of such long signals have a large time spread and are therefore not usable for triggering purposes. We avoid this by introducing a 2 μs dead time after each signal, which retains the time of arrival information of the first cluster but ignores late arriving hits. A count of how many of the above signals overlap in time gives, to very good accuracy, the total number of cells crossed in the first 150 ns following the interaction time. In the following, the hit count so defined is called N_c.

If the dead time were not imposed, efficiency and Bhabha rejection would be higher since the longer pulse would allow for collection of a bigger sample of chamber signals, resulting in better signal to background discrimination. However, for any given background rejection power, the time of arrival of the corresponding trigger signal is larger without dead time than with it. For example, without the dead time, a simple DC trigger requiring $N_c < 80$ would achieve an efficiency of ~97% for $\pi^{\pm,\pm}$ events with a Bhabha rate of ~2 kHz; however, the average trigger delay from the ϕ decay would be ~280 ns, with comparable r.m.s., a clearly unacceptable result from the FEE's point of view.

The trigger arrival time distribution for $\pi^{\pm,\pm}$ events, after having introduced a dead-time of 2 μs, is shown in fig. 3.10 for different values of the cut on N_c. The corresponding integral time distributions are also shown. Almost all the events the DC can trigger are collected within 150 ns from the ϕ decay time. For instance, choosing a cut at $N_c = 15$, the trigger efficiency for $\pi^{\pm,\pm}$ and $\pi^{\pm,\pi\ell}$ events is ~98% with a mean arrival time for the trigger ~55 ns. On the other hand, the Bhabha rate has increased, with respect to the

previous example, to ∼5.1 kHz.

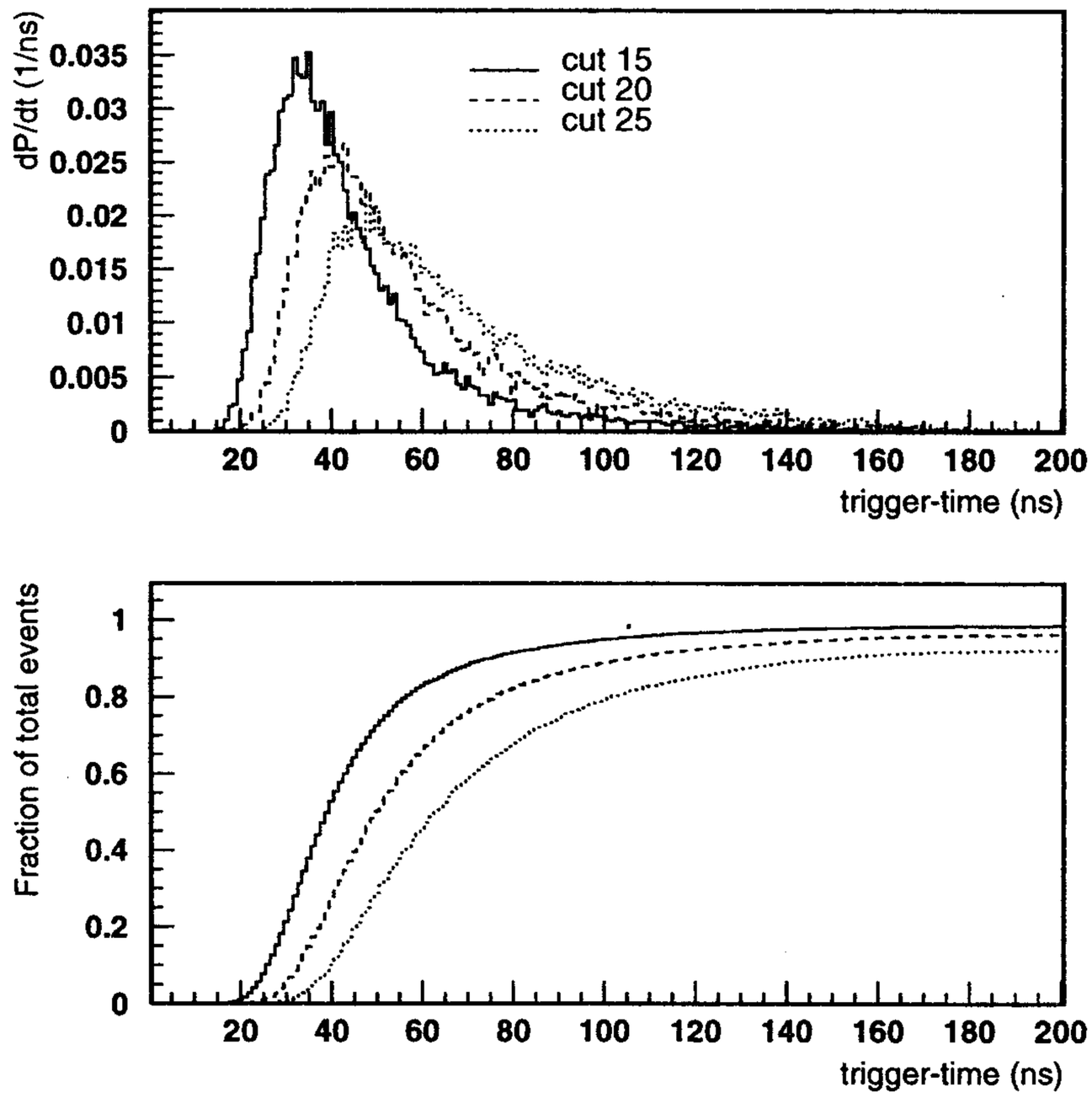

Figure 3.10. Differential and integral arrival time distribution of the first level DC trigger for $\pi^{\pm,\pm}$ events.

The superlayer structure

Bhabha events in which one or both of the outgoing particles interact on the quadrupoles, can be discriminated against ϕ decays by using their peculiar hit topology. In fact, due to the magnetic field, the low energy charged particles created in the interaction with the quadrupoles are confined in the inner region of the detector on their way through the chamber. Conversely, due to the long radius of curvature (∼1 m) of the K^0 decay products and to the long K_L decay path, the hits in the ϕ decays are spread out all over the DC. The occupancy of the chamber planes vs the plane radius* , shown in fig. 3.11, reflects this different signal/background topology. We therefore do not use the four innermost planes in the hit count, improving the background rejection with a negligible loss of efficiency for ϕ decays.

⋆ A plane is defined as a group of wires with the same radial distance to the beam pipe. The planes are ordered with growing radius.

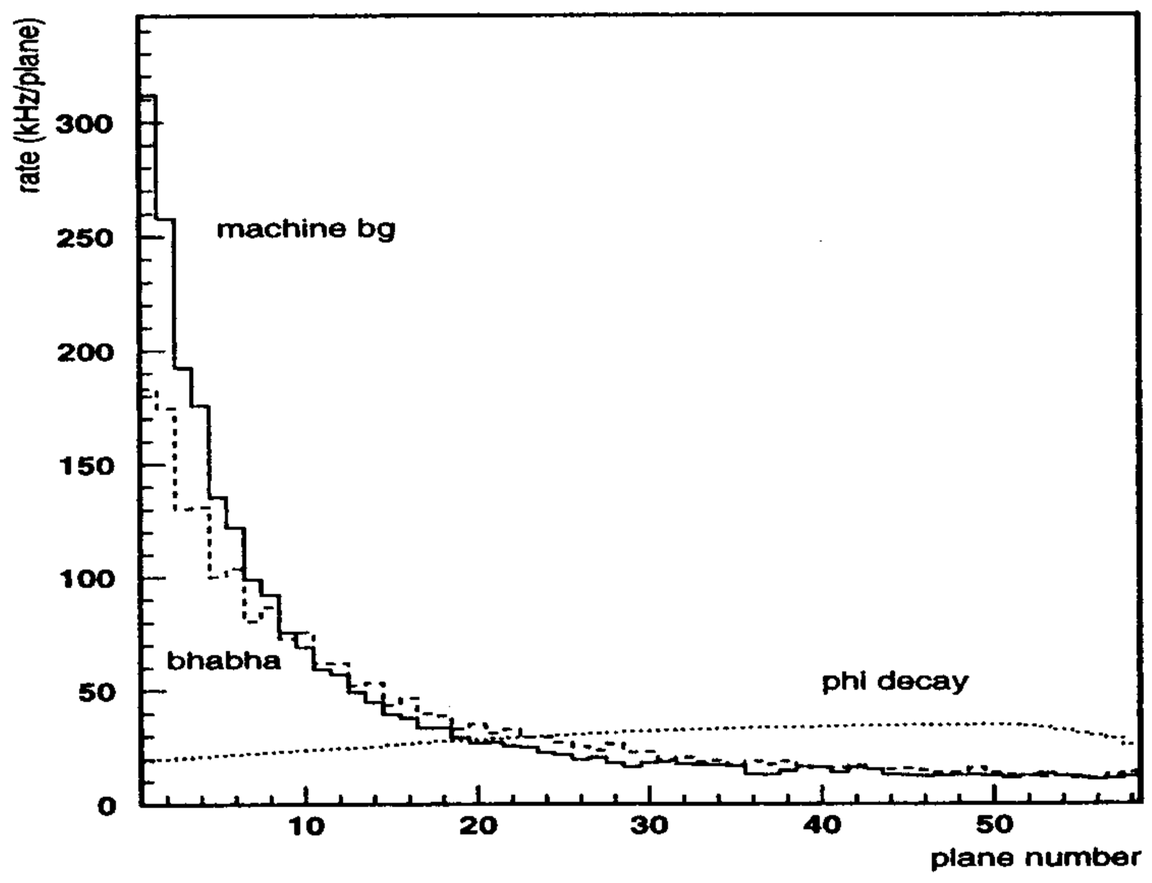

Figure 3.11. Plane distribution of the D.C. hits

A major source of low energy electrons is the conversion of photons on the EMC or DC walls. Both these electrons and those escaping from the quadrupoles have, on average, a transverse momentum <10 MeV/c (see fig. 3.12) and therefore spiralize in the chamber with short radius of curvature(r_c <10 cm).

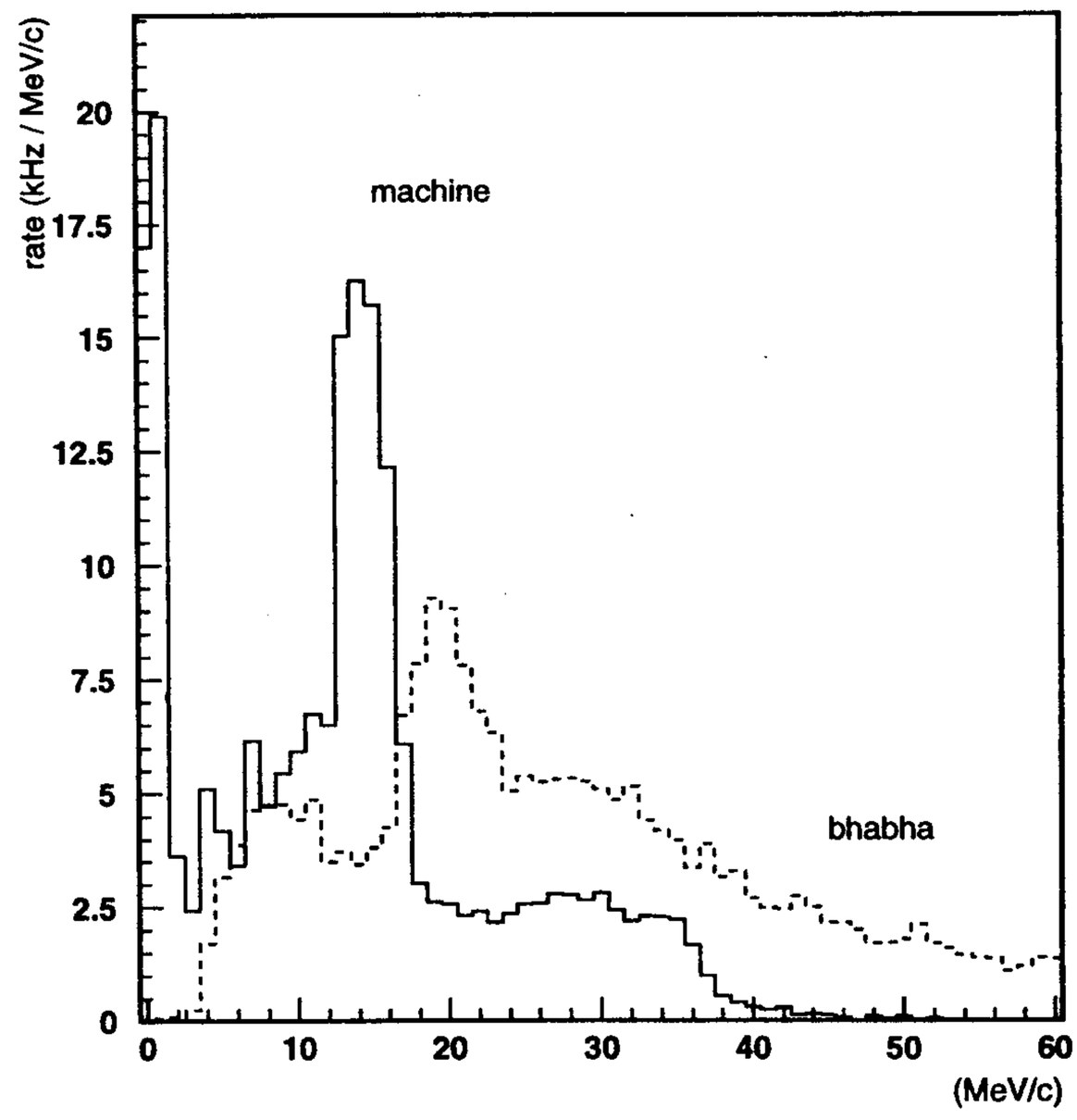

Figure 3.12. Transverse momentum distribution of charged particle in bacground events

To take advantage of this feature, we group the DC wire planes into concentric ring sections ("superlayers") with almost fixed radial spacing. The innermost of these superlayers is formed by the eight 2 cm thick planes from plane number 5 to plane number 12, corresponding to a total radial depth of 16 cm. Then, seven superlayers follow, each made of six 3 cm planes, with a radial depth of 18 cm. The last four 3 cm planes are grouped in the outermost, 12 cm thick, superlayer.

The sum of DC hits in coincidence is first done at the superlayer level. All the sums are then clipped to a given threshold, and finally they are added to the total number N_c. This procedure automatically limits the contribution to N_c of the low p_t spiralizing particles, as can be seen in fig. 3.13: here the number of hits counted by the most populated superlayer, at the moment in which the condition N_c=15 is satisfied, is shown (clipping is not yet applied). It can be seen that, in most of the background events, only one superlayer contributes to the hits count; conversely, in ϕ decays the hits are distributed in more than one superlayer. Therefore, we choose to clip to 5 hits the outputs of the first eight superlayers and to 2 hits the outputs of the remaining ones. These cuts do not significantly modify the efficiency on ϕ decays but suppress a considerable fraction of the background in the DC.

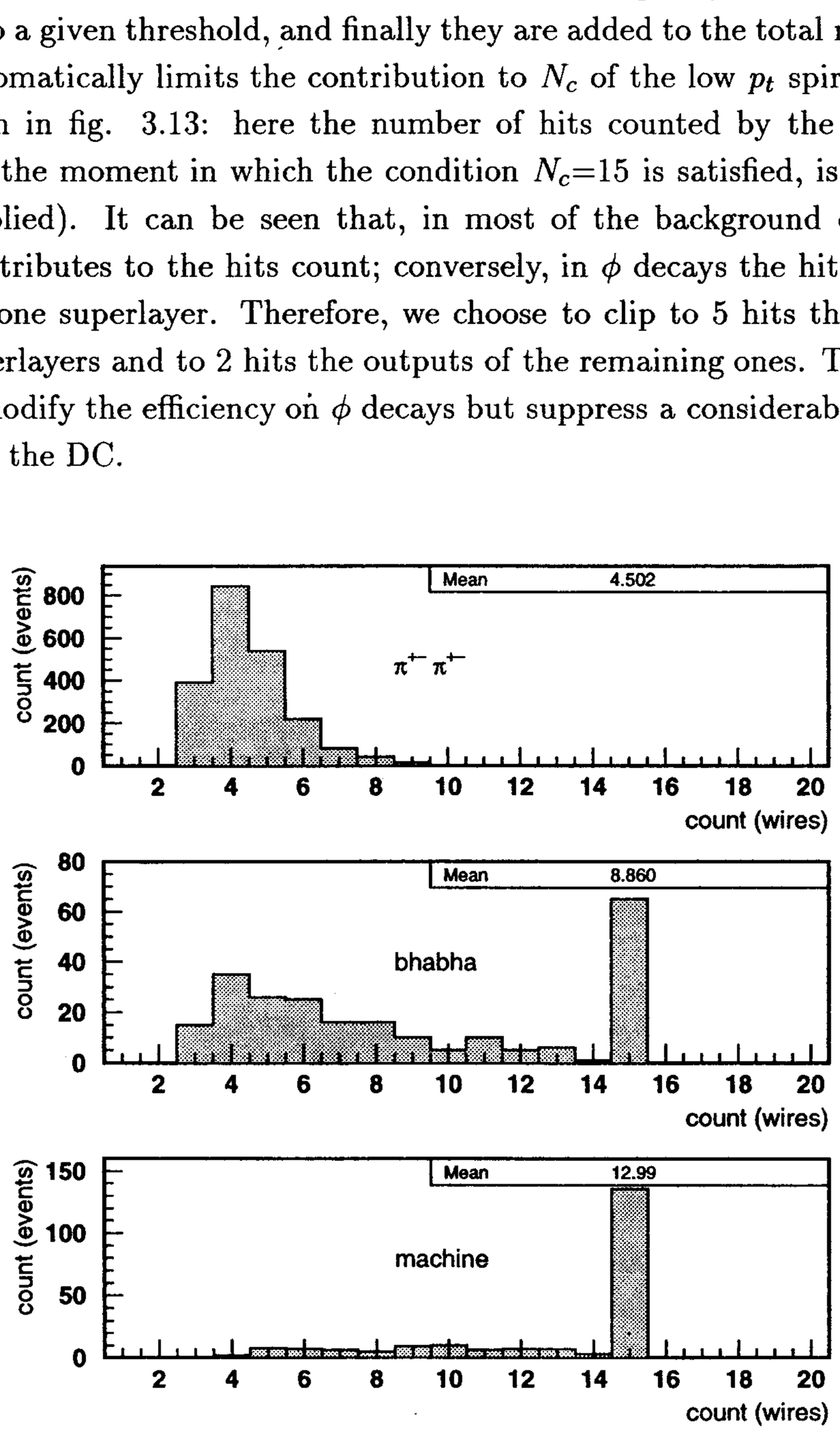

Figure 3.13. Number of hit wires in the most populated superlayer for $\pi^{\pm,\pm}$ and background events

A two level trigger

A single level DC trigger has to find a compromise between a good background rejection and a fast trigger output, while maintaining a high trigger efficiency on the $\pi^{\pm,\pm}$ channel. A two level structure can instead retain both features at the cost of a few per cent extra dead time, because of the higher first level trigger rate allowed. In this scheme, the 2 μs dead time of the wire is retained after the shaping. A low threshold on the hit coincidence, *e.g.* ~15 hits, generates a fast first level trigger used to start the calorimeter ADC's and TDC's. The second level trigger processes all the chamber information available in the following 850 ns, therefore using information of ~70% of the total chamber hits, see fig. 3.9.

The simplest algorithm for the second level decision is to count the number of hits in the DC in the $t_2 = 850$ ns following the first level trigger decision, N_{2l}, and to accept the event if this number exceeds a given threshold. In fig. 3.14 the distribution of this variable is shown for $\pi^{\pm,\pm}$ and Bhabha events: the difference in the mean values is the reason why this algorithm efficiently suppresses the Bhabha events.

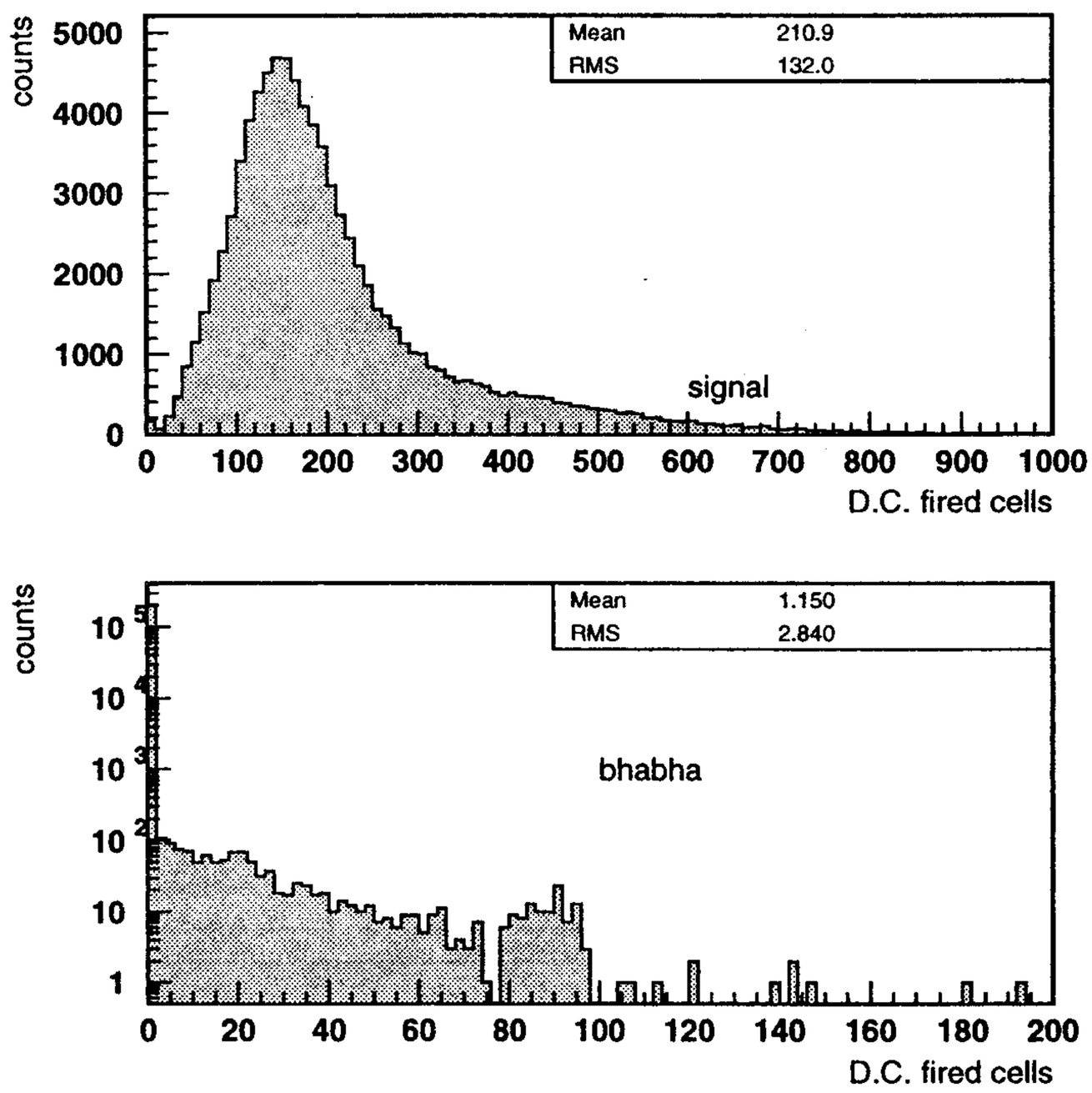

Figure 3.14. Number of DC hits in the 850 ns following the first level decision for $\pi^{\pm,\pm}$ and Bhabha events.

A note on the first level trigger: a low threshold means a higher efficiency and a faster trigger, but also implies a higher background rate. Since to each first level trigger there corresponds a DAQ busy time 2 μs long, there will also be an increased DAQ integrated

dead time.

A comment about noise: due to the narrow time window allowed for the coincidence, ~150 ns, and to the digital nature of the signal processed, very high rates, like *e.g.* 10 MHz, of uncorrelated noise in the chamber can be tolerated for the choice of N_c=15. This remains true also for the second level, because the higher threshold setting balances the larger statistics sampled in 850 ns.

3.2.4 Triggering on Cosmic Ray Events

A simple cosmic rays veto can be implemented using the analog sums of the signals of adjacent P.M.'s in the outmost layer of the calorimeter. The P.M's signals are summed six at a time, defining 48 "sectors". The signals from these sectors are then treated the same way as those used to define the ϕ or Bhabha calorimetric triggers, but with thresholds chosen to be equal to the average energy release in a cell of a minimum ionising particle. Once two of the sectors are above threshold, the cosmic rays veto is implemented.

Monte Carlo studies show that this trigger is sufficient to reject about 70% of the cosmic rays events, with a loss on ϕ decays of few parts in a thousand. It also shows that the inefficiency on muon pairs impinging on the barrel is about 5%.

4. MONTE CARLO TRIGGER SIMULATIONS

4.1 Monte Carlo Simulation

Monte Carlo events have been generated to study all the relevant aspects of the trigger system and to optimize its parameters. For each of the decay channels $\pi^{\pm,\pm}$, $\pi^{\pm,00}$, $\pi^{00,00}$, respectively ~90,000,~90,000 and ~70,000 events were generated. To study the performance of the trigger in suppressing the main background sources of KLOE, in addition 200,000 Bhabha, 5,000 cosmic ray and 250,000 machine background events were generated.

The calorimeter elements response was fully simulated, properly taking into account the experimentally measured light yield, its attenuation along the fibres and its collection efficiency. To simulate the analog sum of the photomultiplier signals their shape was approximated by a rectangle. Results turned out to be almost independent of the choice of the rectangle's width, varied in the range between 2-10 ns. Whenever one of these sums exceeded its threshold, the corresponding logic variable was set. The logic variables were then combined according to the scheme discussed in chapter 3.

The drift chamber response was simulated taking into account the measured space-time relation and the propagation of the signal along the wires. To simulate the first level trigger a 150 ns long signal for each hit wire was produced, followed by a 2 μs dead-time. The hit count was performed according to the superlayer structure described in the previous chapter including clipping of the superlayer yield. In order to model the second level trigger the number of non clipped hits N_{2l} arriving within 850 ns after the first level trigger was counted too.

In the following sections the results for the calorimeter and drift chamber standalone triggers are briefly reviewed. In the last sections the performances of the KLOE combined trigger (EmC+DC) are reported for a "standard" choice of the trigger parameters (EmC tresholds, EmC and DC multiplicity,..). This trigger strategy will guarantee high efficiency for all physical relevant channels and acceptable background rates.

4.2 Results

The EmC trigger performance

The EmC trigger has two parameters to be optimized: the sectors thresholds and the minimum number of fired sectors required to generate the trigger. These two parameters are separately set in the barrel and in the endcaps, as a consequence of the different relative rates of the signal and background events in these two parts of the calorimeter.

In fig. 4.1 the fired sectors multiplicity for $\pi^{\pm,\pm}$, $\pi^{00,00}$ and Bhabha events are shown, with a choice of the effective threshold of 50 MeV for the barrel and 70 MeV for the endcaps; sectors of both the normal and overlap series are added in the plot. The distribution for $\pi^{00,00}$ and Bhabha events are clearly well separated: for instance, a cut at 4 fired sectors, that in the figure corresponds to requiring two independent releases,

suppresses most of the Bhabha background and keeps ~99.9% of the $\pi^{00,00}$ signal (note the different vertical scale for signal and background). It is also interesting to note that, with this choice of trigger parameters, the sector multiplicity is very redundant, allowing careful checks of the sectors efficiency with the data themselves.

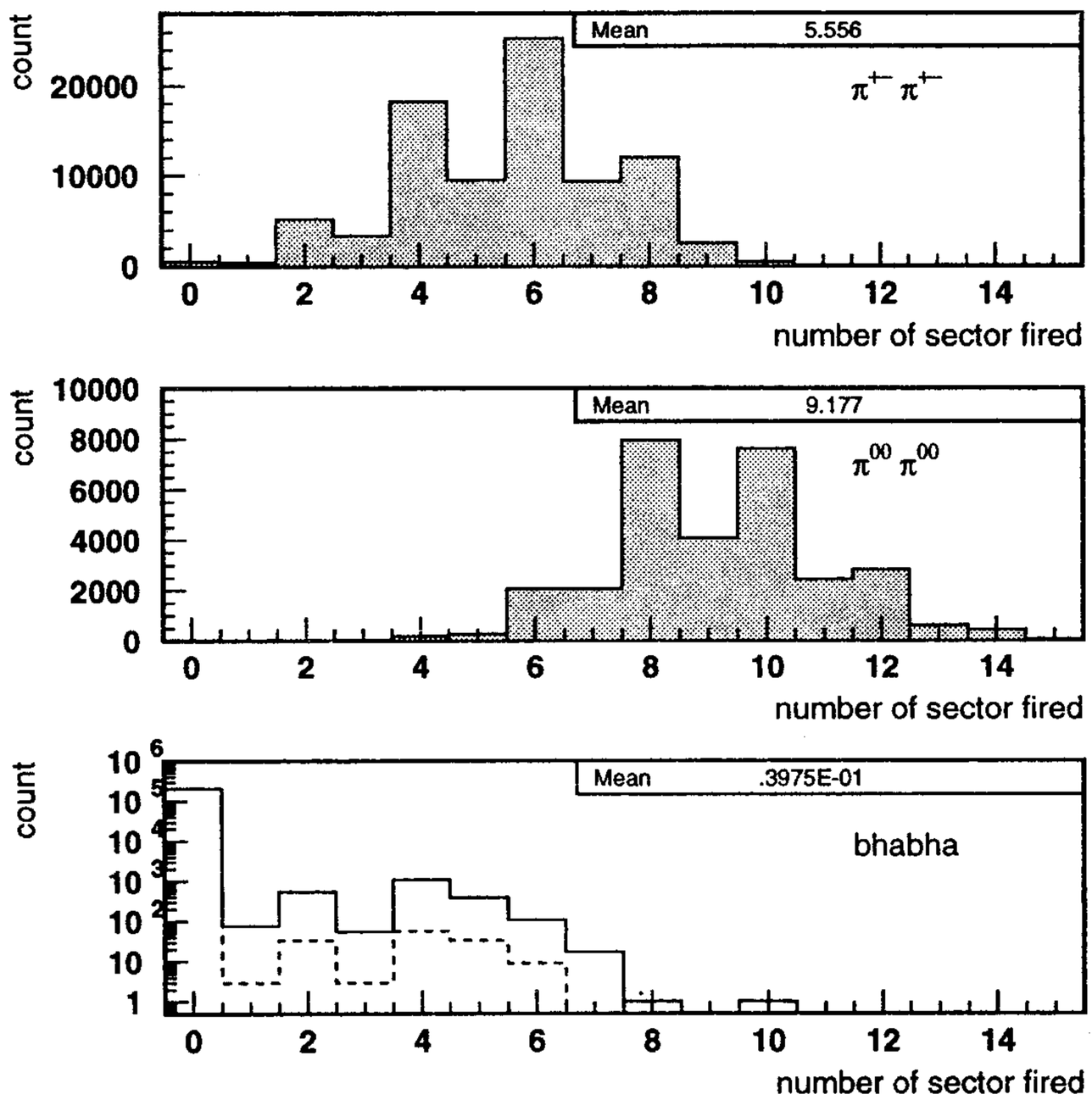

Figure 4.1. Distributions of the number of fired trigger sectors in EmC. The overlap and normal series are added together, which accounts for the structure of the plots.

On the other hand, this same trigger request lowers the efficiency for $\pi^{\pm,\pm}$ to an unacceptable level. In fact, a strategy of selectively raising the endcap threshold, which would exploit the forward peaked angular distribution of the backgrounds, leads to a lower efficiency on $\pi^{\pm,\pm}$ decays because of the effect of the magnetic field that forces the charged pions to spiralize towards the endcaps.

Threshold on (MeV)	Barrel = 20		Barrel = 30		Barrel = 40	
Endcap	eff	rate (kHz)	eff	rate (kHz)	eff	rate(kHz)
30	0.994	10.25	0.991	9.99	0.985	9.82
45	0.990	8.23	0.984	8.06	0.976	7.98
60	0.981	7.14	0.982	6.90	0.960	6.81

Table 4.1 Level 1 EMC trigger performances vs thresholds values in barrel and endcaps

This effect is shown in table 4.1, where the efficiency on $\pi^{\pm,\pm}$ decays and the Bhabha rate are given as a function of three different values of the thresholds in the barrel and the endcaps. The same thresholds scan for $\pi^{00,00}$ and $\pi^{\pm,00}$ events gives efficiency values always above 99.9% and 99.6%, respectively.

The EmC is, therefore, a device perfectly suited for triggering on events containing neutral pions. However, high efficiencies on the $\pi^{\pm,\pm}$ channel can be achieved only at the price of accepting very high background rates.

The DC trigger performance

Efficiencies for $\pi^{\pm,\pm}$ and Bhabha rates for the stand alone DC-trigger are shown in fig. 4.2 as function of N_c, the number of hits within 150 ns. Here the calorimeter is used only to veto on large angle Bhabhas and cosmic rays.

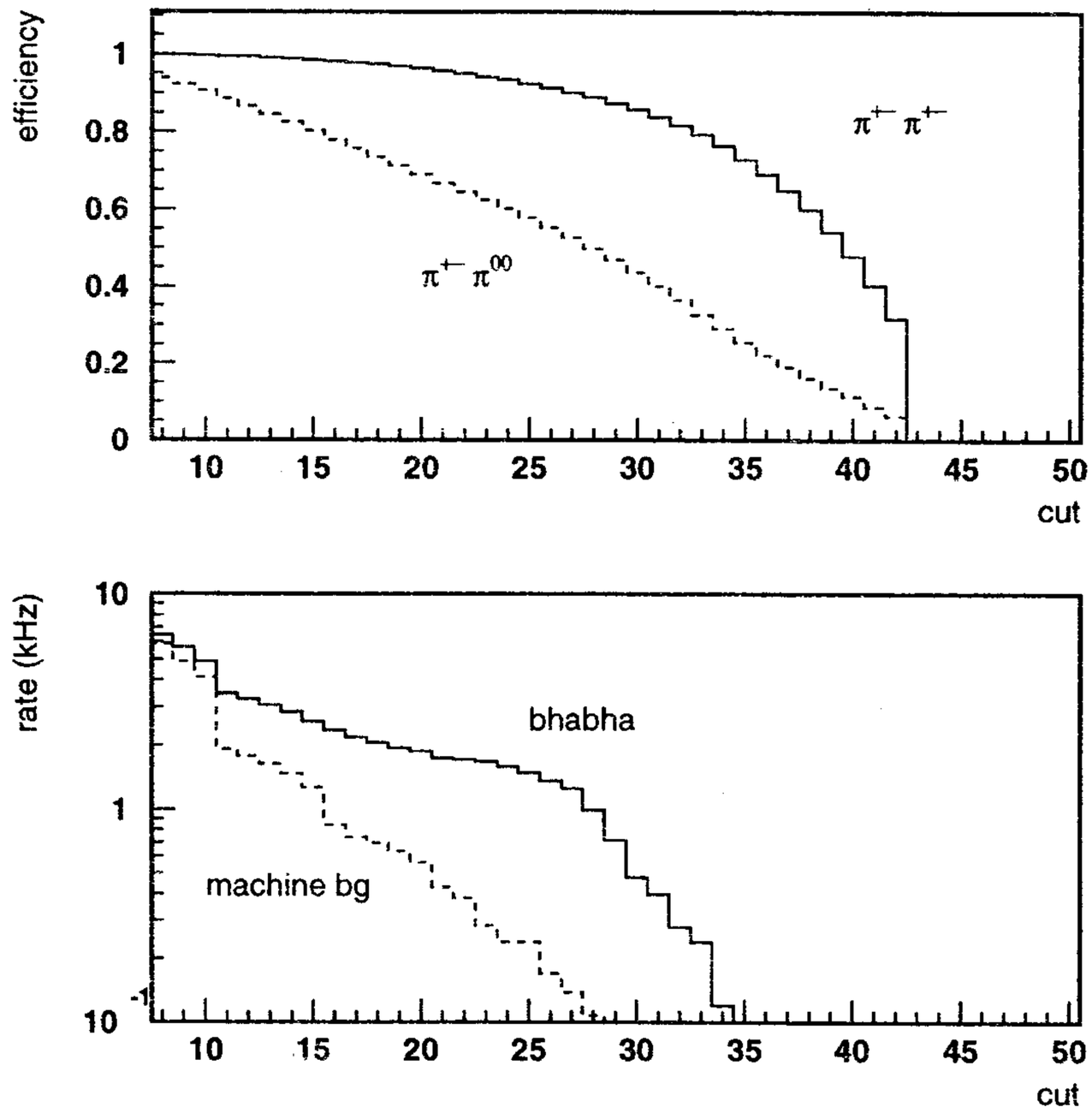

Figure 4.2. Efficiency and background rates as a function of the cut on the parameter N_c.

With the request N_c>15, an efficiency of ~98% for the $\pi^{\pm,\pm}$ channel can be achieved; ~97% of these events are triggered within t_{max} = 150 ns from the bunch crossing (see fig. 4.10). The total background rate is obtained by adding the contribution of the Bhabha events (~2.4 KHz), the machine background (~1.5 KHz), and cosmic rays (~0.6 KHz) survived to the calorimeter veto . These figures include also pile-up effects in the chamber which contribute to about 10% of the rate. (Pile-up does not occur in the EmC trigger because a shortest time window is used to set the coincidence). From fig. 4.2 the effect of the clipping procedure, which cuts the distributions at the value N_c=42, can also be seen.

Fig. 4.3 shows the correlation between efficiency on $\pi^{\pm,\pm}$ decays and Bhabha background rate as a function of the cut on the second level variable N_{2l}. The "standard" cut $N_{2l} \geq 40$ is indicated by the arrow and corresponds to a 98% efficiency on $\pi^{\pm,\pm}$ decays and a 2.6 kHz Bhabha rate.

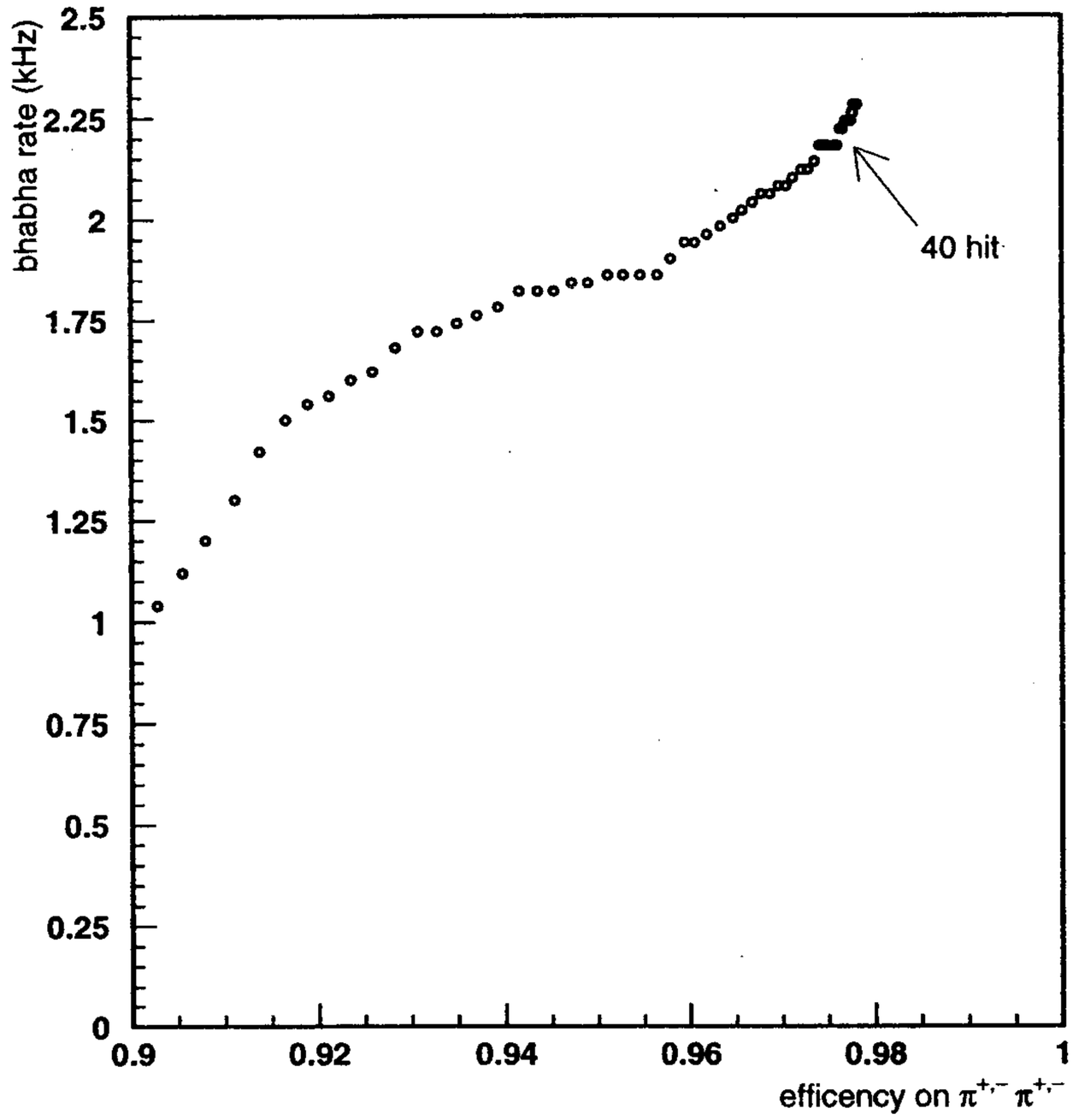

Figure 4.3. Efficiency on the $\pi^{\pm,\pm}$ decays vs background rate for level two DC standalone trigger .

The combined KLOE trigger performance

The combined trigger of the KLOE experiment was generated by requiring for the first level at least two signals above threshold in the calorimeter or at least 15 hits in the previous 150 ns in the drift chamber. Given a valid first level trigger, regardless which device has fired, a second level was generated if at least one of the following three conditions was satisfied: the presence of one sector above threshold in the calorimeter barrel; the presence of three sectors above threshold in one endcap; more than 40 hits collected in the DC in the 850 ns following the level one signal.

The efficiencies for different ϕ decay channels and background rates obtained with this strategy are listed in table 2. The use of the drift chamber increases by $\sim$ 3 % the efficiency on $\pi^{\pm,\pm}$ events, while increasing the Bhabha and machine background rates, at the first level, by $\sim$2.5 kHz and $\sim$1 kHz, respectively. As previously stated, the request of having at least two calorimeter channels above threshold is a moderate requirement on

particle multiplicity and is intended to remove background.

ϕ decays	lev. 1	lev.2
	eff	eff
$\pi^+\pi^-\pi^+\pi^-$	0.997	0.996
$\pi^+\pi^-\pi^0\pi^0$	0.998	0.996
$\pi^0\pi^0\pi^0\pi^0$	0.999	0.999
background	lev. 1	lev.2
	rate (kHz)	rate (kHz)
bhabha	7.22	3.10
machine	1.30	0.98
cosmic rays	1.55	1.55
total backg.	10.07	5.53

Table 4.2 Efficiency on ϕ decay channels and background rates with level one and two trigger.

All estimates assume the accelerator is running at full luminosity (that is $\mathcal{L}$=10^{33} cm^{-2} s^{-1}), and the final trigger rate is equal to the conservative DAQ-limit. The contribution to the total rate of the machine backgrounds, i.e. the more poorly known component, amounts to less than 1 kHz. It has also been verified that, accepting efficiencies down to 99.0%, the trigger rates can be brought well below 10 kHz. Such an efficiency still allows reliable estimates of systematic effects in the trigger to be made.

Since the level 1 trigger provides the start signal to the calorimeter's TDC's, it is particularly interesting to know its time performances for the various ϕ decay channels. The distribution of the level 1 production time, with respect to the ϕ decay time, is shown in fig. 4.4; the formation time of the electronic signal as well as its propagation along the cables between the FEE and the various trigger racks is not included and is not relevant to the present discussion.

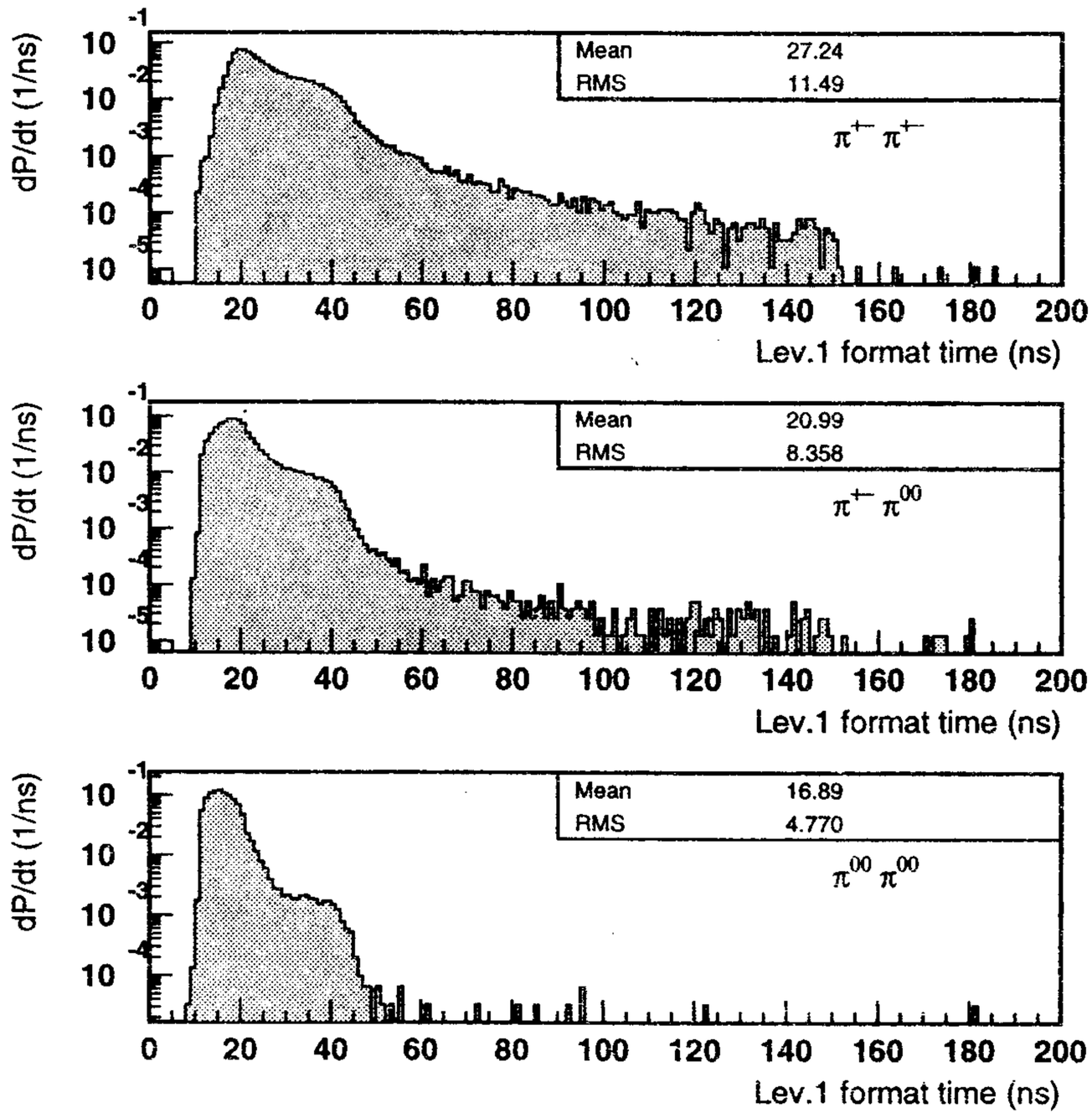

Figure 4.4. Distribution of the level one trigger time formation for ϕ decays.

On average, level 1 is formed after 10-15 ns after the fastest P.M. has produced its signal; in about 2% of the $\pi^{\pm,\pm}$ and $\pi^{\pm,\pi\ell}$ events this happens after more than 40 ns, while in the other cases this fraction is of the order of few per mil (see fig. 4.5).

It is also important to know the distribution of the time difference between the level 1 formation and the last photomultiplier signal in the event, because a too large difference would cause the corresponding TDC to go in overflow, consequently losing its information. This distribution is shown in fig. 4.6. Since the calorimeter's TDCs are designed to go in overflow 220 ns after the level 1 signal[11] , it can be seen that almost all the arrival times of the neutral particles are correctely measured, while for ~6% of the charged particles they are not.

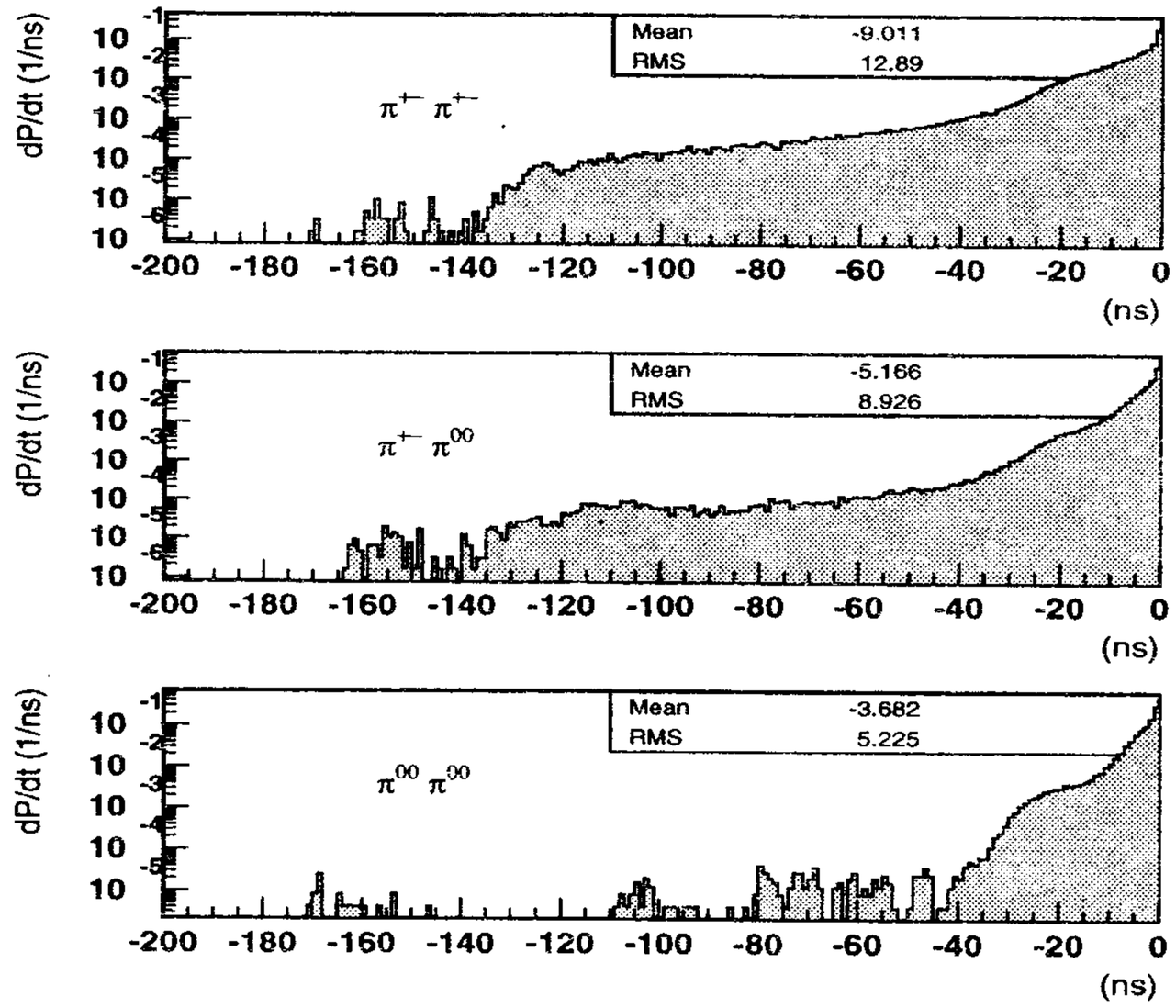

Figure 4.5. Time difference between the trigger formation and the first P.M. signal; only signals above 10 MeV have been considered.

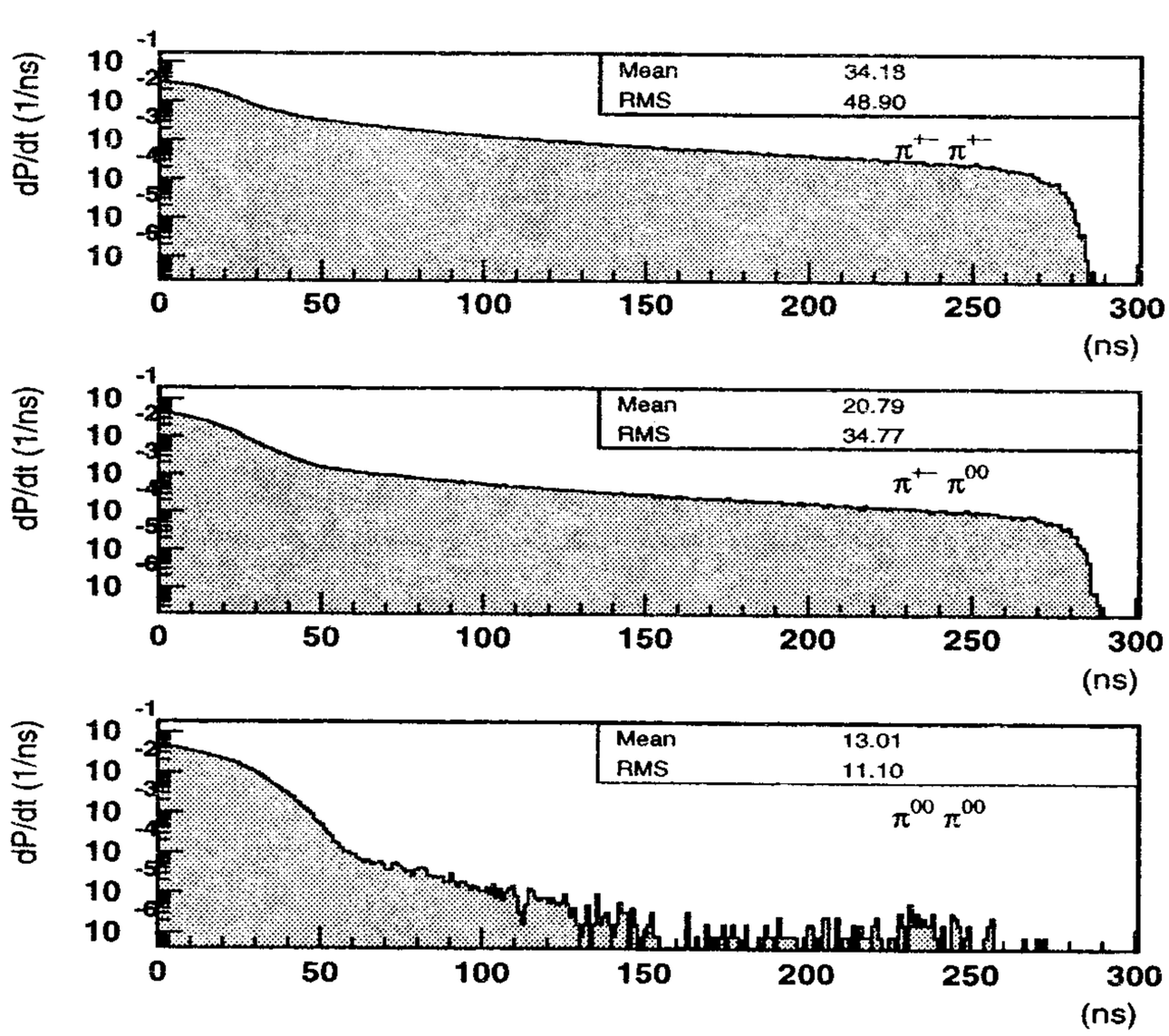

Figure 4.6. Distribution of arrival times at the calorimeter, after the trigger; only signals above 10 MeV have been considered.

Results are stable with respect to the cut values. Moving the calorimeter's thresholds by 10 MeV, *i.e.* ~20%, causes variations of the order of two parts in a thousand in the efficiencies and of the order of 2-3 kHz in the level 1 rate. Also moving the level 2 drift chamber cut from 40 to 50 hits, causes a decrease of the efficiencies of the same order, but helps in rejecting 1 kHz more of machine background.

5. IMPLEMENTATION OF THE TRIGGER HARDWARE

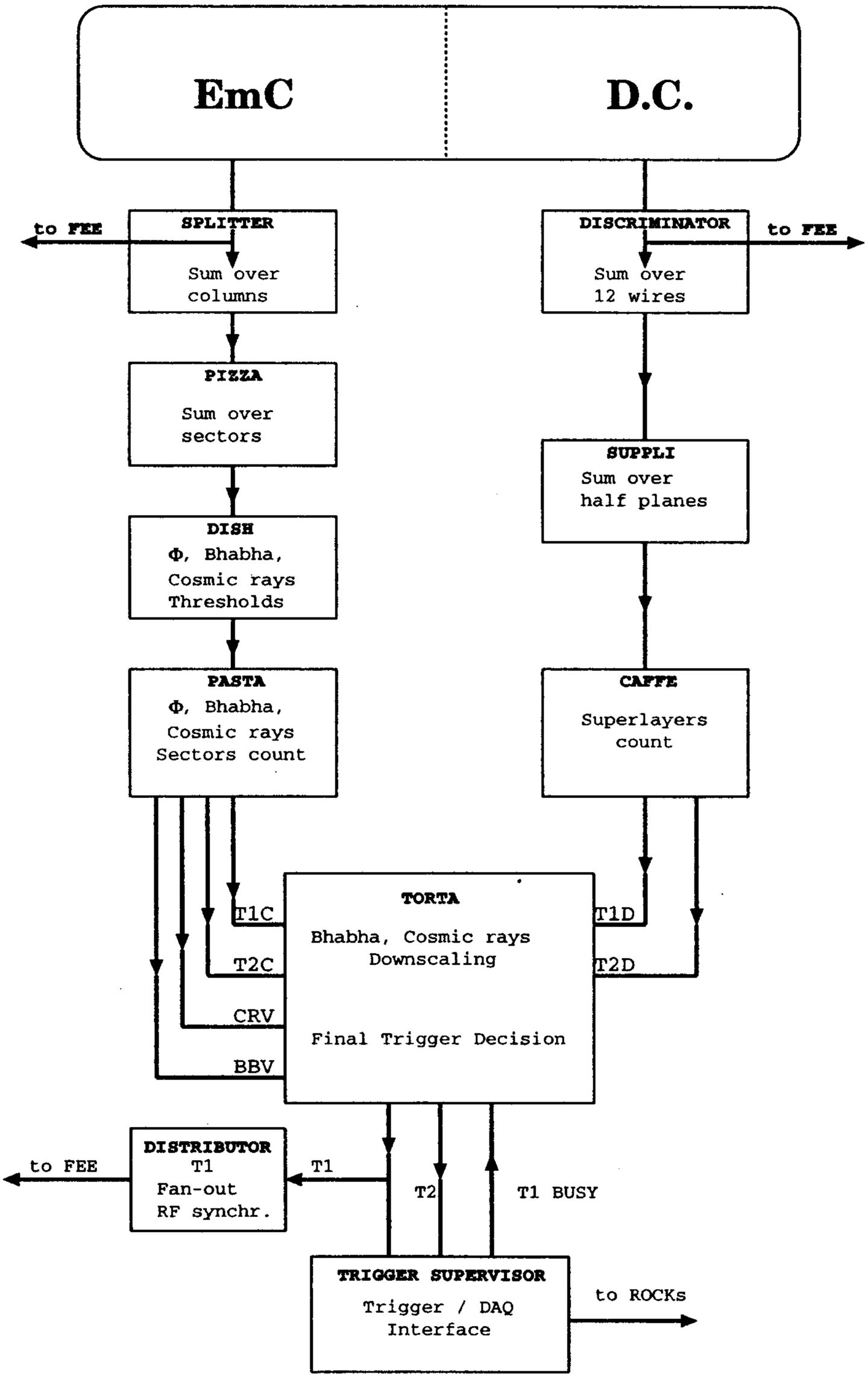

Figure 5.1. Block diagram of the Trigger System Architecture.

The KLOE trigger uses signals from both the electromagnetic calorimeter and the

central drift chamber. A simplified block diagram of the trigger architecture is shown in fig. 5.1. Details are given in the following.

5.1 Trigger Hardware for the EMC

Within 150 ns after an interaction the calorimeter has to provide a set of signals which together with corresponding signals of the drift chamber form the basis for the trigger decision of the experiment. In parallel, monitoring information written to tape with every triggered event has to be generated. These data permit the offline determination of all trigger efficiencies with the required precision and detailed investigation of systematic effects of the trigger system. In addition they help to study systematic effects in the physics analysis. Redundancy in the monitoring data is desired in order to perform consistency checks of the data.

Monitoring data also have to be provided online in order to survey the correct functioning of the system. In case of a possible malfunction the shift crew must be able to localize quickly the non-working module by use of the monitoring data.

The detailed design of the trigger electronics is optimised for maximum reliability and a high degree of flexibility, in order to allow for possible future modifications with minimal effort in cost and time.

To achieve these scopes the following techniques where used throughout the design:

- *ECL-technology* is used for all time critical digital signals in order to minimise propagation delays.
- *Multilayer boards* allow for a controlled impedance environment for interboard connections. Use of stripline techniques for signal paths longer than a few centimeters avoids electrical reflections of the signals on the board and therefore reduces the noise level on the board. This increases the reliability of the system.
- *SMD (Surface Mounted Device)* technology allows for the highest component density, reduces signal path lengths and therefore propagation delay and noise level on the board.
- *Use of Discrete Components* wherever it is adequate, minimises power consumption and thus reduces cooling requirements.
- *Use of Submodules* plugged onto a motherboard allows for easy substitution of non working parts and flexibility for cost insensitive design changes and upgrades. In addition, design, prototyping and production is also made easier and more economical.
- *Use of FPGA (Field Programmable Gate Arrays)* for the interface to the DAQ or VME saves pcb-board area and eases the design of the layout. Debugging and even changes of the interface design are much simpler compared to conventional techniques because they can be realized simply by reprogramming the FPGA device.

The Modules of the Calorimeter Trigger

The signals from the calorimeter's PM's are collected on 164 boards ("*Splitter boards*")

and are divided into three different paths to the ADCs, the TDCs, and the trigger. For the trigger, five adjacent PM signals corresponding to one calorimeter column are summed, for each side of the calorimeter, separately. In addition, groups of 6 adjacent PM signals in the outmost layer of the calorimeter are summed in order to form the fundamental signals for the cosmic trigger (cosmic trigger channel).

The overlapping sums explained in chapter 3 are formed in the so called "*Trigger Pizza*"* by adding the output signals of the Splitter in groups of 4 to 6 columns (calorimeter trigger channel).

These analog signals are compared to eight different thresholds each and processed in a simple logic stage. This task is performed by the "DIgitiser-SHaper (*DISH*)" module. It provides output signals which indicate that a local energy deposit above a certain threshold is in the calorimeter.

To form the final trigger decision in the Trigger Box, the number of hits in the calorimeter is determined in the "Precise Analogue STage (*PASTA*)" by forming current sums.

In the following, the architecture of these modules will be discussed in detail.

5.1.1 The Splitter Boards

Here, only the portion of the Splitter which is relevant to the trigger system is discussed. The preamplified calorimeter signals are received in an emitter follower stage† . The circuit forming the sum over the calorimeter columns or over the six adjacent PM signals for the cosmic trigger is based on the calorimeter-preamplifier circuit. A maximal time walk of 5 ns is expected for signals emerging from the same particle, taking into account the time of flight of the particle or shower in the calorimeter, different path lengths for the signals and various tolerances of electronic components. Therefore, a small integration constant is added to the circuit, calculated to keep the error of the analog sum below 5% for signals arriving in a time window 5 ns wide.

5.1.2 The Trigger Pizza

The trigger Pizzas sum adjacent columns to form analog signals corresponding to the various trigger channels. In total there will be 4 Pizzas, one for each readout side of the barrel and one for each endcap. To form overlapping sums over six columns in the barrel region without having significant signal path length differences the adders have to be organised in a circular geometry. A schematic view of this boards is shown in fig. 5.2; each input signal is fed into two different sum series, shifted by three columns with respect to each other. The same summing circuit as in the Splitter board is used. The barrel Pizza has 288 inputs and 96 outputs.

⋆ Its name is derived from the symmetric circular architecture in the case of the barrel which guarantees perfect symmetry for all signals reguarding signal pathlengths.

† Since the power supply of the Splitter is the same as the one for the preamplifiers there are no problems of differential potentials between the output stage of the preamplifier and the input stage of the Splitter.

The geometry of the endcap readout does not require the circular architecture of the Pizza board (the "rightmost" and the "leftmost" channels do not need to be overlapped). In addition, the overlap of the endcap channels cannot be performed at the right and at the left border of the beampipe hole (see fig. 5.4). In total, the endcap Pizza has 200 inputs and 72 outputs.

The Pizzas are completely passive modules which do not need a computer interface. Therefore they can be placed anywhere around the detector in order to optimise cable lengths.

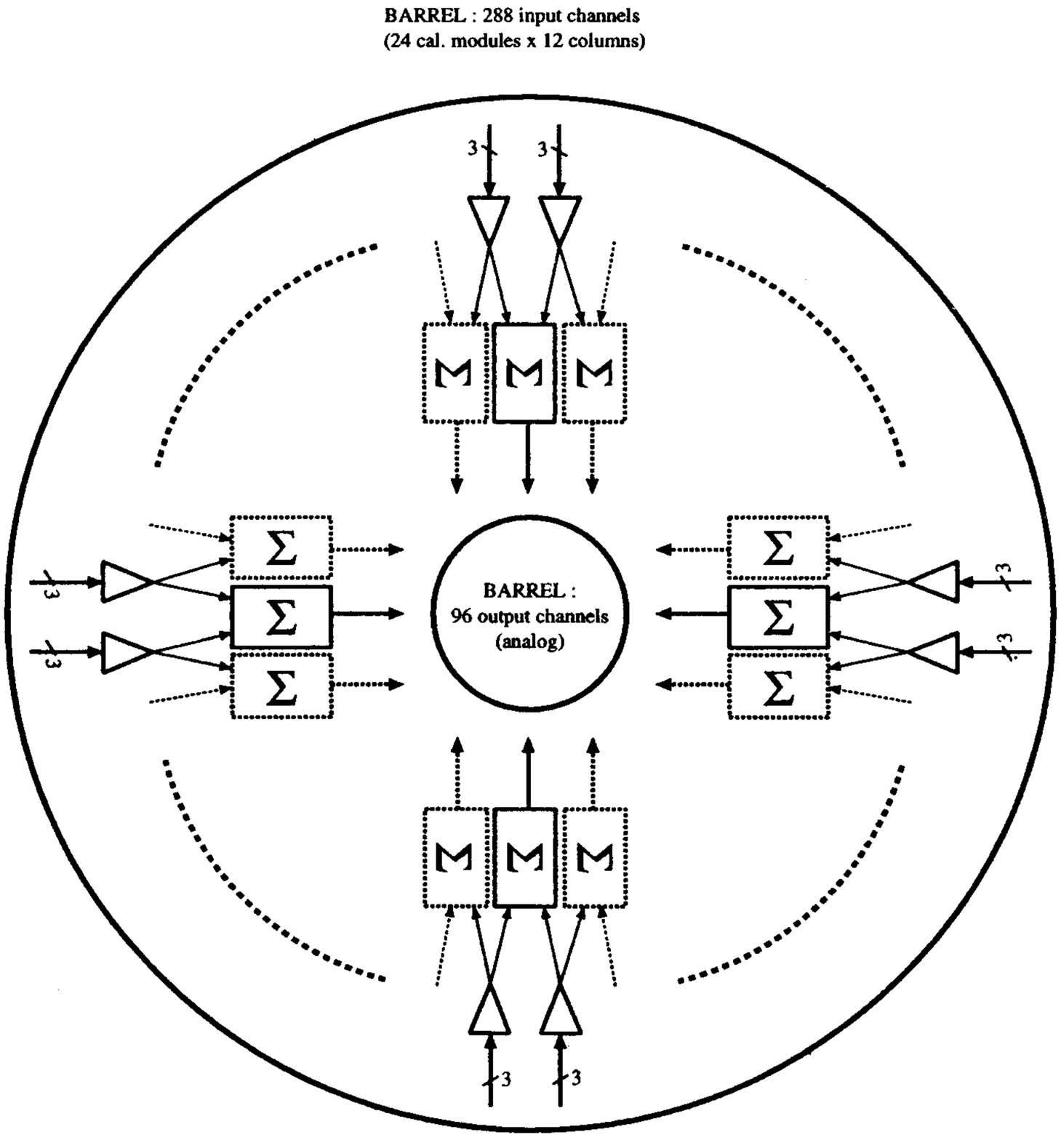

Figure 5.2. Block diagram of the barrel Trigger-Pizza.

5.1.3 The DISH

In the DISH, signals are generated which indicate that an energy deposit above a certain threshold has occurred in a calorimeter region corresponding to a certain trigger channel. For each channel two signals corresponding to the two different energy thresholds

LET and BBT are formed. Every DISH module comprises six trigger channels. In addition to the single channel outputs the module forms analog sums over the LET and the BBT signals for all six channels. Fig. 5.3 shows the block diagram of the DISH.

After reception, the two incoming signals for each trigger channel are compared to eight thresholds. Four of these serve to form the LET, the other four to form the BBT. The output signals of the comparators have to be combined in a simple logic to perform the algorithm discussed in chapter 3. In particular, signals from both sides of the calorimeter have to be combined. Since the light in the barrel region needs 27 ns to travel from one side of the calorimeter to the other, the time walk of the electrical signals at the input is expected to range from 0 to $\approx$ 30 ns (cable length- and component tolerances are included). To achieve a sufficient overlap of the comparator output signals generated by the same particle, the digital shaping time of the One-Shot is adjusted to 35 ns. To prevent a trigger possibly generated by two different particles hitting the same trigger segment one after the other, the signals should not be stretched more than this amount. The One-Shot has to be retriggerable, in order to avoid trigger inefficiencies due to low energy particles which do not generate a LET or BBT signal, but activate some of the comparators. A summing circuit counts the number of LET and BBT triggers on the DISH module so that at its output these sums and the single channel BBT and LET signals are available. The sum is done under the consideration that the signals to be summed, in general, come from different particles of the same event. Monte Carlo studies have shown that signals arrive within a time window of 70 ns. The signals are shaped to this time before being added.

For monitoring purposes, for any triggered event, the status of all comparators and the LET and BBT bits are recorded. This means that the status of these 10 bits has to be memorised until the first level trigger is delivered, within ~200 ns from the arrival of the first particle in the detector. Therefore, the 10 signals are additionally shaped to a length of 200 ns, after being converted to TTL levels. Again, the One-Shot used is retriggerable. On arrival of the second level trigger, the on-board trigger counter will be incremented and the monitoring data is written into a FIFO memory from where it will be read by the DAQ via the AUX-bus[12] .

In order to monitor the analog trigger electronics in the Splitter and the PIZZA, the analog signals in the DISH are sent to a standard ADC. The trigger timing monitoring is performed by sending the outputs of the lowest threshold comparators to a standard TDC. The ADCs and TDCs will be modified to fit the needed dynamic range, at the expense of lowering resolutions.

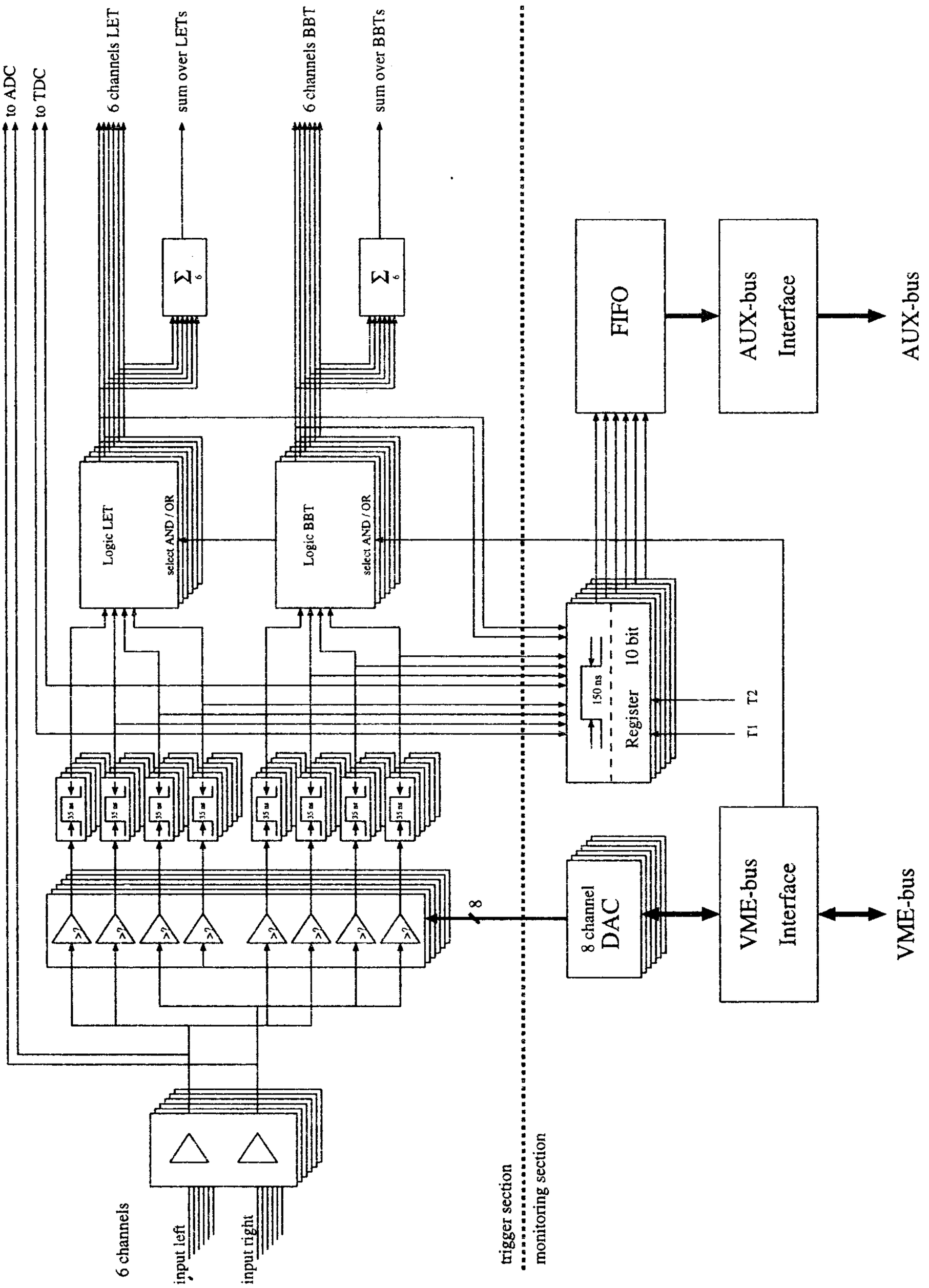

Figure 5.3. Block diagram of the DISH board. Only one trigger channel is shown in detail. In total the module comprises 6 channels.

5.2 Trigger hardware for the drift chamber

For the drift chamber an efficient, low bias, trigger can be easily implemented by just requiring a minimum number of hit wires in a fixed time window. After the amplification stage, the signals are discriminated and shaped at 150 ns. The shaper output is converted to a signal whose current is added to the outputs of all the other comparators. Therefore the resulting current is proportional to the number of hit wires. The sum is performed in several steps:

- the signal corresponding to the multiplicity in 12 contiguous wires in a plane is formed,

- all the signals from each half plane are summed together[⋆] ,

- since noise and accuracy considerations make it unwise to continue the summing process to include all the >12,000 chamber wires, at this step the sum signal is regenerated,

- the two half plane multiplicities are summed together,

- the 9 superlayers signals are formed and clipped to a given threshold to reduce the contribution of low energy electrons spiralizing in the chamber (see chapter 3),

- a global current sum is formed and discriminated to produce the "chamber first level" trigger signal. The same current signal is integrated, to count the multiplicity in a larger time window, to produce the second level trigger.

The Modules of the Drift Chamber Trigger

The trigger electronics for the drift chamber is made of two components:

- *48-channel discriminator cards* that provide the digital signals for the TDCs and the signals for the trigger.
- *"Sum Unit Providing PLane Information (SUPPLI)" boards* where the counting of the hit fired in an half plane is performed.

5.2.1 The discriminator card

Each sense wire signal, after preamplification, is fed into the discriminator cards where signals for the TDCs and the trigger are formed; the signals are shaped at 2 μs to provide the dead time mechanism described in chapter 3. They are then formed to a width of 150 ns, i.e. the coincidence width which optimizes between efficiency and background rejection, and produces a fast trigger signal.

The outputs of the 48 comparators are transformed into 4 current signals, where each corresponds to 12 contiguous wires located on the same chamber plane. Each fired wire produces a 1 mA current, with an accuracy of 1%. Even though the 2 μs dead time reduces noise problems in the hit count, the possibility to veto each single channel is still implemented.

⋆ To reduce the cable length each wire plane is readout by two crates located in the opposite sides of the KLOE detector. For this reason in each drift chamber readout crate only information of one half plane is available.

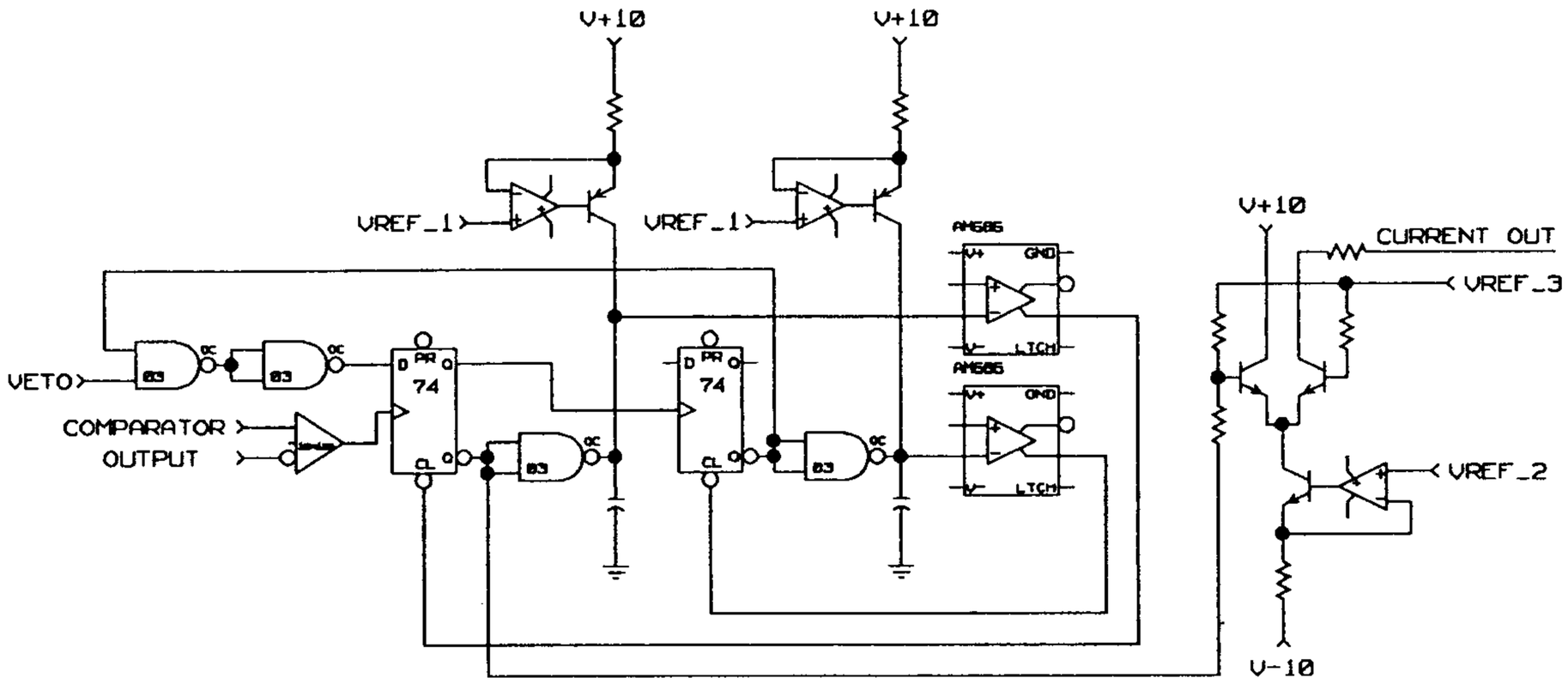

Figure 5.4. Simplified layout of one of the 48 channels of the discriminator card.

5.2.2 The Sum Unit Providing PLane Information (SUPPLI) board

The 4 sum signals from each of the 16 discriminator cards housed in a crate are delivered to a SUPPLI board in the same crate. 12 identical submodules are located in this board; each of them performs the analogue sum of a maximum of 8 current signals, corresponding to to a maximum of 96 contiguous wires.

A signal regeneration algorithm controls the signal to noise ratio for the sum:

- each sum is digitized by means of 8 comparators, with linearly increasing thresholds, to detect from 1 to 8 active wires,

- the outputs of the comparators (see fig. 5.5) are converted into current signals and summed.

As shown by Monte Carlo simulation, this "limitation" alghoritm does not affect the trigger efficiency.

The output signals from the 20 SUPPLI boards are sent to the trigger box where the final multiplicity count is performed.

The 64 analog signals from the first level 12 wires sums are also available on a rear connector of the SUPPLI board for future uses.

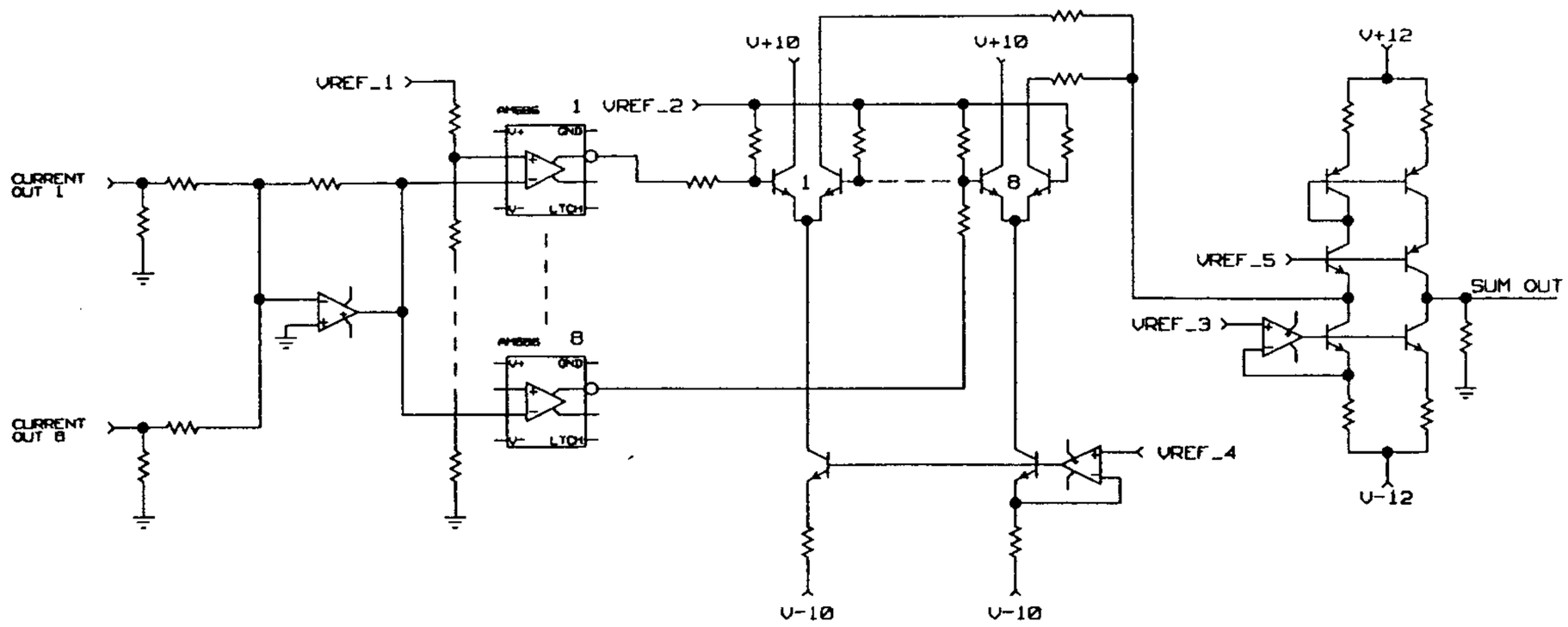

Figure 5.5. Simplified schematics of one of the 12 sum and rediscretization circuits used in the SUPPLI board.

5.3 The Trigger Box

The trigger signals, produced by the boards previously described, are sent to the Trigger Box, a 9U VME crate with AUX-bus backplane, where the generation of the first and second level triggers is performed. The trigger crate sends the level one and level two trigger signals to the Trigger Supervisor crate, which distributes them to the FEE crates and produces a synchronization signal used to desable the trigger crate.

The Modules of the Trigger Box

The different operations of the Trigger Box are performed by dedicated double 9U boards, used because of the high density of connectors:

- the PASTA (Precise Analogue STAge) board collects the signals from the 38 DISHes.

- the CAFFE (Chamber Activity Fast FEtch) board collects the signals from the 20 SUPPLI boards.

- the TORTA (Trigger ORganiser and Timing Analyser) provides the final trigger decision and delivers it to the FEE and DAQ system via the Trigger Supervisor (see next chapter).

5.3.1 The Precise Analogue STAge (PASTA) Board

The function of this board is to measure the energy deposit multiplicity in the calorimeter. The LET and BBT signals provided by the DISHes are separately processed in two identical sections of the PASTA, to produce the calorimeter first level trigger T1C and the Bhabha signal (BBV). The second level trigger T2C uses only the LET signals from the DISHes.

As previously discussed, each DISH provides a current signal that is proportional to the number of active trigger channels in the DISH. The PASTA receives 16 signals from

the barrel, 14 from the endcaps for both LET and BBT thresholds and 8 from the cosmic ray DISHes.

A T1C signal is produced from the coincidence of at least two energy releases above the LET threshold with the condition that they do not come from the same endcap (see fig. 5.6). When at least one barrel element or at least three elements in one endcap are active, the PASTA produces also a level two trigger (T2C) and sends it to the TORTA.

To add flexibility to the trigger system and for test and monitoring purposes, the trigger scheme can be modified by changing the majority and/or the topological requests by means of a VME register.

We recall that the calorimeter elements are organized in two, overlapping, series of 168 trigger channels; therefore the multiplicity measurement is not a trivial task because we must avoid that a single particle would be counted twice. As an example, the PASTA board can count a multiplicity of two in the barrel, if one of two different conditions is satisfied: either there are two deposits in one series, or one channel is active in one series and one in the other, provided that the second channel does not overlap with the first. Moreover, both electronics schematics and layout require particular care, such that a prompt trigger signal is formed with a delay independent of the signal path inside the circuit.

A different section of the PASTA is used to produce a cosmic ray trigger veto (CRV) that makes use of the signals from the calorimeter's outermost layers. The signals from groups of 6 outermost barrel photomultipliers are summed in the splitters and sent to 8 dedicated DISHes, where they are compared to a threshold corresponding to the signal of a minimum ionizing particle. Each DISH then provides an output which is proportional to the number of cosmic channels above threshold it contains. These signals are added in the dedicated section of the PASTA and the CRV is produced whenever this sum exceeds the value corresponding to two fired channels. The possibility to set, via VME, topological requirements on the 2 fired sectors is also foreseen.

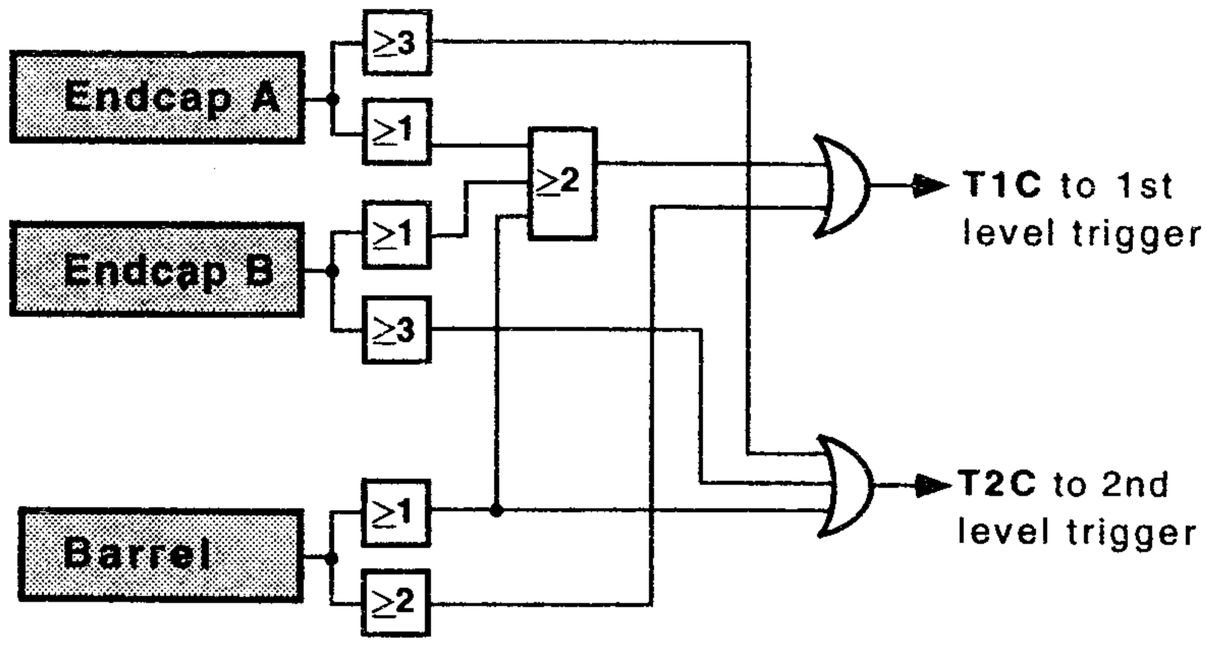

Figure 5.6. Block diagram of the LET section of PASTA where the level one and level two calorimeter trigger signals are formed.

5.3.2 The Chamber Activity Fast FEtch (CAFFE) Board

In this board the first and second level drift chamber triggers are produced using the chamber activity information produced by the SUPPLI boards (see fig. 5.7).

Each of the 20 SUPPLI boards provides the CAFFE with signals proportional to the number of hits in the last 150 ns. In the CAFFE three levels of analogue sums are performed. First, 58 signals corresponding to the chamber planes are produced. They are added again, according to the scheme discussed in chapter 3, to form the 9 superlayer sums. To reduce the contribution of low energy background electrons, the current signals from each superlayer are limited at the value corresponding to a VME programmable number of crossed cells. The current obtained by finally adding the superlayer signals (T0D) is proportional to the number of fired wires in the chamber within 150 ns. A level one drift chamber trigger signal (T1D) is produced whenever this current exceeds the value corresponding to 15 fired wires.

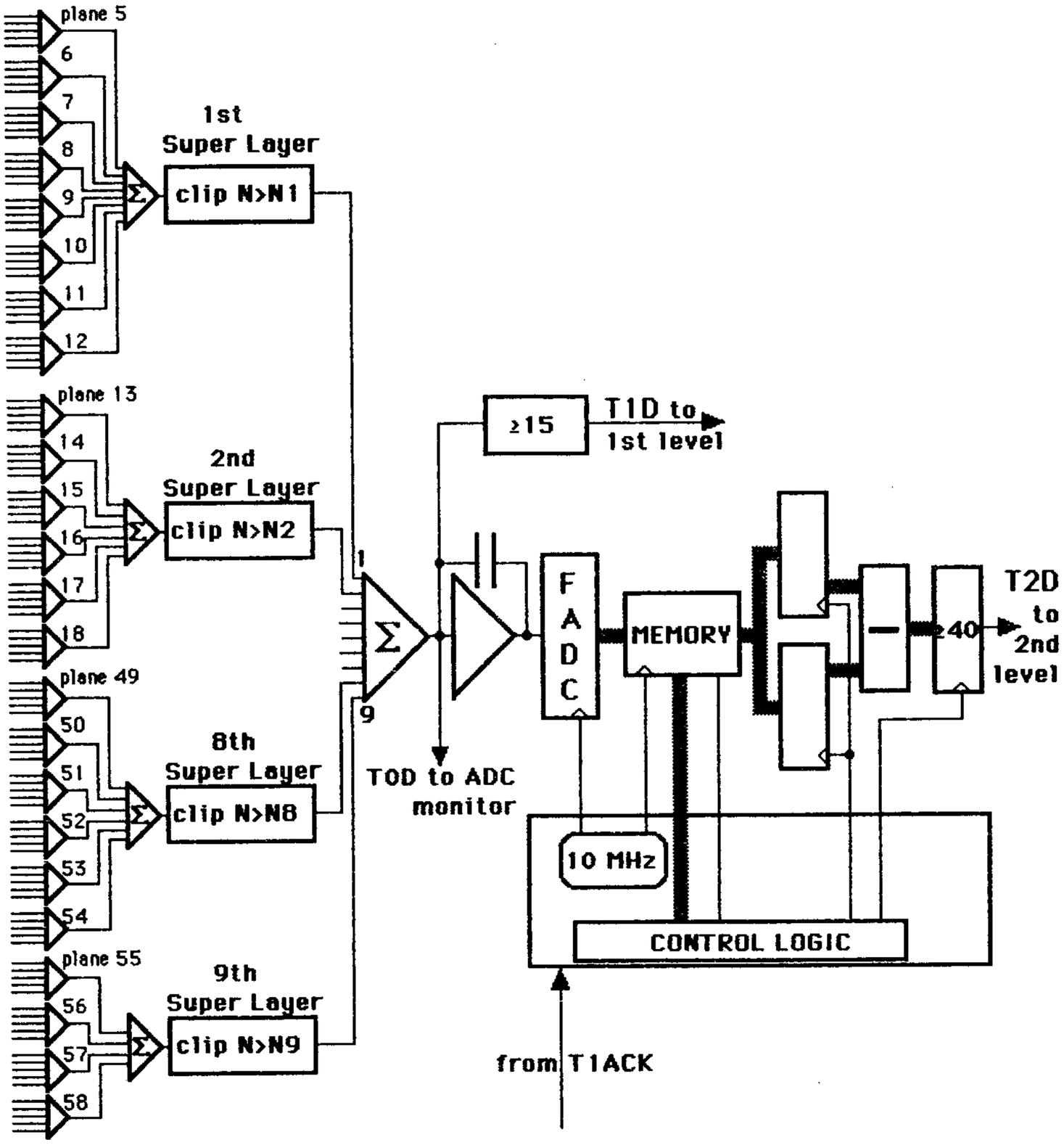

Figure 5.7. Block diagram of the CAFFE where superlayers are formed and level one and two chamber trigger signals are produced. Note that, as mentioned in chapter 4, the four innermost layers are not used.

At second level the T0D signal is integrated with a long decay time constant T_d $\sim$100 μs. The integrator output, which is proportional to the sum of all the chamber hits over a time of order T_d, is converted by a flash ADC every $\sim$0.1 μs and fed into a pipeline 1–2 μs long. Upon receipt of a first level trigger, the number of hits in the chosen time interval is obtained from subtracting the values of two appropriate words in the register, corresponding to the integrated multiplicity just before the first level trigger and after 1μs delay. If the measured multiplicity is higher than the given threshold, the second level trigger (T2D) is generated and fed into the TORTA.

In addition, for monitoring purposes, T0D is also discriminated with a lower threshold and sent to the TORTA where chamber signals before the triggered event are recorded. The amplitude of the 9 superlayer sums are measured using low resolution ADCs, to allow a continuous control of the thresholds and to monitor the activity in different parts of the

chamber.

5.3.3 The Trigger ORganiser and Timing Analyser (TORTA) Board

The final calorimeter (T1C, BBV, CRV, T2C) and chamber (T1D, T2D) trigger signals, produced by the PASTA and CAFFE boards, are transmitted to the TORTA where the final decision is taken. A level one trigger (T1) is obtained if the condition $(T1C+T1D)\cdot\overline{(BBV+CRV)}$ is satisfied. These operations are performed by the TORTA, after having appropriately downscaled the BBV and CRV signals (see fig. 5.8). Once a T1 is produced, the TORTA checks for the presence of T2C or T2D, to produce the level two trigger T2Y. T2Y is defined as $T2Y = T1 \cdot (T2C + T2D)$.

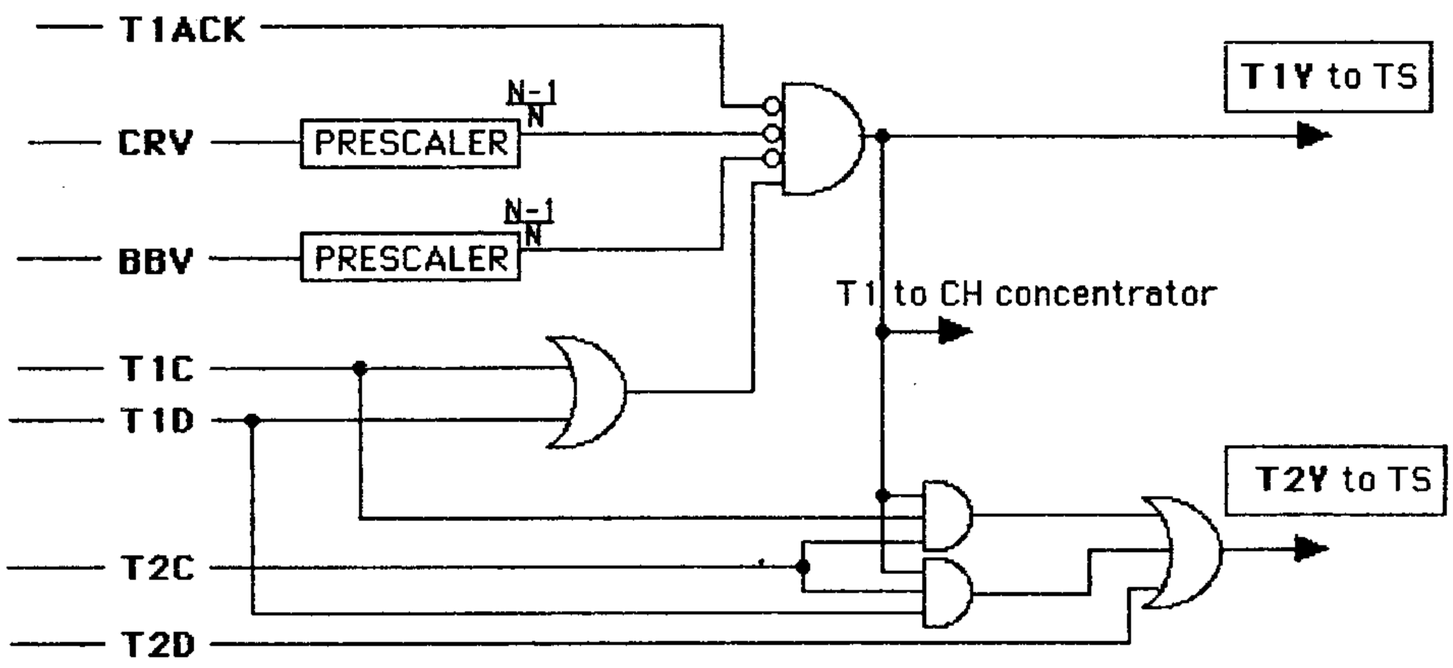

Figure 5.8. When the downscaled BBV and CRV do not veto the calorimeter's or chamber's first level trigger, a T1 signal is sent to the Trigger Supervisor and to the Trigger Distributor. The event readout starts if a second level trigger is produced by at least one of the two detectors.

The TORTA distributes T1 to the Trigger Supervisor and to the FEE boards via the Trigger Distributor module; the Trigger Supervisor sends back the T1ACK signal to disable trigger generation for a fixed amount of time (see next chapter). If, for some reason, a synchronization error is detected by the TORTA (T1 not followed by T1Y, or T2Y not followed by T2) an error signal is asserted by the latter.

T1 and/or T2Y signals can be generated in the TORTA without detector inputs for test or calibration runs. Moreover, in order to check the second level trigger performances, a programmable fraction of T1 signals will force the T2Y generation.

Other monitoring features are also implemented:

- a status pattern of the T1C, T2C, T1D, T2D, BTV and CRV signals for each event,

- counting of the number of the T1C and T1D signals vetoed by BTV or CRV, of the T1 vetoed by the DAQ, of the T1 not followed by a T2Y,

- measurements of the dead time integrated between two acquired events, the time between two consecutive T1, between two consecutive T2 and between the last activity

in the drift chamber and the T1Y.

For monitoring purposes the possibility to separately operate the calorimeter and the drift chamber would be very useful. In such a scheme ("partitioning") the drift chamber signals are rerouted to a dedicated TORTA section where, with the same timing, the final T1 and T2Y signals are formed and sent to a second trigger supervisor for a separate acquisition.

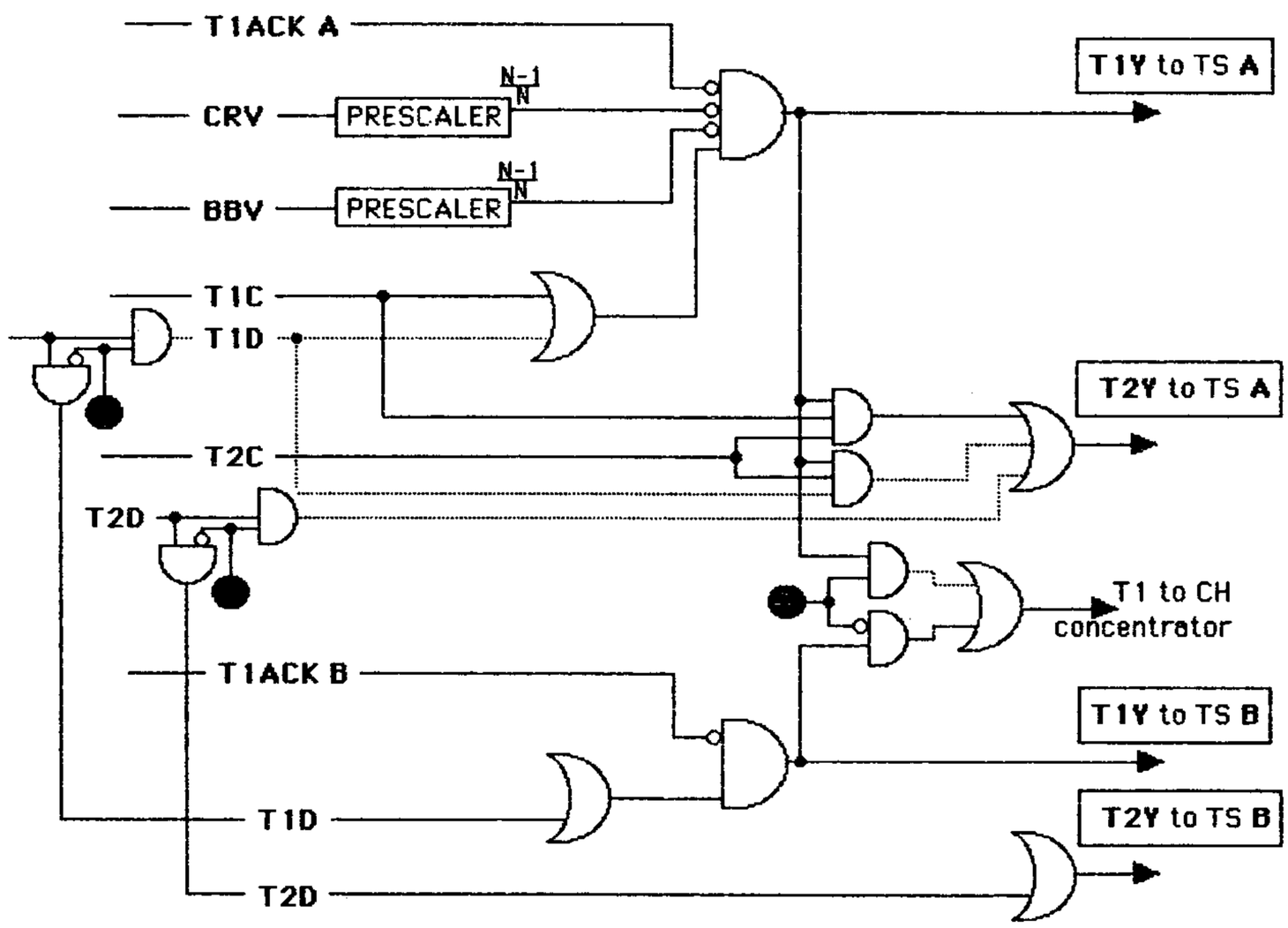

Figure 5.9. The partitioning capability of the trigger system is sketched: the calorimeter and chamber information is independently managed by two identical sections of the TORTA and two trigger supervisors (TS A and TS B).

Timing

Using the measurements of the delays introduced by the various electronics components and the knowledge of the needed cable lengths, the following timing table has been

obtained:

Item	delay(ns)	total delay	Item	delay(ns)	total delay
Drift Chamber Trigger			Calorimeter Trigger		
wire	0-20	20	PM	10-20	20
preamplifier	5	25	preamplifier	2	22
13 m	65	90	13 m	65	87
discriminator	25	115	splitter	4	91
0.5 m	3	118	12.5 m	63	154
SUPPLI	15	133	PIZZA	3	157
14 m	70	203	3 m	15	172
CAFFE	20	223	DISH	20	192
0.5 m	3	226	1 m	5	197
			PASTA	16	213
			0.5 m	3	216
TORTA	12	238	TORTA	12	228
physics	100	338	physics	70	298
0.5 m	3	341	0.5 m	3	301
Trigger Distributor	22	363	Trigger Distributor	22	323
2 m	10	373	2 m	10	333
TM	5	378	TM	5	.338

Table 5.1 Production time of level one trigger signal with respect to the ϕ decay time.

The delay due to physics includes the time of signals formation in the detector and corresponds to the time within which 99.9 % of the triggers are produced. All included, the drift chamber trigger provides its signal within 378 ns and the calorimeter trigger within 338 ns from the bunch crossing. On the other side, since the signals from the splitter (91 ns) arrive to the ADCs after 8 m x 5 ns/m = 40 ns, the ADC must store the analogue information for at least 378 - (91 + 40) = 247 ns, a value compatible with the chosen integration gate of the FEE ADCs. The inputs to the TDC arrive from the splitters (91 ns) after 16.5 m x 5 ns/m = 83 ns, while the start arrives 378 - (91 + 83) = 204 ns later. The One-shot in front of each TDC channel can easily provide this delay, without introducing time jitters at the level of 50 ps.

6. TRIGGER DAQ INTERFACE

In this chapter the DAQ protocols and operations related to the distribution of the level one and level two trigger signals to the FEE crates are described. A complete description of the KLOE DAQ architecture can be found in reference 4.

Both T1 and T2 are needed by the calorimeter's ADCs and TDCs, while only the T2 signal is required for the ROCKs and the TDCs of the Drift Chamber. The very high precision required in the ECAL time measurement can only be achieved if the T1 signal is distributed with a stability of about 50 ps to the calorimeter TDCs; instead, a precision of about 1 ns on the T2 distribution is sufficient. This allows the use of different hardware solutions in the distribution of the two signals, which are described in the following. To exploit the two level trigger strategy, a few modifications of the ROCKs and ADCs design are needed with respect to those shown in[4] .

6.1 The Trigger Supervisor Crate

The interface between the Trigger and DAQ systems is provided by the modules inside the Trigger Supervisor Crate (TSC), a 9U VME crate with AUX-bus, see fig. 6.1. In the TSC are located the Trigger Supervisor, the Trigger Distributor, and as many Fan in-out boards as readout chains. These modules are described in the following.

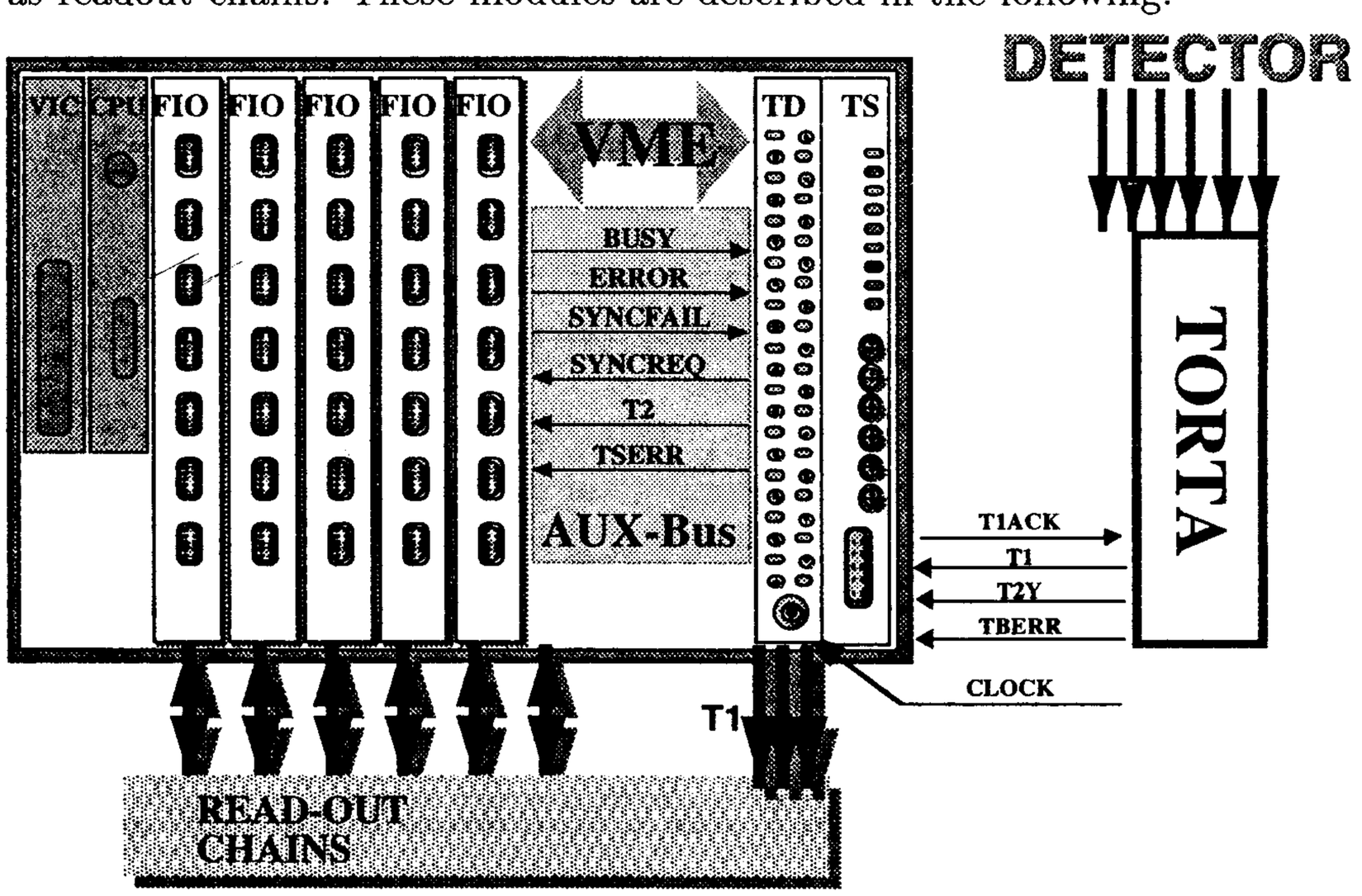

Figure 6.1. Trigger supervisor crate.

6.1.1 The Trigger Supervisor

The Trigger Supervisor (TS) receives T1 from the TORTA and disables it via the T1ACK signal. In the case where a second level trigger T2Y is generated by the TORTA, it also asserts T2 2 μs after T1. The TS must also control the correct synchronization

of event numbering in all the readout chains, as will be explained in more detail later. During the synchronization cycle, or if a BUSY condition is detected in any of the L1 crate, the TS disables the TORTA. The dead time is measured by an internal TDC system which measures also the time needed for the synchronization cycle.

6.1.2 The Trigger Distributor

The time stability of the T1 signal, which is used as a reference for the ECAL TDCs, must be of the order of 50 ps. This means that a synchronization must be performed between the T1 signal and the 78 MHz downscaled RF clock distributed by the accelerator. Therefore the T1 signal, provided by the TORTA, is fed into a Trigger Distributor board where the synchronization is performed. The synchronized signal is then distributed to the FEE modules via Trigger Monitor (TM) boards. These are dedicated boards sitting in each FEE crate, in a position from where it is possible to monitor the activity of the AUX-bus. The same module distributes the T1 signal to the 16 FEE boards on the crate via 2 dedicated differential lines in the backplane, and checks the validity of the data on the AUX-bus, ensuring the good working conditions of the DAQ.

6.1.3 The FIO

The Fan in-out modules (FIO) receive the T2 and SYNCREQ signals from the TS via backplane and distribute them to the corresponding readout chain via NIM, 1 ns precision, signals. Each FIO redirects also to the TS the OR of the BUSY and SYNCFAIL signals of the corresponding ROCK(M)s. Special VME registers will be dedicated to the monitoring of the signals in case of error conditions.

6.2 Operation of the Trigger

6.2.1 Normal Running

Operations during normal running are shown in figure fig: 6.2 and explained below.

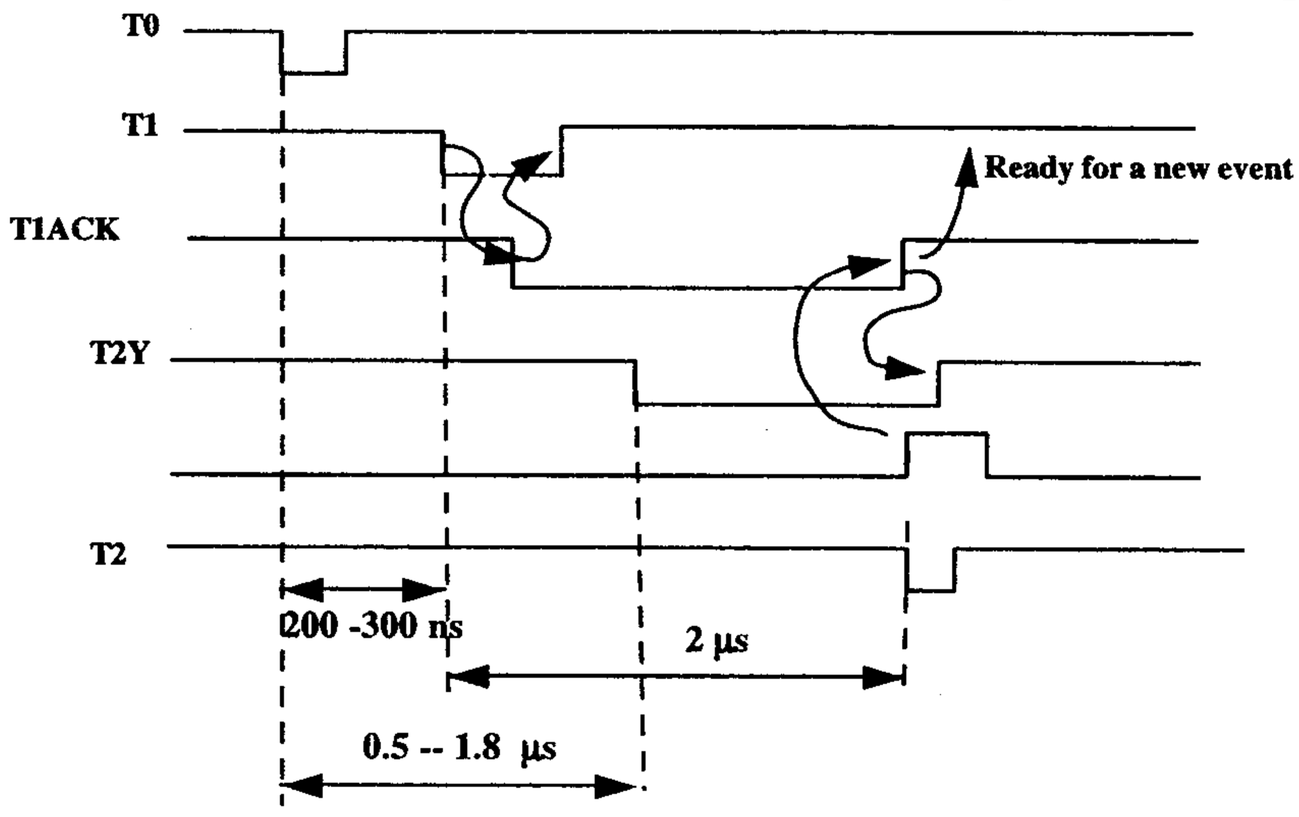

Figure 6.2. Normal cycle.

A T1 is delivered by the TORTA and synchronised by the TD with the accelerator R.F. signal, before being distributed to the readout chains. It is also given to the TS which

asserts the T1ACK. T1ACK is deasserted at the end of a fixed time delay, independently of the T2 generation, and if no BUSY condition is detected by TS. The T1 signal is received by the Trigger Monitors via a dedicated front-panel coaxial connector. The Trigger Monitors assert the T1 signal on the corresponding AUX-bus. A T2Y, generated by the TORTA, is delivered to the TS that generates the T2 signal with a constant delay of 2 μs from T1, and distributes it to the FIOs. The ROCKs receive the T2 signal from the corresponding FIO on the front-panel connector and implement the function of trigger assertion (T2) on the AUX-bus. The other lines in the front-panel connector are dedicated to the SYNCREQ, SYNCFAIL and BUSY signals.

6.2.2 Errors and error lines

A BUSY condition is given by a L1 crate if, after T2, in any of its local buffers there is space only for the present event and for a possible next one. In this case, the T1ACK is not released and therefore the TB is disabled, increasing the dead time. If a T1 is not followed by a T1ACK from the TS, the TB asserts the TBERR signal to the TS. TBERR is also asserted in cases where internal TB errors are detected. TSERR is the error line asserted by the TS on the backplane, it causes the freezing of the status of all the signals monitored in the FIOs. The ROCK can produce an Error signal on the FAIL line to the FIOs and is ORed on the backplane to the TS. In case of ANY Error, the TS will block the Trigger generation, leaving the T1ACK asserted to the TB and generating a VME interrupt to the CPU sitting in its crate.

6.2.3 Trigger Synchronization Cycle

The synchronization test cycle is required to check that the trigger number independently generated by ROCKs, ROCKMs, ADC/TDC and trigger boards are aligned during the run. The TS is in charge of requiring the execution of this cycle any time the last generated trigger number is a Golden Number, i.e. a global 12 bits parameter defined at the start of run. The cycle is activated by all the ROCKs and ROCKMs when the SYNCREQ signal is asserted by the TS and when the previous readout cycle is completed. The correlated signal, SYNCFAIL, is asserted by the ROCK when the synchronization cycle starts. SYNCFAIL is deasserted at the end of the cycle if no error is detected.

In the SYNCREQ cycle, the ROCK tests that the last generated trigger number is equal to the Golden number memorised at the run parameter configuration time. If no internal error (check of its own trigger counter) is found, the ROCK reads the last generated trigger number from every ADC/TDC[12] . If an error is detected, the address of the slave with a wrong trigger number is written in a dedicated register in the ROCK and can be read-out by VME. Then the XSYSHALT and BUSY signals are asserted at the completion of the cycle, while the SYNCFAIL remains asserted until a general reset is generated. The SYNCREQ cycle can be 3-4 μs long in a completely configured crate, but the start time in every crate depends on the completion of the remaining read-out operations in the ROCK state machine; this because a synchronization cycle can only be started in between two event readouts. After a timeout, or when the BUSY is raised, a

DAQ Error is generated and logged, a special event is generated containing information about the status of every ROCK after the SYNCREQ cycle, and finally the Run is stopped writing on tapes the End Of Run (EOR) records.

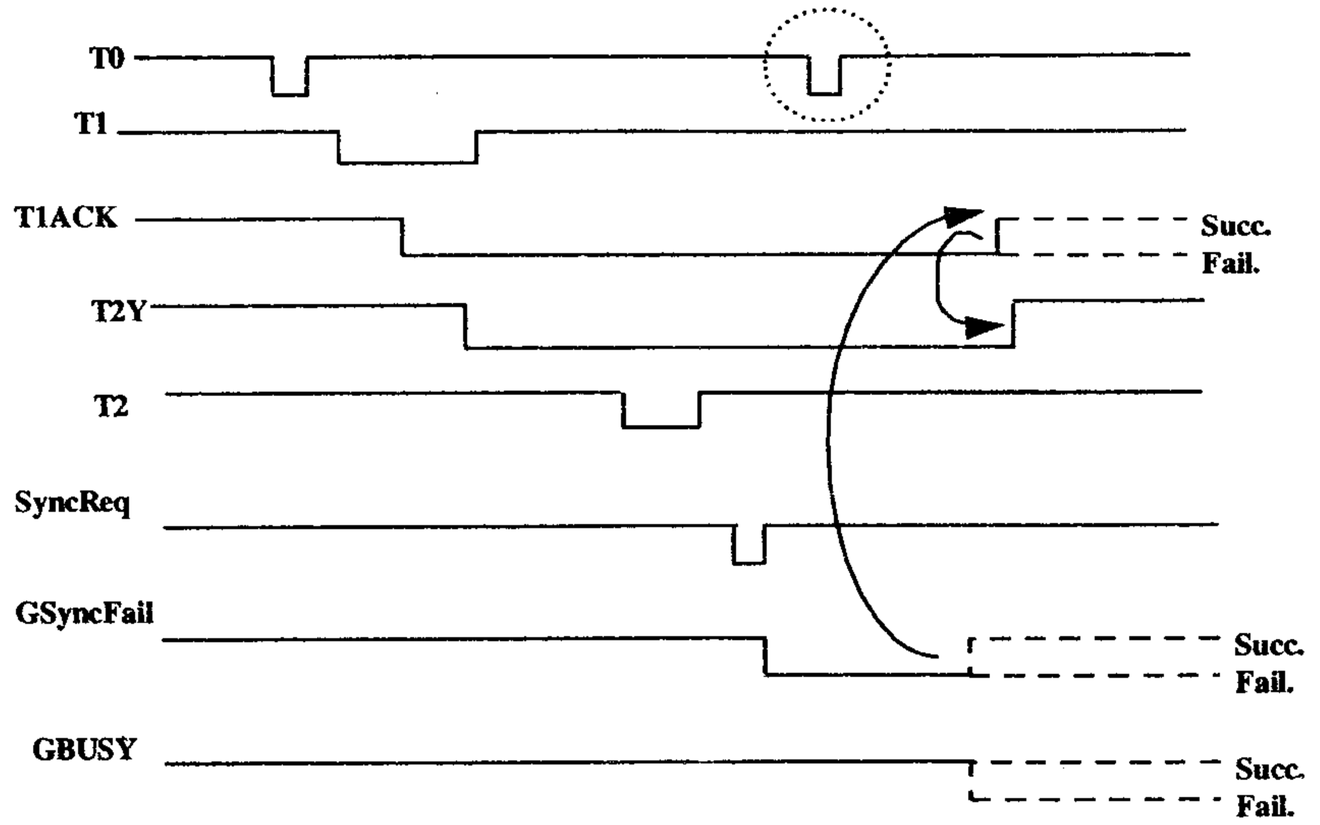

Figure 6.3. Synchronization cycle

6.2.4 Run Control and Trigger

All the Trigger operations are activated and deactivated by the RUN CONTROL system, via a Trigger Control program running on the VME CPU resident inside the TSC. Before the start of the run this program configures the run parameters by:

1. Creating a shared memory, visible to all the L1 and L2 crates through the crates interconnecting VICs, where global parameters are written and remain permanently available.
2. Writing the Golden number (12 bits long) in the shared memory.
3. Sending an INIT-RUN message to the L2-VME and Trigger-CPUs, to configure run parameters in the ROCK special registers (Golden number) and reset the systems.

At START of RUN the Trigger Control program sends a START-RUN message to every CPU, including the Trigger Control. Then, the Trigger Control enables the trigger system and starts the Trigger Supervisor.

6.3 PARTITIONING

As has been already mentioned, the possibility of operating separately the Calorimeter's and Drift Chamber's Trigger and DAQ systems is useful for debugging purposes. In this configuration two partitions will operate independently:

- a MAIN partition containing everything but excluding the drift chamber;
- a secondary partition containing only the drift chamber.

A second Trigger Supervisor will sit in the crate which will operate only when partitioning is required. Some FIOs will be reconfigured by software to belong to this new partition and will no longer be available to the MAIN partition. The DAQ chain will follow this configuration and will be splitted in two parts: the chains belonging to the drift chamber will be assigned to different FARM processors and different output tapes. Separate Run Controllers and Processor Tables will be needed to allow asynchronous operation of the two partitions at the same time on different trigger sources.

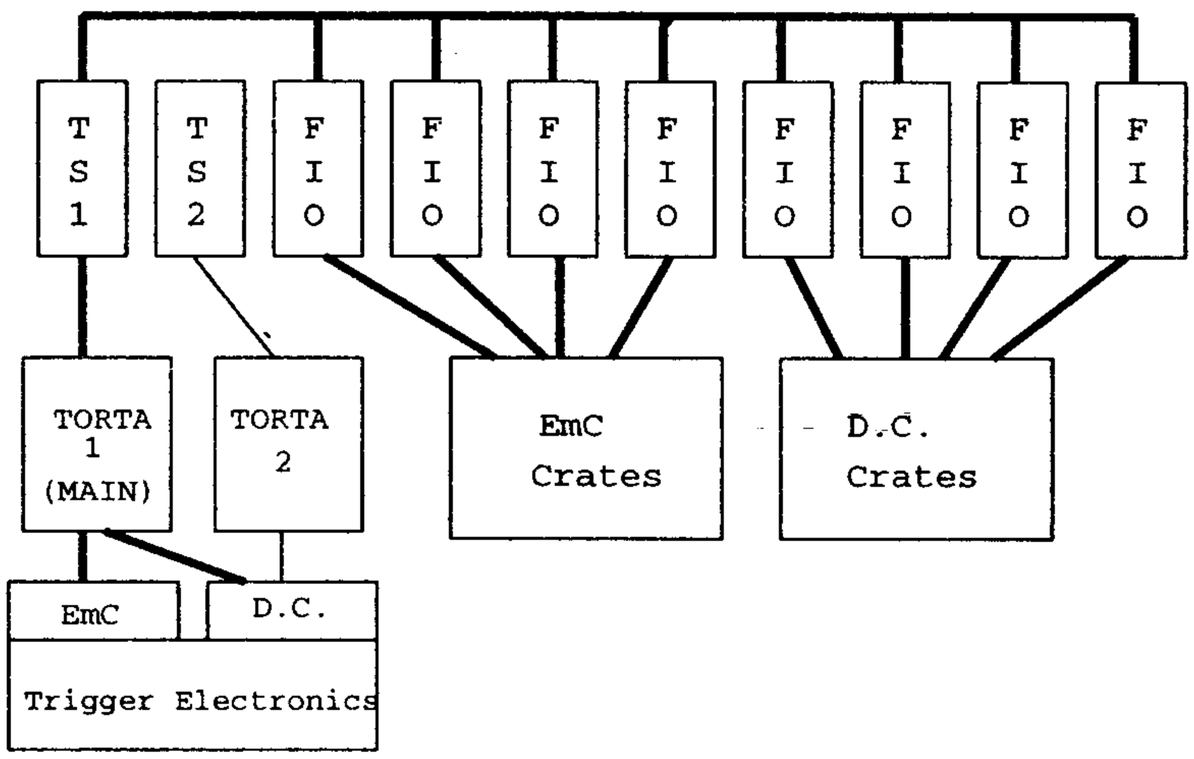

Figure 6.4. Partitioning: in normal run conditions only the main section of the TORTA and only one trigger supervisor are active.

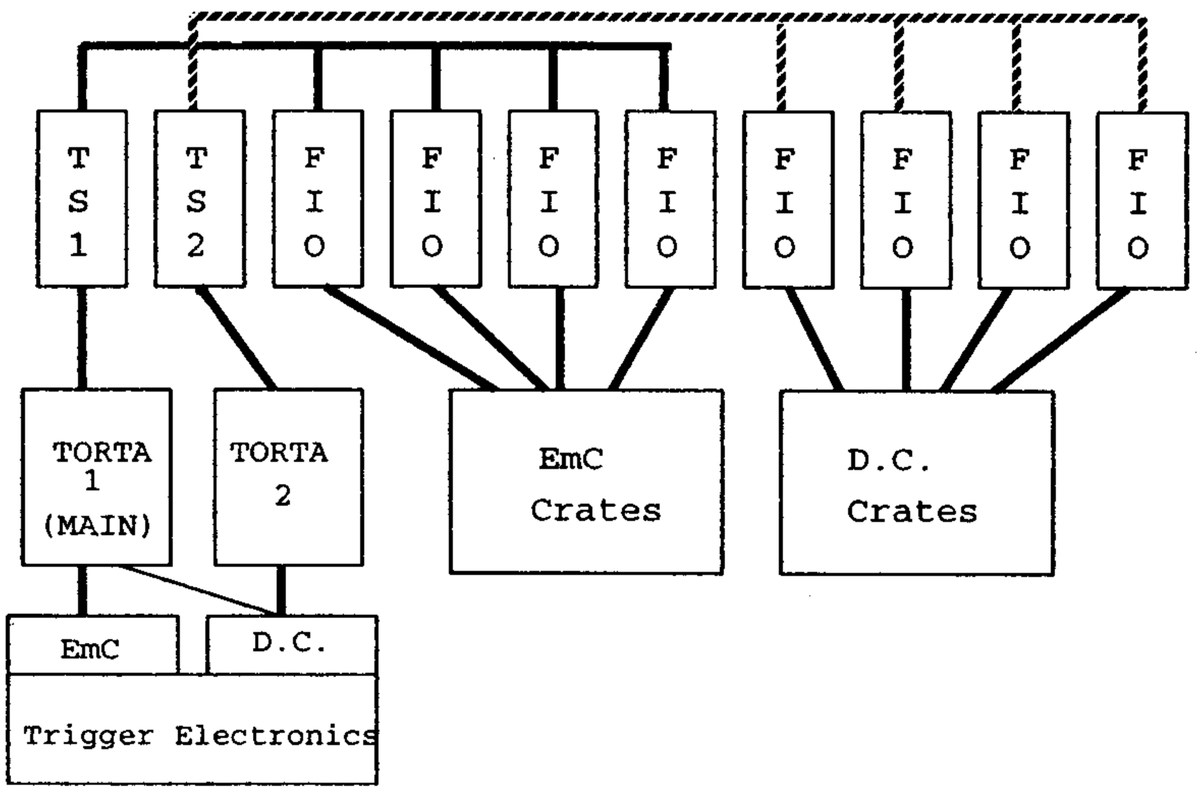

Figure 6.5. Partitioning: the two TORTAs communicate with the corresponding trigger supervisors dedicated to the two detectors.

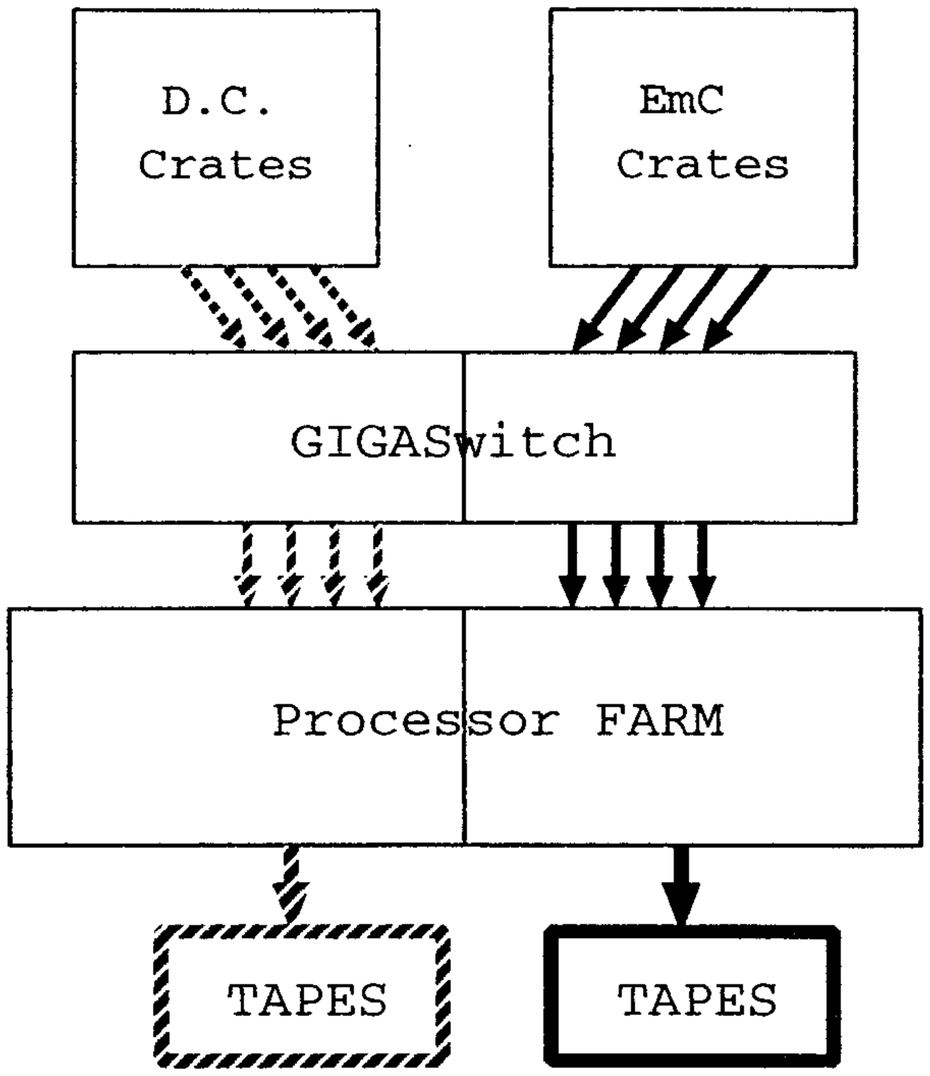

Figure 6.6. Partitioning scheme at the FARM level.

7. COST ESTIMATES AND TIME SCHEDULES

The trigger system is expected to operate in a reduced hardware configuration by the end of '96 when a global test of the trigger and DAQ systems will be performed, using some calorimeter modules input. In April '97 the chamber electronics will also be tested on the real detector. The trigger system will be fully implemented during '97.

Data collected during the first running period, in which DAΦNE would operate at a reduced luminosity, can be helpful in the understanding of the real background conditions and the tuning and optimization of the thresholds setting. The flexibility and modularity of the basic components of the calorimeter and drift chamber trigger allow an easy modification of the trigger conditions, if needed.

Several components are already in the protoptyping phase, while a final design of all the boards composing the trigger box is under way. A rough estimate of the time schedule and costs is given in the following.

7.1 Time schedule

In parallel with the full simulation of the physics and background signals, several hardware components of the trigger have been built and tested. In particular, attention has been devoted to the choice of the analog components, such as line drivers and receivers, adders, comparators, DACs, etc. The layout of the DISH and the chamber discriminator card is ready and prototypes are under construction. The layout of critical parts of the other boards has been tested on preprototypes while awaiting the final design. The success of the preliminary phase makes us confident of the time schedule. Some more complex items like the FIO and the trigger monitor board are not in the critical path, even if the monitor of the trigger-DAQ system will take advantage of their presence. The ADC-TDC system devoted to the calorimeter trigger monitoring is required to be operational during the setting-up of the trigger system. However, since we intend to use the same devices used for the calorimeter FEE, the hardware will be ready from the beginning of the first data taking.

The amount of hardware components needed is listed below.

Calorimeter Trigger

• Trigger Pizza: there are two kinds of analog adders that define the calorimeter trigger elements for the barrel and the end caps, respectively. In total 6 elements are needed, including 1 spare for each type.

• DISH boards: the 96 barrel elements, the 36 elements for each end-cap side and the 48 cosmic ray channels from the barrel require 40 boards, including 2 spares.

• PASTA board: only two modules, including the prototype as a spare, are required.

• Calorimeter Trigger Monitor: the standard calorimeter ADCs and TDCs FEE modules (16 each) have to be modified, in order to increase the dynamic range, at expenses of the resolution in order to control the stability of the calorimeter trigger. The readout of these modules requires 2 additional crates.

Drift chamber trigger

- DC discriminator cards: the readout requires 320 cards, including spares.
- SUPPLI boards: 22 modules, including two spares, are needed.
- CAFFE board: only two modules, including the prototype as a spare are necessary.

Trigger-DAQ interface

- TORTA board: only two modules, including the prototype as a spare, are necessary.
- Trigger Supervisor and FIOs: the trigger supervisor has to be produced in 5 pieces although only one is needed constantly on the experiment. The FIOs modules will be at least 20; 12 are needed in the TS crate to support the 12 different chains and 8 will be used as spares.
- Trigger Distributor: only three modules, including two spares, are necessary.
- Trigger Monitor boards: 50 TM cards, including spares, are needed.

Cabling

About 10 km of cables are needed. SMA connectors must be used for the calorimeter TDCs, for which high stability is required.

	Year	1996									1997				
Item/pieces	Version	04	05	06	07	08	09	10	11	12	01	02	03	04	05
PIZZA:	prototypes														
1+1	pre-production														
2+2	production														
DISH:	prototypes														
5	pre-production														
35	production														
PASTA:	scheme														
	layout														
	prototypes														
1	production														
ADC/TDC monitor:	2+2														
	14+14														
DC discriminator:	production														
SUPPLI:	layout														
	prototypes														
2	pre-production														
20	production														
CAFFE:	scheme														
	layout														
	prototypes														
1	production														
TORTA:	scheme														
	layout														
	prototypes														
1	production														
TS, FIO:	layout														
2+2	prototypes														
3+18	production														
TM:	layout														
4	prototypes														
46	production														

7.2 Cost Estimates

The cost estimate, IVA included, of the trigger system is presented in table:

Items	Units	ML/U	Tot(ML)	
Pizza's	6	6.2	38	
DISH boards	40	3.6	144	
PASTA board	1	10	10	
Crate and VIC	4	20	80	
CALORIMETER TRIGGER				272
CAL Trigger monitor ADC	16	7.2	115	
CAL Trigger monitor TDC	16	7.2	115	
Crate and VIC	2	20	40	
CAL TRIGGER MONITOR				270
DC card modification	320		300	
SUPPLI boards	22	3.6	79	
CAFFE board	1	10	10	
DRIFT CHAMBER TRIGGER				389
TORTA board	1	10	10	
Trigger Supervisor	5	8	40	-> 28
FIO	20	4	80	-> 58
Trigger Monitor	50	3.8	190	->180
Crate and VIC	1	20	20	
TRIGGER-DAQ INTERFACE				296
CABLING	10 km		30	30
Total				1256

REFERENCES

1. The KLOE Collaboration, *A GENERAL PURPOSE DETECTOR for DAΦNE*, **LNF-92/019** (1992).
2. The KLOE Collaboration, *THE KLOE DETECTOR, Technical Proposal*, **LNF-93/002** (1993).
3. The KLOE Collaboration, *The KLOE CENTRAL DRIFT CHAMBER, Addendum to the KLOE DETECTOR Technical Proposal*, **LNF-94/028** (1994).
4. The KLOE Collaboration, *The KLOE DATA ACQUISITION SYSTEM, Addendum to the KLOE DETECTOR Technical Proposal*, **LNF-95/014** (1995).
5. G. Vignola, *Proc. of the Workshop on Physics and Detectors for DAΦNE*, ed. G. Pancheri , Frascati (1991) p. 1; G. Vignola, *Proc. of the XXVI International Conference on High Energy Physics, Dallas, 1992*, ed. J. R. Sanford, AIP Conf. Proc. No. **272** (1993) p. 1941.
6. A. Antonelli, C. Bloise, A. Calcaterra, *Geanfi Program - Version 1.2*, KLOE Note **23** (1992); *GEANFI Handbook vers. 1.3.3*, KLOE Note **52** (1992).
7. E. Gero, *The KTURTLE Program*, KLOE Memo **11** (1995); E. Gero *Beam-gas Background Simulation for KLOE*, KLOE Memo **21** (1995).
8. S. Guiducci, *Background in the KLOE I.R. due to the Touschek scattering*, DAΦNE Technical Note **IR 5** (1994).
9. E. Drago, A. Smilzo, *Cosmic Muon Generator and Its Application to KLOE*, KLOE Note **57** (1993).
10. A. Dar *Atmospheric Neutrinos, Astrophysical Neutrons and Proton Decay Experiments*, Phys. Rev. Letters **51** (1983) p. 227
11. P. Franzini et al. *Tests of the KLOE EM Calorimeter TDC Board*, KLOE Memo **34** (1995).
12. A. Aloisio et al. *Fast Readout System for KLOE*, KLOE Note **88** (1994).